

WELL PRODUCTIVITY PREDICTION FOR THINLY LAMINATED
RESERVOIR USING INTEGRATED HIGH-RESOLUTION LOGS.

Mr. Suchart Chokthanyawat

A Thesis Submitted in Partial Fulfillment of the Requirements
for the Degree of Master of Engineering Program in Petroleum Engineering
Department of Mining and Petroleum Engineering
Faculty of Engineering
Chulalongkorn University
Academic Year 2011
Copyright of Chulalongkorn University

บทคัดย่อและแฟ้มข้อมูลฉบับเต็มของวิทยานิพนธ์ตั้งแต่ปีการศึกษา 2554 ที่ให้บริการในคลังปัญญาจุฬาฯ (CUiR)

เป็นแฟ้มข้อมูลของนิสิตเจ้าของวิทยานิพนธ์ที่ส่งผ่านทางบัณฑิตวิทยาลัย



The abstract and full text of theses from the academic year 2011 in Chulalongkorn University Intellectual Repository (CUiR)

are the thesis authors' files submitted through the Graduate School.

การพยากรณ์ความสามารถในการผลิตของหลุมน้ำมันในแหล่งกักเก็บลักษณะเป็นชั้นบางๆด้วย

ข้อมูลที่มีความละเอียดสูง

นายสุชาติ โชคธัญญาวัฒน์

วิทยานิพนธ์นี้เป็นส่วนหนึ่งของการศึกษาตามหลักสูตรปริญญาวิศวกรรมศาสตรมหาบัณฑิต

สาขาวิชาวิศวกรรมปิโตรเลียม ภาควิชาวิศวกรรมเหมืองแร่และปิโตรเลียม

คณะวิศวกรรมศาสตร์ จุฬาลงกรณ์มหาวิทยาลัย

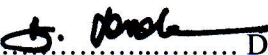
ปีการศึกษา 2554



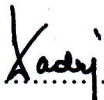
5 2 7 1 6 1 8 1 2 1


Thesis Title WELL PRODUCTIVITY PREDICTION FOR
 THINLY LAMINATED RESERVOIR USING
 INTEGRATED HIGH-RESOLUTION LOGS.
By Mr. Suchart Chokthanyawat
Field of Study Petroleum Engineering
Thesis Advisor Assistant Professor Suwat Athichanagorn, Ph.D.
Thesis Co-advisor Saifon Daungkaew, Ph.D.

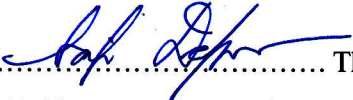
Accepted by the Faculty of Engineering, Chulalongkorn University in
Partial Fulfillment of the Requirements for the Master's Degree


.....  Dean of the Faculty of Engineering
(Associate Professor Boonsom Lerdkhirunwong, Dr.Ing.)


THESIS COMMITTEE

.....  Chairman
(Associate Professor Sarithdej Pathanasetpong)

.....  Thesis Advisor
(Assistant Professor Suwat Athichanagorn, Ph.D.)

.....  Thesis Co-advisor
(Saifon Daungkaew, Ph.D.)

.....  Examiner
(Assistant Professor Jirawat Chewaroungroj, Ph.D.)

.....  External Examiner
(Wisarut Thungsuntonkhun, Ph.D.)

สุชาติ โชคธัญญาวัฒน์ : การพยากรณ์ความสามารถในการผลิตของหลุมน้ำมันในแหล่งกักเก็บลักษณะเป็นชั้นบางๆด้วยข้อมูลที่มีความละเอียดสูง (WELL PRODUCTIVITY PREDICTION FOR THINLY LAMINATED RESERVOIR USING INTEGRATED HIGH-RESOLUTION LOGS.) อ. ที่ปรึกษาวิทยานิพนธ์หลัก:
 ผศ. ดร. สุวัฒน์ อธิชนากร, อ.ที่ปรึกษาวิทยานิพนธ์ร่วม: ดร.สายฝน ดวงแก้ว, 106 หน้า.

เนื่องจากการใช้จ่ายในการสำรวจหาแหล่งน้ำมันในแหล่งที่มีระดับน้ำทะเลสูงมีค่าใช้จ่ายที่สูงขึ้นมากอย่างมีนัยสำคัญ การทำการประเมินหลุมสำรวจในแต่ละหลุมนั้นจำเป็นต้องดำเนินการอย่างมีประสิทธิภาพเพื่อที่จะหลีกเลี่ยงค่าใช้จ่ายที่มากเกินไป การหาคุณลักษณะของแหล่งกักเก็บน้ำมันที่เป็นชั้นบางๆนั้นซับซ้อนเนื่องจากการที่แหล่งกักเก็บเป็นชั้นบางๆในแนวดิ่งไม่เป็นเนื้อเดียวกัน สามารถทำให้เกิดการไหลแบบซับซ้อนและอีกทั้งสามารถส่งผลกระทบต่อการวัดทางด้านที่เกี่ยวข้องกับคุณสมบัติทางกายภาพของหิน ยกตัวอย่างเช่น หินทรายที่มีความต้านทานทางไฟฟ้าต่ำเนื่องจากชั้นของแผ่นหินที่เป็นโคลนแข็งซ้อนอยู่อย่างเป็นชั้นๆภายในหินทรายนั้น ผลที่เกิดขึ้นทำให้แหล่งกักเก็บที่เป็นน้ำมันถูกทำให้เห็นเป็นแหล่งกักเก็บที่เป็นน้ำจากการทำการวิเคราะห์ทางด้านปิโตรฟิสิกส์ทั่วไป ดังนั้นจึงเป็นสิ่งสำคัญที่สามารถนำอุปกรณ์การวัดแบบมีความละเอียดสูงมาช่วยในการวัดและประเมินในแหล่งกักเก็บที่มีชั้น แผ่นหินดินดาน อยู่เป็นชั้นบางๆในแหล่งกักเก็บที่เป็นน้ำมันอย่างมีประสิทธิภาพ

การศึกษานี้มุ่งหมายที่จะสาธิตขั้นตอนในการใช้ข้อมูลจากเครื่องมือวัดความต้านทานไฟฟ้าแบบภาพถ่าย เพื่อที่จะพยากรณ์ความสามารถในการไหลและความสามารถในการผลิตจากแหล่งเก็บกักน้ำมันใน หลุมน้ำมัน จุดประสงค์ของ การศึกษาในครั้งนี้เป็นการศึกษาครั้งแรก ที่จะพยายามพัฒนาขั้นตอนที่เป็นไปได้และเทคนิคทางคณิต ศาสตร์ในการใช้ความต้านทานไฟฟ้าสังเคราะห์มาช่วยพยากรณ์ความสามารถในการไหลจากการวัดจากข้อมูลการไหลแบบพลวัต เช่น คูอัลเพ็คเกอร์ ฟอร์เมชันทดสอบ การพัฒนาขั้นตอนนี้จะนำ มาใช้กับข้อมูลเครื่องมือวัดความต้านทานไฟฟ้าแบบภาพถ่าย เพื่อที่จะนำมาพยากรณ์ความสามารถในการไหลของแหล่งกักเก็บ ในความลึกอื่นที่ไม่ได้ทำการวัดค่าความสามารถในการไหลจริง ไว้ อย่างไรก็ตามขั้นตอนการศึกษานี้ยังไม่เคยได้รับการทดสอบกับข้อมูลจากแหล่งกักเก็บจริงดังนั้นการศึกษาในครั้งนี้จะนำข้อมูลที่แท้จริงมาทดสอบเพื่อที่จะตรวจสอบว่าสามารถนำมาใช้งานได้จริง

ภาควิชา วิศวกรรมเหมืองแร่และปิโตรเลียม ลายมือชื่อนิติ.....Suchast Choethanyawat
 สาขาวิชา วิศวกรรมปิโตรเลียม..... ลายมือชื่อ อ.ที่ปรึกษาวิทยานิพนธ์หลัก.....Som Othm
 ปีการศึกษา 2554.....

5271618121: MAJOR PETROLEUM ENGINEERING

KEYWORDS: WELL PERFORMANCE PREDICTION / HIGH RESOLUTION LOGS/ THINLY LAMINATED RESERVOIR

SUCHART CHOKTHANYAWAT : WELL PRODUCTIVITY PREDICTION FOR THINLY LAMINATED RESERVOIR USING INTEGRATED HIGH-RESOLUTION LOGS. ADVISOR: ASST. PROF. SUWAT ATHICHANAGORN, Ph.D., CO-ADVISOR: SAIFON DAUNGKAEW, Ph.D., 106 pp.

Due to increasing costs in hydrocarbon exploration, formation evaluation needs to be efficient in order to avoid excessive expenditures. Proper reservoir characterization in thinly laminated reservoirs is a key to successful field development. These thinly laminated reservoirs are complex due to their vertical heterogeneity. As a result, there is low resistivity contrast between water and hydrocarbon bearing zones when standard resistivity logs are used. Thus, it is crucial to deploy a high resolution formation evaluation in order to capture reservoir pay and detect hydrocarbon zones.

This study aims to demonstrate a methodology of using borehole electrical image log to determine effective permeability. The study is the first attempt to develop a numerical technique to build a correlation between synthetic resistivity derived from borehole electrical image tool with other dynamic permeability measurements such as dual packer formation tester. A single well predictive model was used in the process to generate high resolution numerical radial model from high resolution log data. This improving workflow is applied to electrical images to predict effective permeability in other intervals where actual permeability measurements were not acquired. However, this methodology has not been tested with the actual field data. Therefore, this study aims to investigate this workflow when applied to actual field data.

Department: Mining and Petroleum Engineering Student's Signature: *Suchart Chokthanyawat*
 Field of Study: Petroleum Engineering Advisor's Signature: *Suwat Athichanagorn*
 Academic Year: 2011

Acknowledgements

I would like to express my appreciation and thankfulness toward my research advisor, Assistant Professor Dr. Suwat Athichanagorn and Dr. Saifon Daungkaew, for their guidance, support and sincere personal advice that helps me mature as a researcher and will deeply influence my career and future life.

I would like to give my special thank to Thaniya Lorlertratna, for her kindness, suggestion, invaluable supporting, personal advice and invitation for me to join Data Consulting Services for exploring oil and gas business in Schlumberger which has totally changed my life for the better since three years ago.

I am heartily thankful to the thesis committee members for their invaluable comments and recommendations.

I wish to give my special thanks to all faculty members in the Department of Mining and Petroleum Engineering who have offered petroleum knowledge, technical advice, and invaluable consultation. I am thankful to all classmates for discussions and true friendship.

I would like to thank Schlumberger Overseas S.A. (Thailand) and Data Consulting Services staffs for their warm support to reduce the workload during my study. Also, I would like to thank Schlumberger for allowing me to use Single Well Predictive Model 3.1 (SWPM) and providing license of ECLIPSE 100 reservoir simulator software. Without the software, this study would not have been completed.

Lastly, I would like to express my sincere gratitude and deep appreciation to my family for their patient a moral encouragement and constant support.

Contents

	Page
Abstract (Thai)	iv
Abstract (English)	v
Acknowledgements	vi
Contents	vii
List of Tables	ix
List of Figures	x
List of Abbreviations	xvi
Nomenclature	xvii
CHAPTER I INTRODUCTION	1
CHAPTER II LITERATURE REVIEW	6
2.1 Previous Works	6
CHAPTER III THEORY AND CONCEPT	10
3.1 Petrophysical Interpretation	10
3.1.1 Nuclear Magnetic Resonance Log (NMR).....	10
3.1.2 Borehole Electrical Imaging Log	13
3.2 Wireline Formation Tester	16
3.3 Welltest Interpretation	18
3.4 Rock Typing using Flow Zone Indicator (FZI) Method	21
CHAPTER IV METHODOLOGY	25
4.1 Preparation of Rock and Fluid Properties Data	25
4.2 Generation of 3D Static Single Well Model	28
4.3 Grid Conversion.....	34
4.4 Well Test Simulation	38
4.5 Single Well Model Calibration	38
4.6 Well Productivity Prediction.....	39
CHAPTER V RESULTS AND DISCUSSIONS	41
5.1 Single Well Model of NMR based method.....	41
5.1.1 NMR-IPTT#1	42

5.1.2	NMR-IPTT#2	44
5.1.3	NMR-IPTT#3	47
5.1.4	Discussion	49
5.2	Single Well Model of Borehole Electrical Image Based Method.....	50
5.2.1	SRES-IPTT#1.....	51
5.2.2	SRES-IPTT#2.....	58
5.2.3	SRES-IPTT#3.....	65
5.2.4	Discussion	72
5.2.5	MODIFIED-SRES-IPTT#1.....	74
5.2.6	MODIFIED-SRES-IPTT#3.....	79
5.3	Result Comparison.....	85
5.4	Well Productivity Prediction.....	85
CHAPTER VI CONCLUSIONS AND RECOMMENDATIONS.....		93
6.1	Conclusions.....	93
6.2	Recommendations.....	95
REFERENCES.....		96
APPENDICES		100
APPENDIX A.....		101
VITAE.....		106

List of Tables

	Page
Table 4.1: Reservoir parameters for all zone of interest.	27
Table 4.2: PVT Data	25
Table 4.3: Radius and Theta Direction of Dual Packer WFT grid	35
Table 4.4: Thickness Direction of Dual Packer WFT grid for both NMR based method and Borehole Electrical Image based method.....	36
Table 5.1: The comparison of interpreted horizontal permeability from the measurement of Interval Pressure Transient Tests and Single Well Model of NMR based method.....	50
Table 5.2: Interpreted horizontal permeability from Interval Pressure Transient Tests	50
Table 5.3: Coefficients of intervals using normalized coefficient result from IPTT#1.	55
Table 5.4: Coefficients of intervals using normalized coefficient result from IPTT#2.	62
Table 5.5: Coefficients of intervals using normalized coefficient result from IPTT#3.	68
Table 5.6: Horizontal permeability from WFT and all single well models.	72
Table 5.7: Coefficients of intervals using normalized coefficient result from IPTT#1.	76
Table 5.8: Coefficients of intervals using normalized coefficient result from IPTT#3.	82
Table 5.9: Horizontal permeabilities from the measurements and all modified single well models.....	84
Table 5.10: Horizontal permeabilities from the measurements and single well models.	85
Table 5.11: Productivity index from the measurement and single well model.	92
Table 5.12: AOFPP from the measurement and single well model.	92

List of Figures

	Page
Figure 1.1: Integration of electrical image logs and permeability derived from formation tester – (green point), and NMR permeability (standard resolution - blue curve) and synthetic resistivity (high resolution – red curve).....	4
Figure 3.1: Example of spin echo record by the tool.....	11
Figure 3.2: Example of T2 distribution obtained from NMR measurement.....	12
Figure 3.3: Example of how to fit curve to T2 distribution obtained from NMR.	12
Figure 3.4: Bound and free-fluid porosity is computed using a T2 cutoff.	13
Figure 3.5: Example of borehole electrical imaging log.....	14
Figure 3.6: Integration of borehole electrical imaging log with other wireline logs to improve interpretation result	15
Figure 3.7: Pressure response of Wireline Formation Tester (WFT)..	17
Figure 3.8: Wireline Formation Tester with optional modules.....	18
Figure 3.9: Build-up test sequence.....	19
Figure 3.10: Example of pressure derivative.	20
Figure 3.11: Histogram plot of log(FZI) to determine possible numbers of rock types or HFUs.....	22
Figure 3.12: Normal probability Plot of log(FZI) to determine possible numbers of rock types or HFUs.....	22
Figure 3.13: Stratigraphic Modified Lorenz Plot (SMLP) to determine possible numbers of rock types or HFUs.	23
Figure 3.14: Example of log(ϕ_z) vs log(RQI) plot.....	24
Figure 3.15: Relationship between actual permeability and permeability calculated from FZI for each rock type or hydraulic flow unit.	24
Figure 4.1: Wireline log data and Interval Pressure Transient Tests (IPTT).....	28
Figure 4.2: Stratigraphic Modified Lorenz Plot showing that there are 5 rock types..	29

Figure 4.3: Log data representing wireline logs and rock types covering all intervals of the demonstrate well.	30
Figure 4.4: Oil and water relative permeability curves at different water saturations for HFU#1. Initially, the water saturation is 0.1306 and the oil relative permeability is 0.8456.....	31
Figure 4.5: Oil and water relative permeability curves at different water saturations for HFU#2. Initially, the water saturation is 0.1312 and the oil relative permeability is 0.8549.....	32
Figure 4.6: Oil and water relative permeability curves at different water saturations for HFU#3. Initially, the water saturation is 0.1437 and the oil relative permeability is 0.8307.....	32
Figure 4.7: Oil and water relative permeability curves at different water saturations for HFU#4. Initially, the water saturation is 0.1499 and the oil relative permeability is 0.7586.....	33
Figure 4.8: Oil and water relative permeability curves at different water saturations for HFU#5. Initially, the water saturation is 0.1382 and the oil relative permeability is 0.8547.....	33
Figure 4.9: Thinly laminated single well model is generated from SWPM.	34
Figure 4.10: Cartesian grids single well model is converted manually to radial grids single well model.	36
Figure 4.11: Reservoir model for IPTT#1.	37
Figure 4.12: Reservoir model for IPTT#2.	37
Figure 4.13: Reservoir model for IPTT#3.	38
Figure 4.14: Workflow of calibrated single well model – Borehole Electrical Image based method using result from the actual measurement.	39
Figure 4.15: Workflow of predicting well productivity using single well model from Borehole Electrical Image.....	40
Figure 5.1: Well schematic for IPTT#1 interval.....	42
Figure 5.2: Log-log plot of NMR-IPTT#1.....	43
Figure 5.3: Semi-log plot of NMR-IPTT#1.....	43
Figure 5.4: History plot of NMR-IPTT#1.	44

Figure 5.5: Well schematic for IPTT#2 interval.....	44
Figure 5.6: Log-log plot of NMR-IPTT#2.....	45
Figure 5.7: Semi-log plot of NMR-IPTT#2.....	46
Figure 5.8: History plot of NMR-IPTT#2.	46
Figure 5.9: Well schematic for IPTT#3 interval.....	47
Figure 5.10: Log-log plot of NMR-IPTT#3.....	48
Figure 5.11: Semi-log Plot of NMR-IPTT#3.....	48
Figure 5.12: History log plot of NMR-IPTT#3.	49
Figure 5.13: Process of case SRES-IPTT#1.	52
Figure 5.14: Log-log plot of uncalibrated model for IPTT#1 interval.	52
Figure 5.15: Log-log plot of actual data and calibrated single well model for IPTT#1.....	53
Figure 5.16: Semi-log plot of actual data and calibrated single well model for IPTT#1.....	54
Figure 5.17: History plot of actual data and calibrated single well model for IPTT#1.....	54
Figure 5.18: Log-log plot of actual data and calibrated single well model for IPTT#2.....	55
Figure 5.19: Semi-log plot of actual data and calibrated single well model for IPTT#2.....	56
Figure 5.20: History plot of actual data and calibrated single well model for IPTT#2.....	56
Figure 5.21: Log-log plot of actual data and calibrated single well model for IPTT#3.....	57
Figure 5.22: Semi-log plot of actual data and calibrated single well model for IPTT#3.....	57
Figure 5.23: History plot of actual data and calibrated single well model for IPTT#3.....	58
Figure 5.24: Process of case SRES-IPTT#2.	59
Figure 5.25: Log-log plot of uncalibrated model for IPTT#2 interval.	59
Figure 5.26: Log-log plot of actual data and calibrated single well model for IPTT#2.....	60

Figure 5.27: Semi-log plot of actual data and calibrated single well model for IPTT#2.....	61
Figure 5.28: History plot of actual data and calibrated single well model for IPTT#2.....	61
Figure 5.29: Log-log Plot of actual data and calibrated single well model for IPTT#1.....	62
Figure 5.30: Semi-log plot of actual data and calibrated single well model for IPTT#1.....	62
Figure 5.31: History plot of actual data and calibrated single well model for IPTT#1.....	63
Figure 5.32: Log-log plot of actual data and calibrated single well model for IPTT#3.....	63
Figure 5.33: Semi-log plot of actual data and calibrated single well model for IPTT#3.....	64
Figure 5.34: History plot of actual data and calibrated single well model for IPTT#3.....	64
Figure 5.35: Process of case SRES-IPTT#3.	65
Figure 5.36: Log-log plot of uncalibrated model for IPTT#3 interval.	66
Figure 5.37: Log-log plot of calibrated model for IPTT#3 interval.	67
Figure 5.38: Semi-log plot of calibrated model for IPTT#3 interval.....	67
Figure 5.39: History plot of calibrated model for IPTT#3 interval.	68
Figure 5.40: Log-log plot of calibrated model for IPTT#1 interval.	69
Figure 5.41: Semi-log plot of calibrated model for IPTT#1 interval.....	69
Figure 5.42: History plot of calibrated model for IPTT#1 interval.	70
Figure 5.43: Log-log plot of calibrated model for IPTT#2 interval.	70
Figure 5.44: Semi-log plot of calibrated model for IPTT#2 interval.....	71
Figure 5.45: History plot of calibrated model for IPTT#2 interval.	71
Figure 5.46: Modified Log-log plot of WFT measurement at IPTT#1 interval.	73
Figure 5.47: Modified Log-log plot of WFT measurement at IPTT#3 interval.	73
Figure 5.48: Radial composite model.	74
Figure 5.49: Log-log plot of actual data and calibrated single well model for IPTT#1.....	75

Figure 5.50: Semi-log plot of actual data and calibrated single well model for IPTT#1.....	75
Figure 5.51: History plot of actual data and calibrated single well model for IPTT#1.....	76
Figure 5.52: Log-log plot of actual data and calibrated single well model for IPTT#2.....	77
Figure 5.53: Semi-log plot of actual data and calibrated single well model for IPTT#2.....	77
Figure 5.54: History plot of actual data and calibrated single well model for IPTT#2.....	78
Figure 5.55: Log-log plot of actual data and calibrated single well model for IPTT#3.....	78
Figure 5.56: Semi-log Plot of actual data and calibrated single well model for IPTT#3.....	79
Figure 5.57: History plot of actual data and calibrated single well model for IPTT#3.....	79
Figure 5.58: Log-log plot of actual data and calibrated single well model for IPTT#3.....	80
Figure 5.59: Semi-log plot of actual data and calibrated single well model for IPTT#3.....	81
Figure 5.60: History plot of actual data and calibrated single well model for IPTT#3.....	81
Figure 5.61: Log-log plot of actual data and calibrated single well model for IPTT#1.....	82
Figure 5.62: Semi-log plot of actual data and calibrated single well model for IPTT#1.....	82
Figure 5.63: History plot of actual data and calibrated single well model for IPTT#1.....	83
Figure 5.64: Log-log plot of actual data and calibrated single well model for IPTT#2.....	83
Figure 5.65: Semi-log plot of actual data and calibrated single well model for IPTT#2.....	83

Figure 5.66: History plot of actual data and calibrated single well model for IPTT#2.....	84
Figure 5.67: IPR plot from actual measurement of IPTT#1.....	86
Figure 5.68: IPR plot from actual measurement of IPTT#2.....	86
Figure 5.69: IPR plot from actual measurement of IPTT#3.....	87
Figure 5.70: IPR plot from single well model of borehole electrical image based method calibrated from MODIFIED-SRES-IPTT#1 for IPTT#1.....	87
Figure 5.71: IPR plot from single well model of borehole electrical image based method calibrated from MODIFIED-SRES-IPTT#1 for IPTT#2.....	88
Figure 5.72: IPR plot from single well model of borehole electrical image based method calibrated from MODIFIED-SRES-IPTT#1 for IPTT#3.....	88
Figure 5.73: IPR plot from single well model of borehole electrical image based method calibrated from SRES-IPTT#2 for IPTT#1.....	89
Figure 5.74: IPR plot from single well model of borehole electrical image based method calibrated from SRES-IPTT#2 for IPTT#2.....	89
Figure 5.75: IPR plot from single well model of borehole electrical image based method calibrated from SRES-IPTT#2 for IPTT#3.....	90
Figure 5.76: IPR plot from single well model of borehole electrical image based method calibrated from MODIFIED-SRES-IPTT#3 for IPTT#1.....	90
Figure 5.77: IPR plot from single well model of borehole electrical image based method calibrated from MODIFIED-SRES-IPTT#3 for IPTT#2.....	91
Figure 5.78: IPR plot from single well model of borehole electrical image based method calibrated from MODIFIED-SRES-IPTT#3 for IPTT#3.....	91

List of Abbreviations

BBL/D	barrels per day
cp	centipoises
DST	drillstem test
FVF	volume formation factor
FZI	Flow Zone Indicator
ft	feet
HFU	Hydraulic Flow Unit
IPTT	Interval Pressure Transient Test
MDT	Modular Dynamic Formation Tester
mD	Millidarcies
mD.ft	Millidarcies.feet
NMR	Nuclear Magnetic Resonance
PTA	Pressure Transient Analysis
PVT	pressure-volume-temperature
SCAL	Special Core Analysis
SRES	Synthetic Resistivity
SWPM	Single Well Predictive Model
WFT	Wireline Formation Tester

Nomenclatures

dr	grid block size in the r-direction
dz	grid block size in the z-direction
$d\Theta$	grid block size in the theta-direction
h	formation thickness
k	permeability
k_h	horizontal permeability
k_o	oil permeability
k_r	relative permeability
k_{ro}	relative permeability to oil
k_v/k_h	vertical to horizontal permeability ratio
M	mobility ratio
p	pressure
p_i	initial reservoir pressure
r_w	wellbore radius
S_o	oil saturation
S_{orw}	residual oil saturation to water
S_w	water saturation
s	skin factor
t	time
T_2	T2 Distribution

GREEK LETTERS

Σ	summation
ρ	density
ϕ	porosity
μ	fluid viscosity

CHAPTER I

INTRODUCTION

Laminated formations pose two major evaluation challenges for reservoir engineers as follows:

The first is the classic low resistivity pay problem as seen in vertical wells. Layers of clay, silt and fine-grained sand distributed within a hydrocarbon bearing sand will significantly reduce the apparent resistivity measurement. This low resistivity results in wrong fluid identification and therefore this zone might be overlooked.

The second is the high angle well evaluation problem. The same laminated formation, when measured by an induction tool at moderate - high relative dip, will exhibit an increase in apparent resistivity beyond that measured in the vertical well. Again, the inaccurate calculation of water saturation and hydrocarbon volume may cause the error in reservoir estimation.

Both of these problems can be solved by an integrated method of combination of standard logs (Gamma ray, Resistivity, Neutron Porosity, Bulk Density), new technology logging tools (Tri-axial Resistivity, Borehole Electrical Image, and Nuclear Magnetic Resonance logs), and Wireline Formation Tester. In addition to this combination, advanced petrophysical interpretation method such as Log Enhanced Resolution using Borehole Electrical Image Log has been developed to improve the efficiency of reservoir characterization of thinly bedded reservoirs. The integration of this information is a key in establishing link between fluid dynamic and static reservoir properties. This leads to a better understanding and confidence of the applicability in the result.

However, all sources of logging data are not always available. NMR logging information is very rare in Southeast Asia. The answers above allow us to propose an alternative methodology using Synthetic Resistivity derived from Borehole Electrical Image Log as permeability input to simulate pressure response from numerical single

well model calibrated with the actual measurement from dual packer module of Wireline Formation Tester.

Since the 1980's, micro electrical imaging tools such as Formation MicroScanner (FMS), Formation MicroImager (FMI) and Oil Base Mud Imager (OBMI) have mainly been used for structural and sedimentological interpretation and qualitative interpretation for sand quality. Electrical image log variations are often represented using colors ranging between dark brown to yellow where the light color represents high resistivity, and the dark color represents low resistivity. The shale and silt calculation is based on the cut-off on calibrated high resolution resistivity curves to determine sand count in a clastic reservoir. The primary application of borehole image in this type of reservoir is identification and evaluation of potential reservoir quality rock. For thinly bedded sandstone, image is often practically used for determining net pay of sand and silt other than whole coring which is cost limiting. It could also illustrate reservoir structure/stratigraphy and provide an inference of the reservoir quality. The dip and azimuth analysis is also used to indicate the location of potential high permeability zone.

Nuclear Magnetic Resonance (NMR) records a minimum amount of free fluid and porosity distribution as well as permeability profile from the grain size. However permeability profile needs to be calibrated from core permeability or WFT or Interval Pressure Transient Test (IPTT) or full DST based on information availability.

Wireline Formation Tester (WFT) and Interval Pressure Transient Test (IPTT) are used extensively to measure formation pressure, collect downhole fluids, fluid gradient, fluid contact and estimate near wellbore fluid mobility. A dual-packer module can be performed for local production tests or interference tests along the wellbore which are commonly known as IPTT. It is also used to derive reservoir parameters such as permeability-thickness, skin factor and permeability anisotropy.

In many reservoirs, there are several permeability sources often available from one or as many as four sources such as core data, NMR log, WFT and well testing. However, the permeability values from these sources often differ significantly. Core and NMR permeability values represent a smaller depth of investigation than WFT, which WFT itself measures permeability at a smaller scale than well testing. However, it is impossible to perform well testing for every zone in every well. The

systematic integration of borehole image, NMR, pressure transient analysis from an IPTT in the thinly bedded reservoirs, it is helpful for making critical decision prior to run well testing.

The challenge of this study is how to make the relationship between borehole electrical image and effective permeability. Synthetic Resistivity (SRES) derived from borehole electrical image measurement can be used to compute hi-resolution porosity, sorting index or variations of grain size which are uni-directional with permeability. The observation is illustrated in Figure 1.1, shows SRES (red curve), permeability derived from NMR (blue curve) and permeability derived from formation tester (green point) overlaid on one another.

The use of SRES variations for permeability estimations has not been tested with actual field data. Therefore, this study aims to demonstrate new methodology when applied to actual field data and aims to achieve an integrated and structured approach using SRES to predict permeability and well productivity.

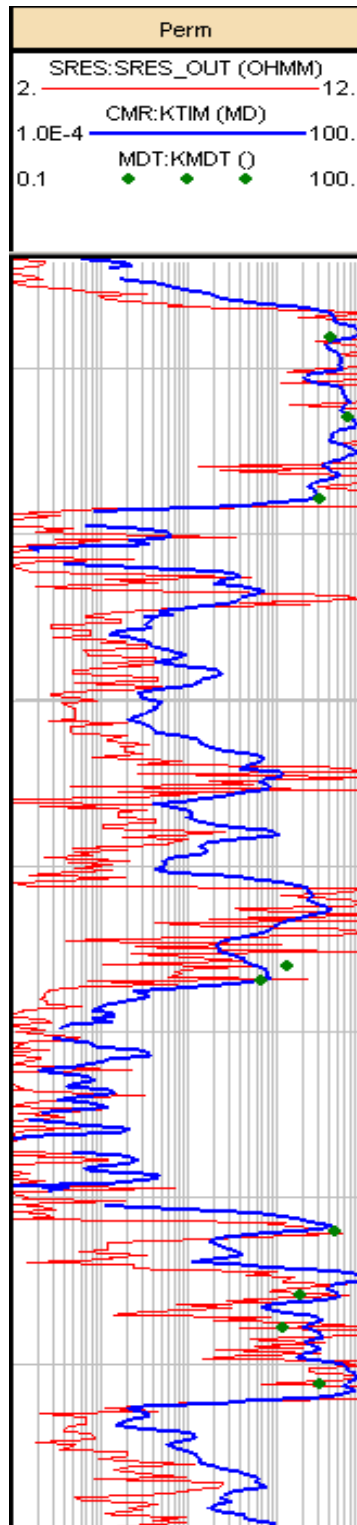


Figure 1.1: Integration of electrical image logs and permeability derived from formation tester – (green point), and NMR permeability (standard resolution - blue curve) and synthetic resistivity (high resolution – red curve)

This thesis paper proceeds as follows:

Chapter II presents review on previous works related to the correlation and prediction of permeability and borehole image resistance and structured approach for calculating the productivity of a laminated clastic reservoir.

Chapter III describes the fundamental of petrophysical interpretation, wireline formation tester, well test interpretation and determination of rock type using Flow Zone Indicator (FZI) Method.

Chapter IV describes the methodology and the single well simulation model used in this study.

Chapter V discusses the results of single well model simulation obtained from permeability derived from NMR and synthetic resistivity calibrated from IPTTs.

Chapter VI provides conclusions and recommendations for further study.

CHAPTER II

LITERATURE REVIEW

This chapter reviews previous works, experiments and developments related to the workflow of integrated hi-resolution logs, petrophysical analysis, PVT data and Interval Pressure Transient Test (IPTT) from Wireline Formation Tester (WFT) to forecast the well performance from numerical single well model.

2.1 Previous Works

Reda and Hashem ^[1] proposed a precise method of using resistivity imaging tool for estimation of high resolution reservoir parameters calibrated to nuclear magnetic resonance data for better reservoir characterization. From their experience, they found that porosity and permeability can be estimated from wireline image logs and then calibrated to any other relevant data measured by NMR or WFT as well as core data. Jennings-Lucia model can be used to predict permeability from high-resolution image base obtained by transforming the porosity hi-resolution image base according to the estimated rock fabric number and petrophysical classification. These parameters can be applied to different wells in the same reservoir. This application can help us map and model porosity and permeability through the entire field.

Elarouci et al. ^[2] proposed a method of integrated WFT, Logs, Core and Well Test data to get hydraulic flow unit permeability. They also discussed key benefits of this cross-discipline method. Their application was performed as step-by-step methodology consisting of porosity and permeability facies determination, hydraulic flow unit identification, synthetic permeability curve generation, and effective-thickness computation. The result of combining all hydraulic flow units coupled with their predicted permeability agree with the result from DST interpretation.

Thomas et al. ^[3] studied correlation of permeability-resistivity and anisotropy permeability. They proposed their own correlation between probe permeability and micro-resistivity to estimate average horizontal and vertical permeability from their regression. Their data set also was divided into zones by gamma ray response to give an indication of how the relationship alters with changing rock fabric.

Anxionnaz et al. ^[4] proposed a technique to derive petrophysical images from borehole electrical conductivity images and high-resolution petrophysical measurements measured along a known path within the borehole. The technique has been successfully applied to generate density images and permeability images for quantitative measurement.

Jackson et al. ^[5] demonstrated that reservoir parameters such as horizontal and vertical permeability may be determined from analysis of Modular Dynamic Tester (MDT) interval pressure transient tests, and the results can be verified via accurate numerical modeling and simulation coupled with a gradient based history matching technique. Interval transient testing and analysis techniques have been presented, and existing interpretation methods for estimating horizontal and vertical permeability were evaluated using simulated and field examples.

Daungkaew et al. ^[6] studied pressure transient response obtained from mini-DSTs in thinly laminated deep water reservoirs from a field example compared to conventional DST. The authors pointed out that with the small scale of pressure transient response obtained from a WFT with dual packer, a more detailed pressure transient response can be seen compared to a larger scale well test where properties derived represent the average reservoir behavior.

Haddad et al. ^[7] studied types of reservoir permeability such as NMR, MDT. Also DST is required to validate NMR, MDT, and/or core data. For reservoir characterization, NMR and MDT permeability from wells in the field, qualified by at least one DST, would result in a more representative reservoir model that may be used for reservoir performance prediction.

Zhou and Chen ^[8] demonstrated an application with a “wizard” based interface called “SWPM” (Single Well Predictive Model). The software is designed to provide the user with the tools to simply and efficiently build 1D and 3D static models from wellbore data, and pass the model to and from ECLIPSE to calibrate the models using well test or production data if available, and finally to use the 3D calibrated model to define future scenarios and predict future performance of the well.

Close and Reynolds ^[9] developed methods of determining pay in laminated sands due to the presence of low-resistivity shale layers within laminated shale-sand sequences. These processes utilize high-resolution resistivity data from imaging tools, such as Formation Micro-Imager (FMI), or directional resistivity data from tri-axial of hi-resolution resistivity, to more accurately represent the bulk properties of a sequence and identify pay by assessing the sand component independently of the shale laminations.

Claverie et al. ^[10] showed that the flow profile of highly laminated reservoir can be predicted by single well model. This single well model have to build at the resolution of the open hole log. The NMR Thin Bed Fraction and borehole image sand count provide insight on the flow capacities of the thin beds.

Daungkaew et al. ^[11] presented an integrated and structured approach for calculating the productivity of a laminated clastic reservoir. A single well predictive model incorporates logs, rock and PVT data, and formation tests to build a flow simulation model at the resolution of the petrophysical analysis. By calibrating the high resolution flow model with dynamic test data from a formation tester Interval Pressure Transient Test (IPTT), the model can be used to predict the well performance.

Daungkaew et al. ^[12] illustrated the wide range of information that can be obtained from WFT data using an advanced well test analysis technique using field examples from the Asia Pacific Region. A single well model numerical simulation for a wireline formation tester deploying a single probe was used to verify the PTA

results presented. An analytical solution in well test analysis software was also used to generate pressure transient response to confirm results from actual field examples.

CHAPTER III

THEORY AND CONCEPT

This chapter presents the fundamental of petrophysical interpretation, wireline formation tester, well test interpretation and determination of rock type using Flow Zone Indicator (FZI) method.

3.1 Petrophysical Interpretation

Petrophysical interpretation is a fundamental role in all exploration and production analysis. Well log data can be used to perform physical property feasibility studies for the area of interest. This physical property framework is used to drive forward to implement reservoir model, to design new acquisition programs, to design production strategy, to assess the feasibility of using various reservoir conditions, and ultimately to improve our understanding of the subsurface. Usually petrophysical interpretation is used to derive porosity, water saturation and permeability based on availability of well log data. This thesis focuses on hi-resolution logs such as NMR and Borehole Electrical Image Log which can help us better evaluate potential reservoir rock in thinly bedded sandstone.

3.1.1 Nuclear Magnetic Resonance Log (NMR)

The NMR offers the potential to measure several important reservoir parameters not measured by conventional logs. Many companies have started to use this measurement as an innovative way to cut coring and well testing costs. Many applications of NMR log available nowadays are listed as follows:

- Porosity and permeability measurements will help make decisions, decrease coring and testing costs, and optimize completion and fracture programs.

- Estimating producible porosity and irreducible water saturation will reduce and/or eliminate water production, maximize hydrocarbon production and improve reserve calculations.
- Possible pay zone identification in areas where standard logs are difficult to interpret.
- Identification of thin permeability streaks in laminated reservoirs.

The fundamental of Nuclear Magnetic Resonance (NMR) logging tool measures density of hydrogen protons in the reservoir fluids either water or hydrocarbon. This tool generates large magnetic field to formation that makes hydrogen protons behave like spinning bar magnet. During changes of magnetic field, they are rotated and spun, producing measurable signals. The received signal consists of a sequence of spin-echo amplitudes that are recorded over a period of time, typically in the range of 0.2 s to 2.0 s. Figure 3.1 shows a spin echo produced by transmitter pulse, and the amplitude of the spin echo is recorded by the tool.

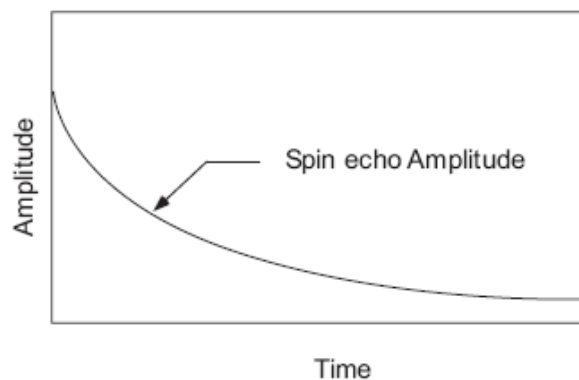


Figure 3.1: Example of spin echo record by the tool.

The volume of rock measured by an NMR logging tool actually contains millions of pores, each pore has different spin echo decay constant. The set of all spin echo decay constants forms the spin echo decay spectrum. Through the mathematical process of inversion, the spin echo decay data can be converted to a T2 distribution. The conversion of set of spin echo decay to T2 distribution is shown in Figure 3.2.

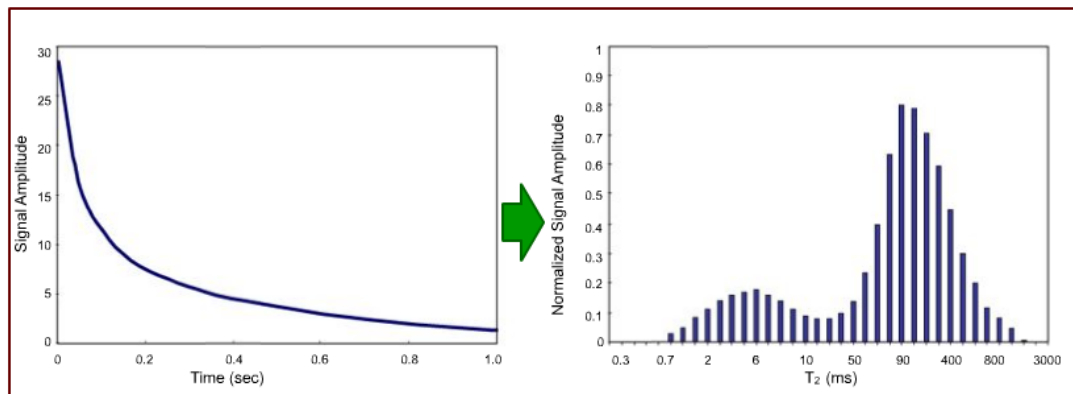


Figure 3.2: Example of T2 distribution obtained from NMR measurement.

Figure 3.3 shows a best fit curve on the T2 components to provide a continuous T2 distribution. The T2 distribution is the basis for all NMR curves. It is always presented on a logarithmic scale. The area under the T2 distribution is equivalent to the sum of all initial amplitudes of the pores in the formation. Therefore, it is proportional to formation porosity.

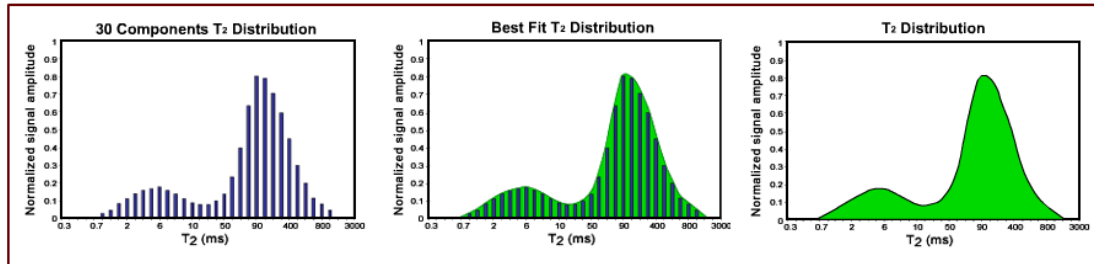


Figure 3.3: Example of how to fit curve to T2 distribution obtained from NMR.

In porous media, T2 has been shown to be proportional to pore size. That is, small pores have short T2 values and large pores have long T2 values as shown in Figure 3.4. An attractive feature of NMR logging is that the borehole measurement can be duplicated in the lab on core samples. The correlation between NMR measurements and petrophysical properties are derived from lab experiments. Lab measurements on water-saturated core samples have shown that T2 cutoff values of 30 ms and 100 ms are appropriate for sandstones and carbonates, respectively. These cutoff values resulted in free-fluid porosities that best are matched with the volumes of water produced from the core samples.

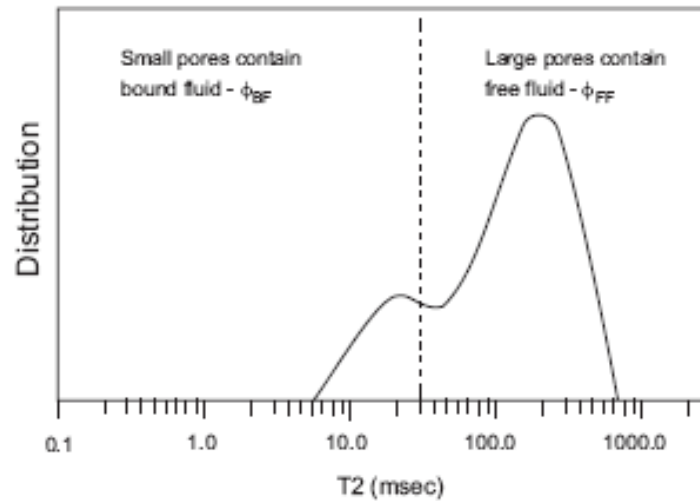


Figure 3.4: Bound and free-fluid porosity is computed using a T2 cutoff.

The NMR estimate of permeability is similarly based on an expectation that permeability will increase with both porosity and pore size. NMR and permeability measurements on water-saturated sandstone samples have shown that permeability can be estimated by:

$$k_{NMR} = a (\phi_{NMR})^4 (T_{2,log})^2 \quad (3.1)$$

where

k_{NMR}	=	estimated permeability, mD
ϕ_{NMR}	=	NMR porosity
$T_{2,log}$	=	logarithmic mean of the T2 distribution
a	=	default value of 4

3.1.2 Borehole Electrical Imaging Log

Borehole Electrical Imaging Log is a new generation of formation imager performing measurement to provide a quality borehole image which has been developed to work in both water based mud and oil based mud systems. The images are sufficiently detailed to give useful structural and stratigraphic information in many geological settings. In the image that the sensors show, darker colored zones are relatively electrically conductive while brighter zones or features are relatively

electrically resistive. Also, some type of borehole electrical imaging can provide a quantitative measurement of invaded zone resistivity from each pair of sensors.

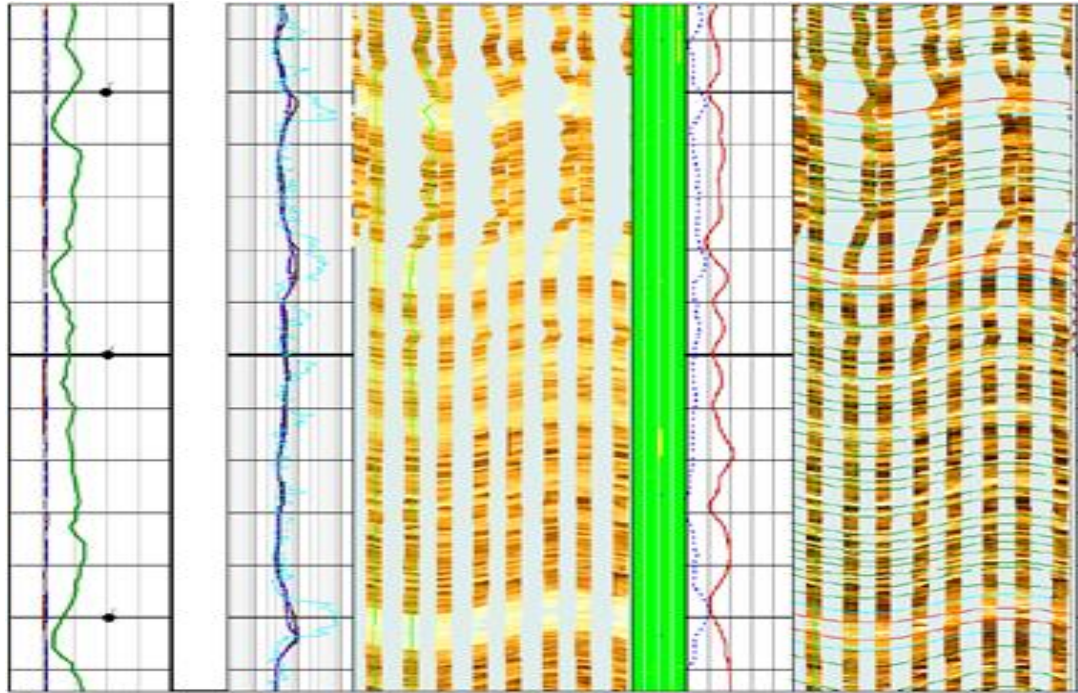


Figure 3.5: Example of borehole electrical imaging log^[15].

Figure 3.5 shows the example of borehole electrical imaging log and other openhole logs contained in seven tracks. Only the third, fourth, fifth and seventh tracks are borehole electrical imaging data. The third track contains openhole resistivity and synthetic resistivity (SRES) from borehole image log. SRES can provide better vertical resolution than openhole resistivity log. The tool vertical resolution is stated as 1.2 in. (3 cm). This means the thinnest bed for which the width can be measured is 1.2 in. A bed with a width less than 1.2 in., or even 0.4 in., can be detected if the resistivity contrast relative to the background rock is strong. However, its apparent width (thickness) could be misleading. The accuracy also depends on the logging speed of the tool as well.

Primary application of borehole images is evaluation of possible quality reservoir rock from the additional post-processing after logging is done from the field. The electrical image processing can help resolve problems that are impossible to resolve with conventional logging tools such as small fractures, vugs, bedding planes, depositional features, thin beds and rock texture. All of these features can have

significant influence on field exploration and development phases. In thinly laminated reservoirs, borehole imaging logs also are often used for net pay determination and rock facies identification which help to indicate additional reserves if these sand laminations are of good porosity and permeability.

Combination of borehole imaging logs and other wireline logs can provide improvement to interpretation of petrophysical properties significantly. One of the first applications of image logs was to help evaluate fluid saturations in thinly laminated reservoirs by using higher resistivity contrast between zones containing two fluid types and higher vertical resolution to integrate all available logs to interpret the potential reservoir for fluid flow qualitatively, is shown in Figure 3.6. the first and second tracks are gamma ray and neutron-density porosities respectively; the third track is bed thickness computed from borehole image log; the fourth and sixth are borehole image log; the seventh is computed SRES (red curve) and squared SRES (blue curve), and the last track is the rock facies computed from the integration of wireline conventional logs and borehole image log.

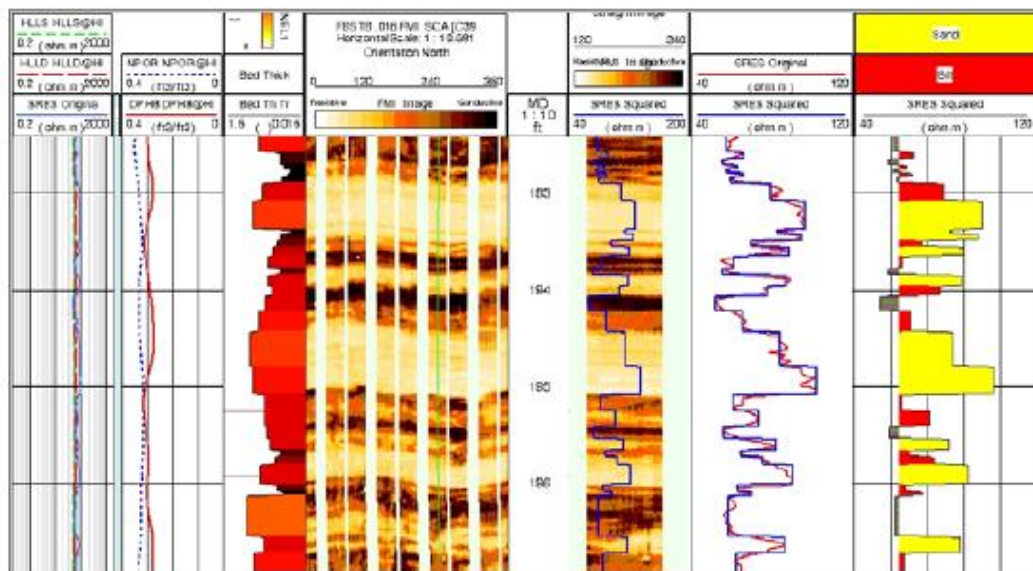


Figure 3.6: Integration of borehole electrical imaging log with other wireline logs to improve interpretation result ^[15].

3.2 Wireline Formation Tester

Wireline Formation Tester (WFT) is used to measure formation pressure with the aim of identifying fluid gradients, fluid contacts, formation mobility, formation permeability (if viscosity data available), and formation effects such as supercharging or fluid density changes along certain depth interval. Although WFT tools provide valuable information in the evaluation of reservoirs, they only provide pressure data at discrete points along the wellbore. Analysis of the recorded pressures is useful for determining reservoir fluid types and for locating the free water level. When an adequate number of pressure tests are performed and stratigraphic units are relatively thick and undisturbed by prior depletion, reservoir fluid types may be determined by constructing a plot of formation pressure versus true vertical depth (TVD) and analyzing the pressure gradients. While the pressure gradient alone may be enough to identify the reservoir fluid, the reservoir fluid density may also be obtained.

In addition, because a continuous log of pressure versus time is recorded, analysis of pressure drawdown and/or pressure buildup is useful for determining near-wellbore formation mobility. WFT tools may also be utilized to obtain reservoir fluid samples and retrieve them to the surface for further laboratory analysis. These fluid samples are routinely sent to a fluid laboratory to determine the PVT properties of the reservoir fluid and for compositional analysis.

The operation practice of recording pressure versus time is shown in Figure 3.7. When the probe from the WFT tool is seated against the formation and a seal is created (1), a pretest piston is withdrawn to a known volume, creating a pressure drop between the WFT tool and the formation (2). The test continues with a buildup period (3). This process is repeated to withdraw fluid by using pump out module from the tool to minimize the effect of fluid invasion while drilling and ensure pressure reading come from the actual formation response (4). The tool stops pumping out and let the pressure build up again until pressure in the tool reaches the formation pressure (5). The pressure test is terminated when the probe is retracted, breaking the seal between the WFT tool and the formation.

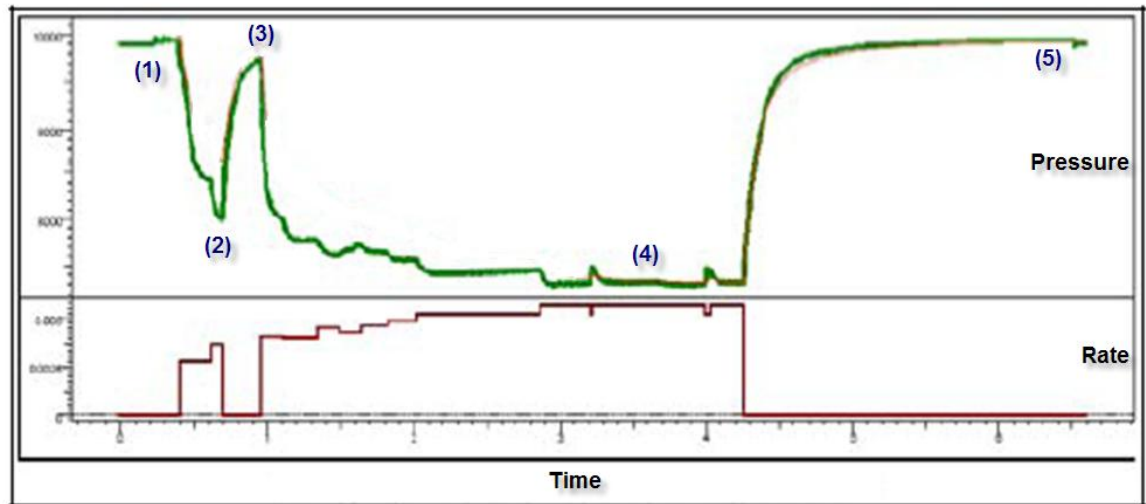


Figure 3.7: Pressure response of Wireline Formation Tester (WFT)^[26].

One type of the wireline formation tester used in this study is dual packers which has the capability of hydraulically isolating a minimum of one meter of formation. The dual packer WFT provides two inflatable packer elements which seal off a meter section of the borehole (can be extended to 13 feet). The elements are inflated with wellbore fluid or with water carried down-hole in a sample chamber. The whole packed off section of borehole wall is open to the formation so that the fluid flow area is several thousand times larger than with the conventional probes. This allows pressure measurements and fluid sampling in laminated, shaly, fractured, vuggy, unconsolidated, or low permeability formations where the probes usually cannot operate. For pressure measurement, enough fluid needs to be removed from the interval to lower pressure below the formation pressure. The dual packers can be set repeatedly at different locations on a single trip in the well. Using these, pressures, real-time formation fluid identification, PVT samples, permeability, and flow rate can all be evaluated in details. In difficult conditions where the single probe wireline formation tester usually cannot operate (i.e., fractured limestone, very low permeability formations, and thin and laminated formations), the dual packers WFT allows pressure measurements, sampling, and formation fluid identification. These applications of the WFT are possible due to the increased area sealed by the packers creating a flow area of 679 in², compared to only 0.1521 in² in a conventional single probe. Dual packers WFT have been applied successfully to many cases such as a

fractured carbonate reservoir, a thinly-bedded reservoir and a formation with very low permeability. There are several available options for wireline formation tester modules that can be added to the basic tool to substantially increase its capabilities as shown in Figure 3.8.

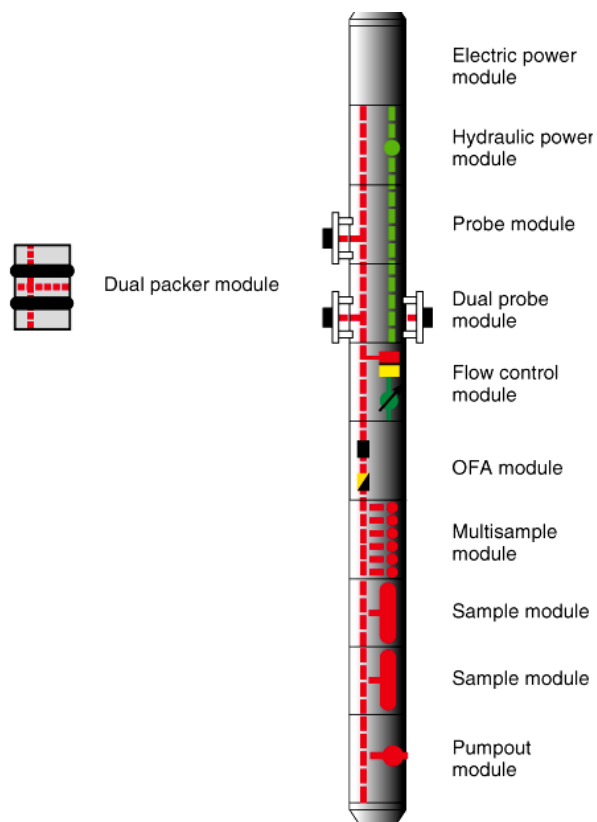


Figure 3.8: Wireline Formation Tester with optional modules ^[21].

3.3 Welltest Interpretation

A well test is a measurement of pressure as a function of time under controlled conditions. While the well is flowing, the quality of data is often poor thus the data during a build up period are usually analyzed. In this study, the principle of well test analysis technique is applied to wireline formation tester data to obtain reservoir information. Build up test sequence as shown in Figure 3.9 is used in most cases and also in this study. The flow rate is usually measured at surface while the pressure is recorded downhole. Before opening the well, the initial pressure is constant and uniform in the reservoir. The drawdown pressure response is recorded during flow

period. When the well is shut in, the build up pressure change is estimated from the last flowing pressure $p(\Delta t=0)$. Then, pressure response is analyzed versus the elapsed time Δt since the start of the period (time of opening or shut-in).

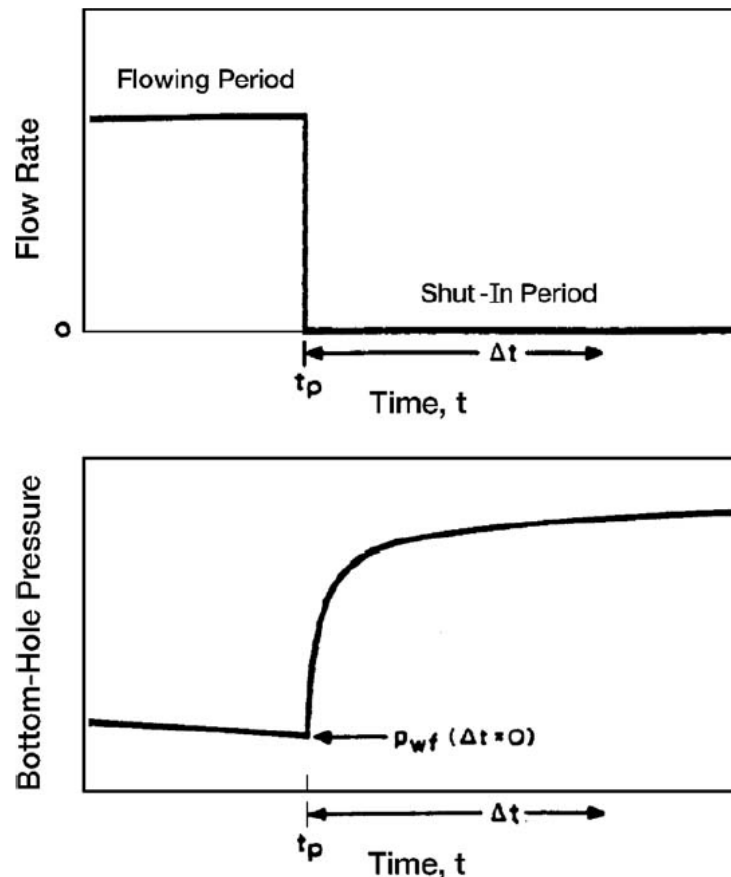


Figure 3.9: Build-up test sequence^[26]

Figure 3.10 shows derivative plot of the pressure response which basically reveals three flow regions: early, middle, and late time. The early time represents wellbore and near wellbore responses such as effects of damage, acidizing, or hydraulic fracture. It is often associated with a (log-log) straight line of fixed slope. A slope equal to “one” means “wellbore storage,” and during that period, nothing can be determined from the reservoir because there is still wellbore response. The middle time represents spherical flow (a negative half slope) and radial flow (a slope of zero). When radial flow is reached, the permeability can be determined. The permeability is calculated from the slope of the semi-log straight line, or the vertical location of the flat portion of the derivative. These two answers should be the same. The late time reflects the effect of the reservoir boundaries and heterogeneities. It is from this

region that the reservoir shape can be determined. However, wireline formation tester rarely sees such pressure response.

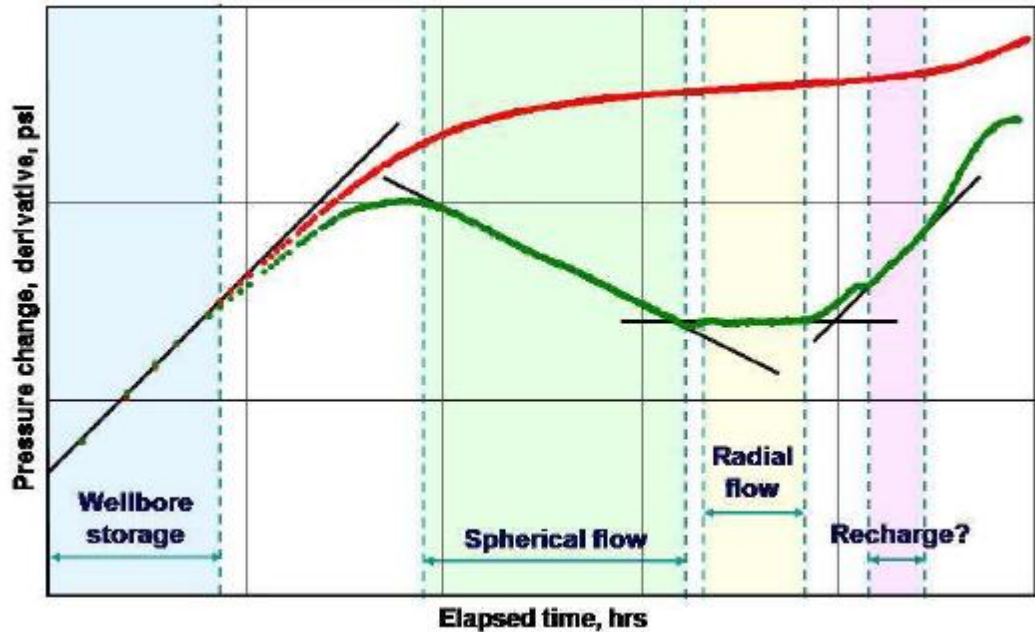


Figure 3.10: Example of pressure derivative.

The interpretation of horizontal permeability is based on build up following a single drawdown. So, the Horner plot is used for calculating permeability from the straight line slope in the Infinite Acting Radial Flow (IARF) regime.

Pressure drop equation during IARF

$$\Delta p = 162.6 \frac{qB\mu}{kh} \left[\log \left(\frac{t_p \Delta t}{t_p + \Delta t} \right) + \log \left(\frac{k}{\phi \mu C_t r_w^2} \right) - 3.23 + 0.87S \right] \quad (3.2)$$

The permeability-thickness product can be determined from the slope of IARF straight line in Horner plot as follows:

$$kh = 162.6 \frac{q\mu B}{m} \quad (3.3)$$

where

k	=	permeability, mD
h	=	formation thickness, ft

q	=	flowrate, STB/day
μ	=	viscosity, cp
B	=	Formation Volume Factor, RB/STB
m	=	slope of IARF straight line in the Horner plot
s	=	skin
ϕ	=	porosity
r_w	=	wellbore radius, ft
c_t	=	total compressibility, psi^{-1}

3.4 Rock Typing using Flow Zone Indicator (FZI) Method

Oil and gas field development plans are usually dependent on static and dynamic models to estimate the hydrocarbon reserves and production prediction. Rock type is one of the essential steps needed in building the models by defining unit of rock that has a unique porosity-permeability relationship and capillary pressure profile. There are many different approaches used in the industry to determine the rock types, such as Pittman, Windland, Lucia, Flow Unit Indicator (FZI), cumulative distribution function, etc. However, this thesis will focus on the FZI method.

The FZI method was developed and based on the Kozeny-Carman permeability equation. The derivation of the FZI equations are based on the assumption that porous medium can be represented by a bundle of capillary tubes. The set of data is gathered in a single group of data and the corresponding parameters Reservoir Quality Index (RQI) and FZI are calculated, using the following relationships:

$$RQI = 0.0314 * \sqrt{\frac{k}{\phi}} \quad (3.4)$$

$$\phi_z = \frac{\phi}{1 - \phi} \quad (3.5)$$

$$FZI = RQI * \phi_z \quad (3.6)$$

$$\log(RQI) = \log(\phi_z) + \log(FZI) \quad (3.7)$$

where

RQI	=	Reservoir Quality Index
FZI	=	Flow Zone Indicator
k	=	Permeability
\emptyset	=	Porosity
\emptyset_z	=	Normalize Porosity Index or pore volume to grain volume ratio

The numbers of possible rock types are determined by looking at the histogram of log (FZI) as shown in Figure 3.11 or Normal Probability Plot of log (FZI) as shown in Figure 3.12.

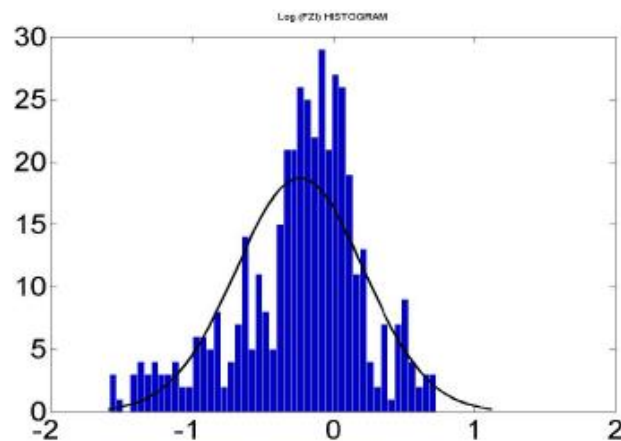


Figure 3.11: Histogram plot of log(FZI) to determine possible numbers of rock types or HFUs.

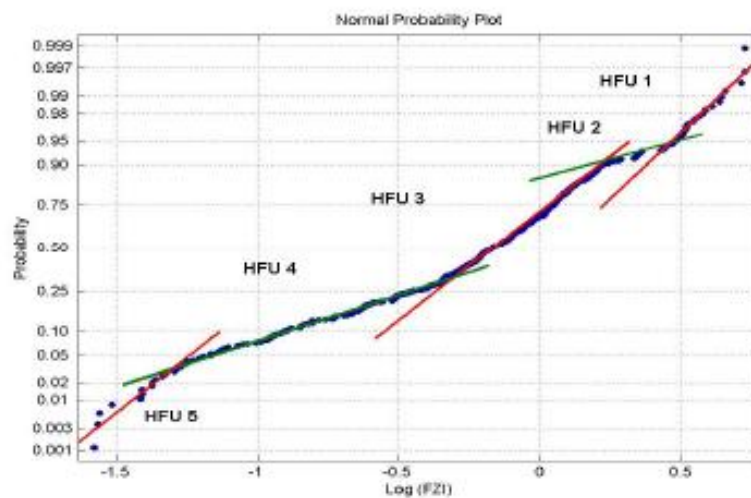


Figure 3.12: Normal probability Plot of log(FZI) to determine possible numbers of rock types or HFUs.

The technique attempts to automatically define hydraulic flow units based on “storage capacity” and “flow capacity” (porosity and permeability), and then automatically group the hydraulic flow units into similar rock types. The methodology adopted is based on the Stratigraphic Modified Lorenz Plot (SMLP) technique described in a paper by Gunter et al ^[19]. This is a graphical technique which SMLP displays cumulative porosity-thickness versus cumulative permeability. Therefore, on the SMLP, straight-line segments represent flow units while inflection points represent flow unit boundaries. Flow units have been identified by boundary strength curve if it exceeds cutoff value of boundary strength threshold. As a result, straight-line segment slope allows grouping into each rock type as shown in Figure 3.13.

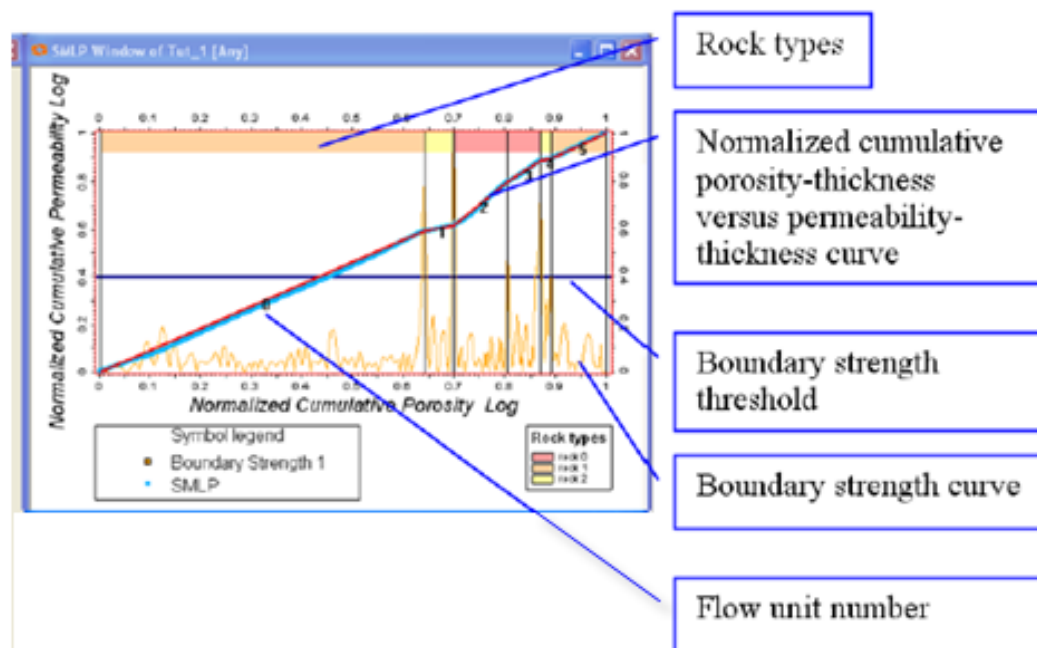


Figure 3.13: Stratigraphic Modified Lorenz Plot (SMLP) to determine possible numbers of rock types or HFUs.

In order to visualize the rock typing or hydraulic flow unit (HFU) result in graphical format, Equation 3.7 is used to display rock typing using FZI method as shown in Figure 3.14. The data can be plotted in log-log plot of RQI vs ϕ_z . The relationship between actual permeability and permeability calculated from FZI for each rock type or hydraulic flow unit is also shown in Figure 3.15.

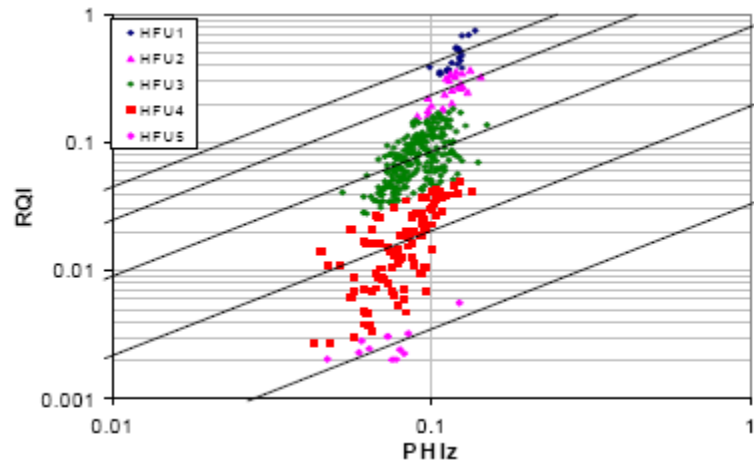


Figure 3.14: Example of $\log(\phi_z)$ vs $\log(\text{RQI})$ plot.

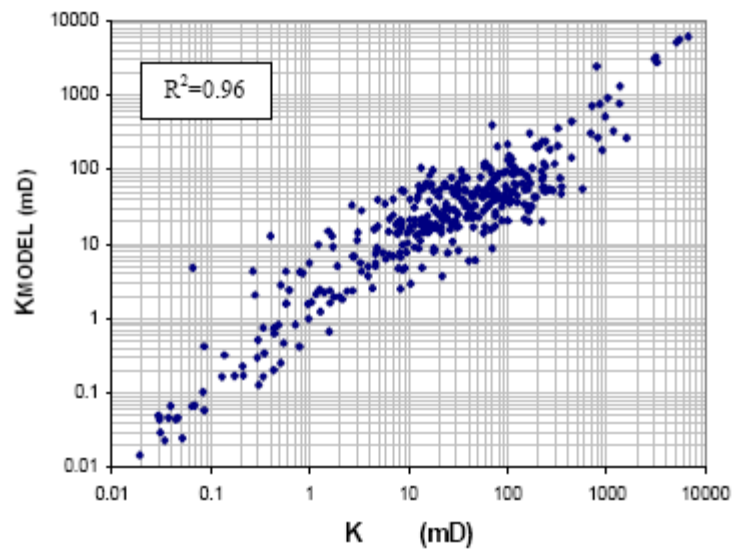


Figure 3.15: Relationship between actual permeability and permeability calculated from FZI for each rock type or hydraulic flow unit.

CHAPTER IV

METHODOLOGY

This study aims to implement a systematic workflow for the use of borehole image log for permeability estimation by using calibrated SRES as permeability from borehole electrical image log instead of permeability derived from NMR logging tool. It is a challenge to perform a numerical experiment using SRES as the permeability input to single well model. The methodology to generate single well models; one from permeability derived from NMR and another one from SRES from borehole image electrical image is described as follows:

4.1 Preparation of Rock and Fluid Properties Data

For the well used in this study, rock properties are depicted in Table 4.1. All three intervals that pressure transient tests were conducted are assumed to contain dead oil having the same fluid properties as shown in Table 4.2. Details of reservoir parameters are shown in Table 4.3. Wireline logs and interval pressure transient tests (IPTT) are depicted in Figure 4.1.

Table 4.1: Rock properties were input to both single well models.

Rock properties	Single Well Model NMR	Single Well Model Borehole Electrical Image
Porosity	Porosity log	Porosity log
Permeability	NMR permeability log	Synthetic resistivity log

Table 4.2: PVT data.

	B_o	μ_o
Pressure (psia)	FVF (rb/stb)	Viscosity (cp)
1764.70	1.3121	0.35996
1814.70	1.3209	0.35512
1864.70	1.3298	0.35045
1914.70	1.3388	0.34593
1964.70	1.3479	0.34156
2014.70	1.3570	0.33734
2064.70	1.3662	0.33325
2114.70	1.3755	0.32929
2164.70	1.3849	0.32544
2214.70	1.3943	0.32172
2264.70	1.4039	0.31810
2314.70	1.4117	0.31535
2364.70	1.4101	0.31679
2414.70	1.4086	0.31827
2464.70	1.4072	0.31978
2514.70	1.4058	0.32132
2564.70	1.4044	0.32290
2614.70	1.4032	0.32451
2664.70	1.4019	0.32615
2714.70	1.4007	0.32782
2764.70	1.3996	0.32953
2814.70	1.3985	0.33126
2864.70	1.3974	0.33303
2914.70	1.3964	0.33483
2964.70	1.3954	0.33665
3014.70	1.3945	0.33851

Table 4.3: Reservoir parameters for all zones of interest.

Reservoir Model of IPTT#1		
Boundary	No flow	
Reservoir radius	2839	feet
Datum depth	5384.498	feet
Pressure @ datum depth	2767.11	psia
Top of reservoir depth	5375.9	feet
Thickness	10.00005	feet
Packer interval	5382.53-5385.81	feet
Wellbore ID	0.2159	feet
Horizontal permeability, k_h	116	mD
k_v/k_h	0.25	

Reservoir Model of IPTT#2		
Boundary	No flow	
Reservoir radius	2839	feet
Datum depth	5201.1	feet
Pressure @ datum depth	2722.9	psia
Top of reservoir depth	5180.83	feet
Thickness	29.62589	feet
Packer interval	5199.31 - 5202.41	feet
Wellbore ID	0.2159	feet
Horizontal permeability, k_h	193	mD
k_v/k_h	0.94	

Reservoir Model of IPTT#3		
Boundary	No flow	
Reservoir radius	2839	feet
Datum depth	5036.074	feet
Pressure @ datum depth	2530.8	psia
Top of reservoir depth	5034.36	feet
Thickness	3.28	feet
Packer interval	5034.434-5037.714	feet
Wellbore ID	0.2159	feet
Horizontal permeability, k_h	29.5	mD
k_v/k_h	0.512	

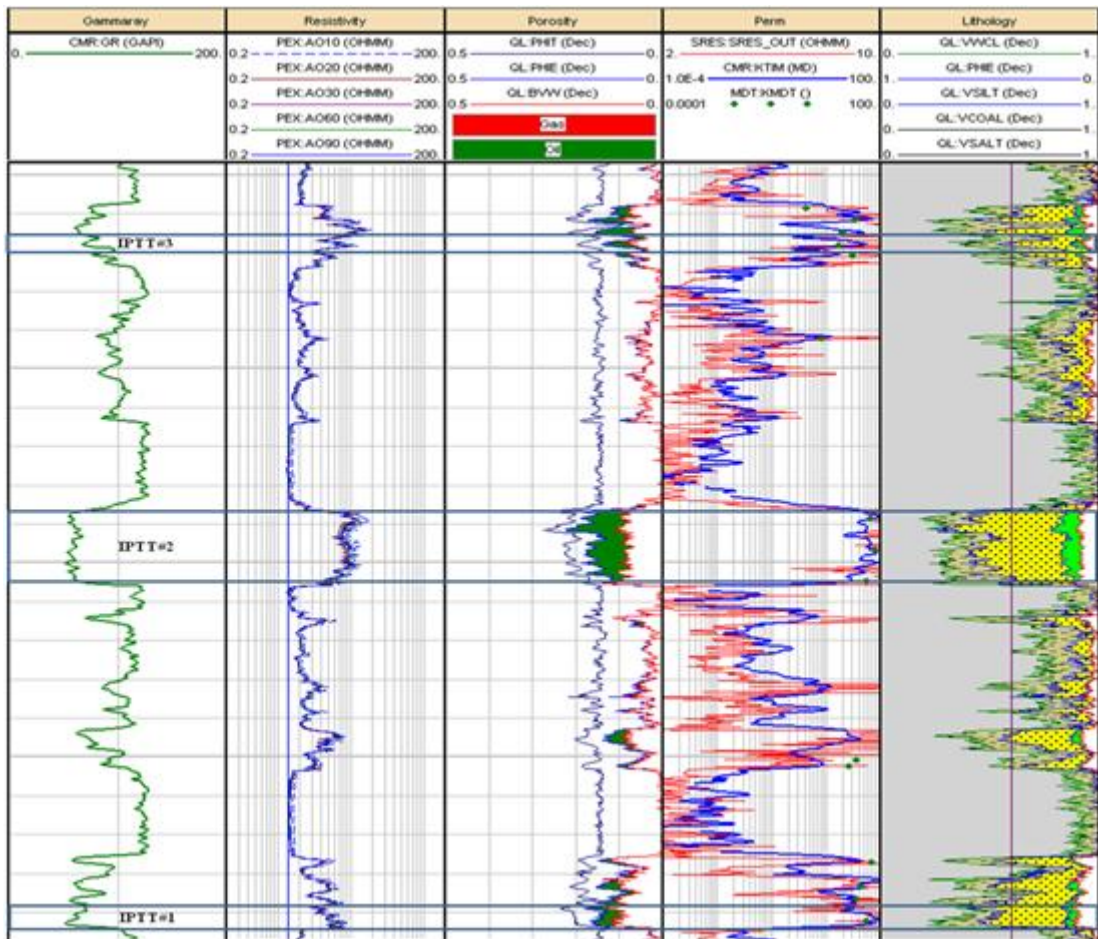


Figure 4.1: Wireline log data and Interval Pressure Transient Tests (IPTT).

4.2 Generation of 3D Static Single Well Model

The values of petrophysical data from actual measurement were input to the single well model by using SWPM (Single Well Predictive Model) in order to identify rock type, populate rock properties, fluid properties, SCAL, etc to the single well model. Thinly bedded laminated feature is simulated by assigning porosity and permeability to be homogeneous in each layer and heterogeneous in the vertical direction. Initial reservoir conditions and numerical grid specifications of both single well models are defined based on field data.

To identify rock types or hydraulic flow units, Stratigraphic Modified Lorenz Plot Analysis (SMLP) technique was performed in order to analyze cumulative porosity-thickness versus cumulative permeability. In Figure 4.2, there are five peaks of boundary strength curve which are over the boundary strength threshold.

Therefore, flow unit have been identified by boundary strength curve if it exceeds threshold value of boundary strength threshold. As the result, straight line segment slope allows grouping into five rock types.

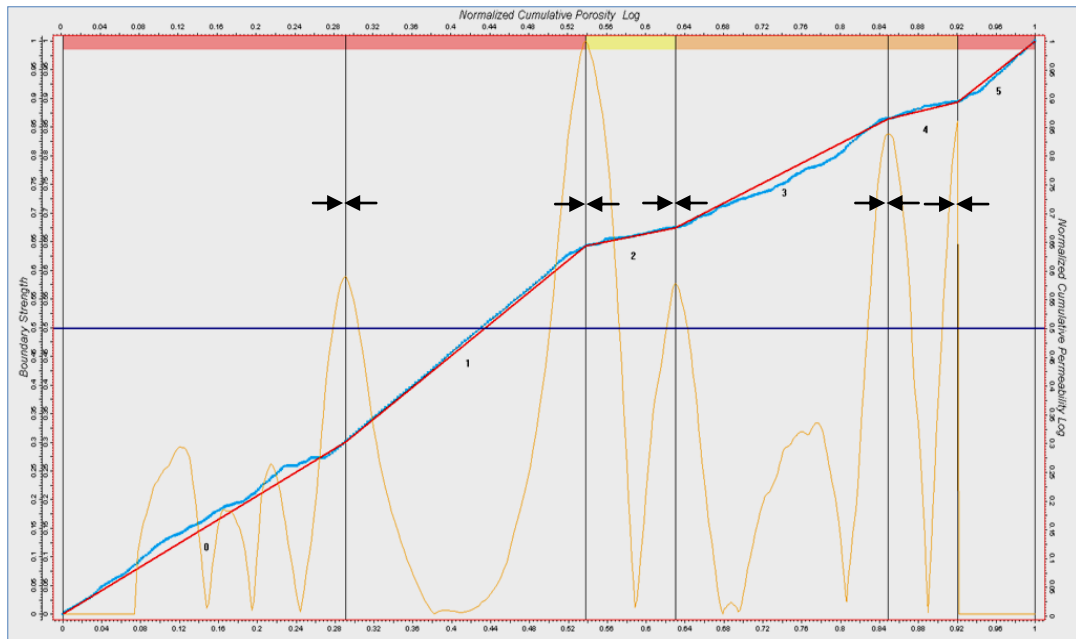


Figure 4.2: Stratigraphic Modified Lorenz Plot showing that there are 5 rock types.

According to rock type analysis, results were generated by using Stratigraphic Modified Lorenz Plot Analysis (SMLP) technique as illustrated in Figure 4.3. The porosity-permeability relationship for each rock type of single well model using permeability derived from NMR and single well model using SRES as permeability from borehole electrical image are shown in APPENDIX A.

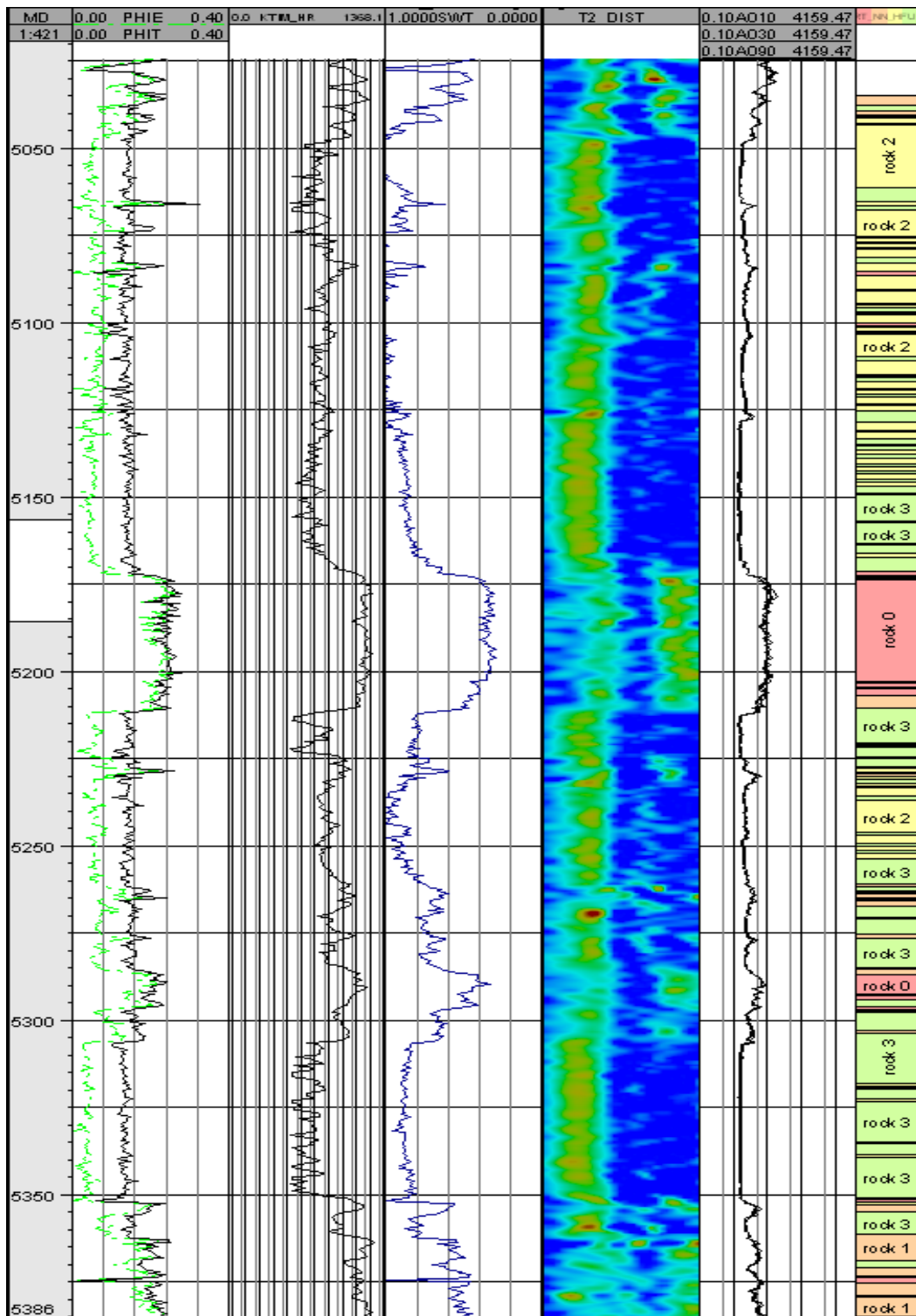


Figure 4.3: Log data representing wireline logs and rock types covering all intervals of the demonstrate well.

As there are 5 Hydraulic Flow Units (HFU) in this well, five oil and water relative permeability curves are needed. These curves are shown in Figures 4.4, 4.5, 4.6, 4.7 and 4.8. For all flow units, capillary pressure is assumed to be zero. After all information was populated to each layers. Thinly laminated single well model is generated from SWPM as illustrated in Figure 4.9.

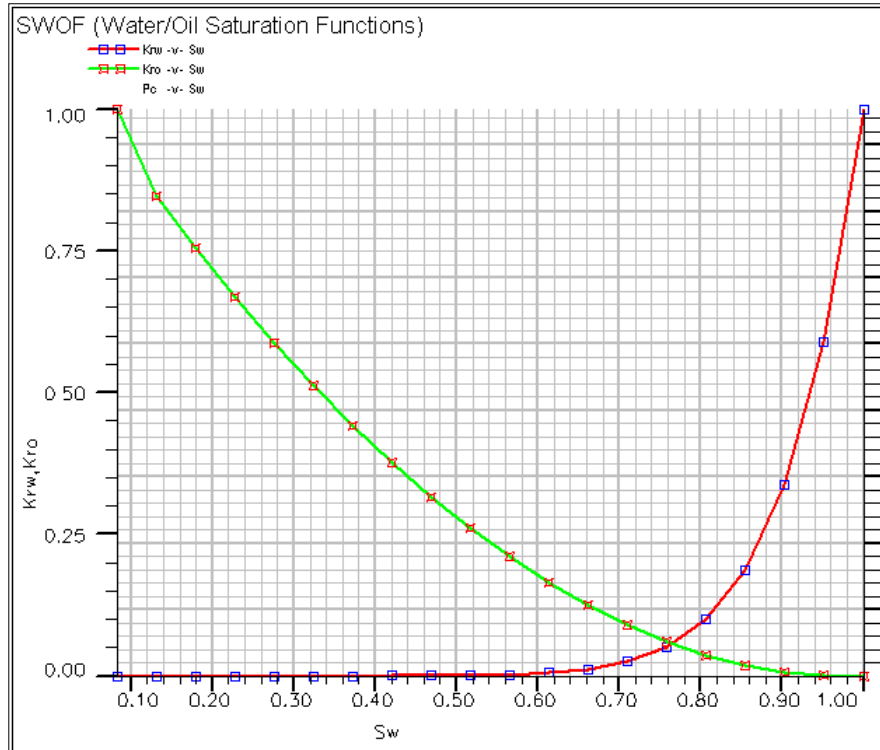


Figure 4.4: Oil and water relative permeability curves at different water saturations for HFU#1. Initially, the water saturation is 0.1306 and the oil relative permeability is 0.8456.

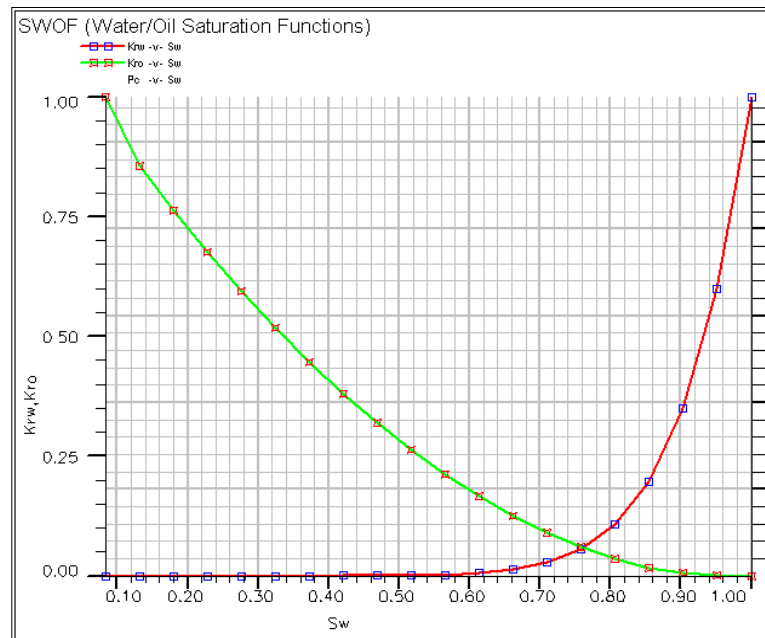


Figure 4.5: Oil and water relative permeability curves at different water saturations for HFU#2. Initially, the water saturation is 0.1312 and the oil relative permeability is 0.8549.

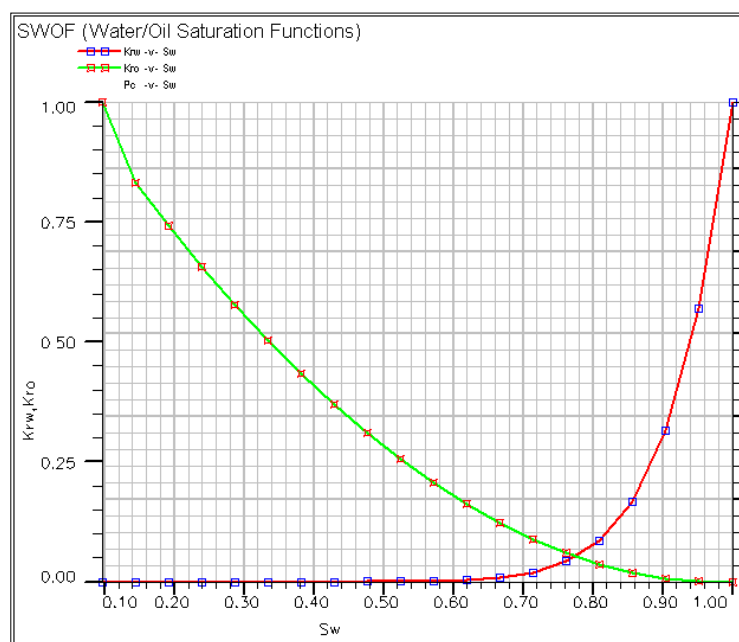


Figure 4.6: Oil and water relative permeability curves at different water saturations for HFU#3. Initially, the water saturation is 0.1437 and the oil relative permeability is 0.8307.

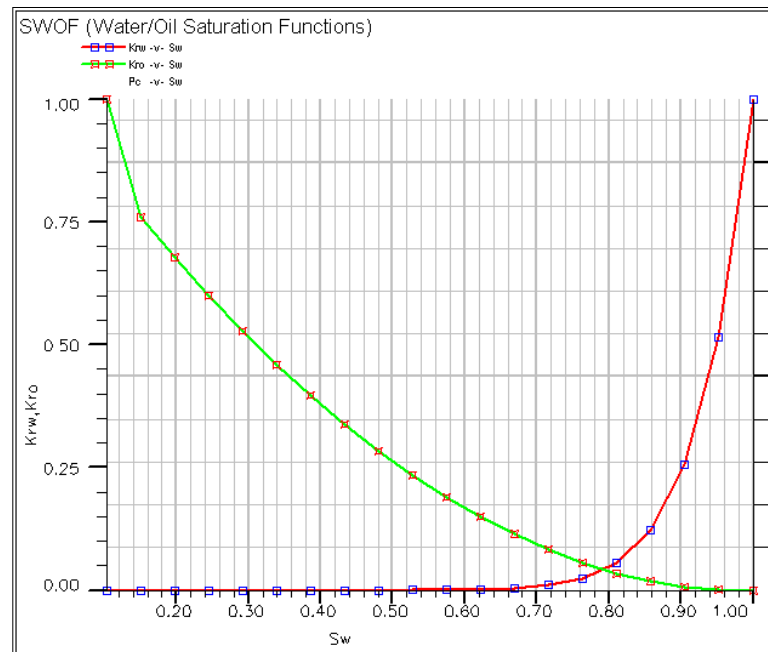


Figure 4.7: Oil and water relative permeability curves at different water saturations for HFU#4. Initially, the water saturation is 0.1499 and the oil relative permeability is 0.7586.

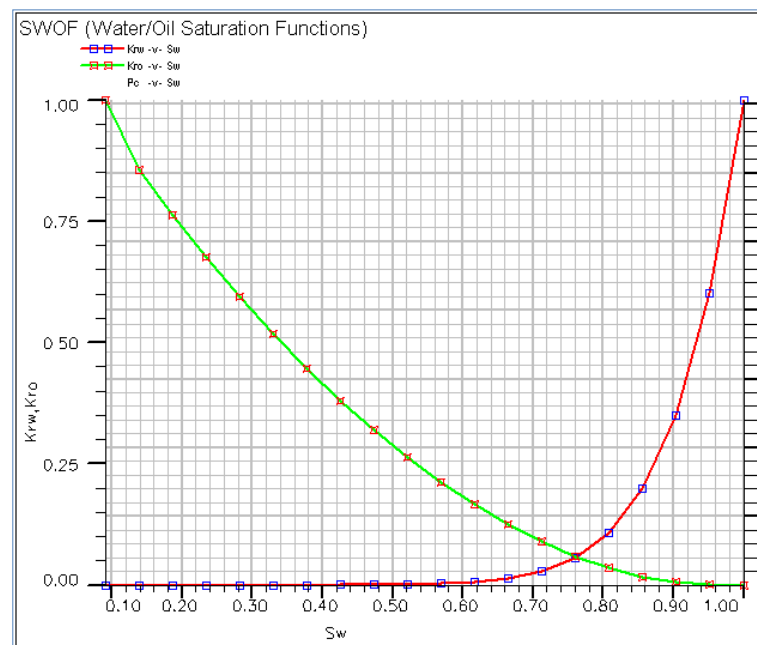


Figure 4.8: Oil and water relative permeability curves at different water saturations for HFU#5. Initially, the water saturation is 0.1382 and the oil relative permeability is 0.8547.

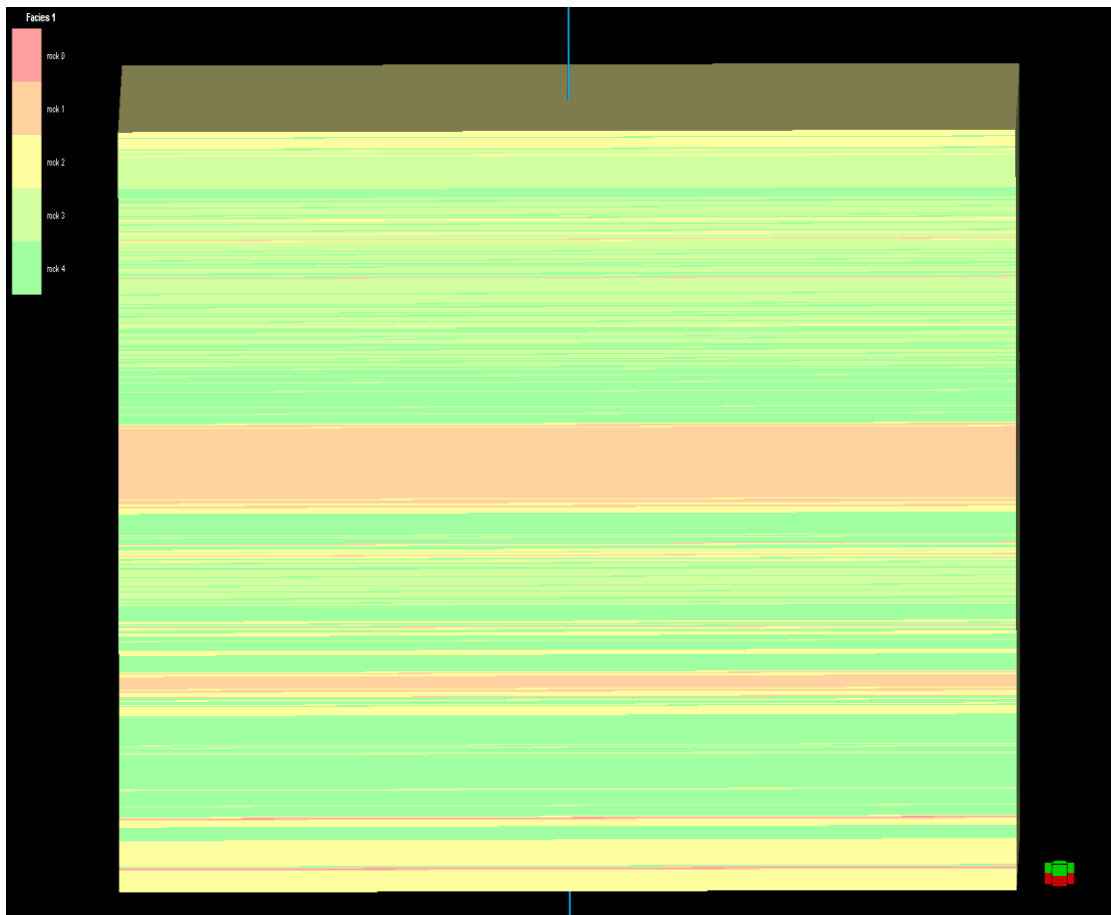


Figure 4.9: Thinly laminated single well model is generated from SWPM.

4.3 Grid Conversion

SWPM is a tool to create static models in order to populate all rock and fluid properties from available petrophysical data to export the static models to ECLIPSE for simulation purpose. Single well model which is exported from SWPM is under Cartesian grid format. It needs to be converted to radial grid format manually in order to perform well testing simulation. The single well model is based on a circular boundary, radial grid model with the dimension of 50 x 8 grid blocks in the r and θ direction, respectively. Thickness (dz) varies on a case by case basis. The thickness of each single well model was based on identification of flow units and rock types derived from permeability and porosity logs using Neutral Net Analysis or Stratigraphic Modified Lorenz Plot algorithm. The size of grid blocks in the r -

direction increases logarithmically from a small grid at the wellbore toward the reservoir boundary. The fluid flow area was calculated from the flow area of Dual Packer WFT which is flowing around wellbore for 3.28 ft open interval.

Table 4.4 shows the grid cell dimension in the r and θ direction for the single well model. The grid block in z direction is based on acquisitions of NMR or Borehole Electrical Image and thickness of each zone of interest as shown in Table 4.5. The connection between the wellbore and the reservoir is represented by grid cell (1,1-8) which is the packer interval of each zone of interest. Figure 4.10 shows the conversion of Cartesian grids single well model into radial grids single well model.

Table 4.4: Radial and Theta direction of Dual Packer WFT grid.

Radial direction (ft)								Theta direction	
n	Δr	n	Δr	n	Δr	n	Δr	n	$\Delta \theta$
1	0.03227	14	2.14247	27	105.713	40	105.713	1	45
2	0.05877	15	2.89109	28	105.713	41	105.713	2	45
3	0.07931	16	3.90128	29	105.713	42	105.713	3	45
4	0.10702	17	5.26446	30	105.713	43	105.713	4	45
5	0.14441	18	7.10396	31	105.713	44	105.713	5	45
6	0.19487	19	9.58621	32	105.713	45	105.713	6	45
7	0.26296	20	12.9358	33	105.713	46	105.713	7	45
8	0.35484	21	17.4633	34	105.713	47	105.713	8	45
9	0.47883	22	23.5755	35	105.713	48	105.713	Σ	360
10	0.64614	23	31.8269	36	105.713	49	105.713		
11	0.87192	24	42.9663	37	105.713	50	105.713		
12	1.17658	25	58.0046	38	105.713	Σ	2839.08		
13	1.5877	26	78.3062	39	105.713				

Table 4.5: Thickness direction of Dual Packer WFT grid for both NMR based method and Borehole Electrical Image based method.

Single Well Model - NMR based method			
Station	Layer size (ft)	Number of layers	Total thickness (ft)
IPTT#1	0.5000	20	10.0005
IPTT#2	0.5021	59	29.6121
IPTT#3	0.4690	7	3.28

Single Well Model - Borehole Electrical Image based method			
Station	Layer size (ft)	Number of layers	Total thickness (ft)
IPTT#1	0.1695	59	10.0005
IPTT#2	0.1673	177	29.6121
IPTT#3	0.1640	20	3.28

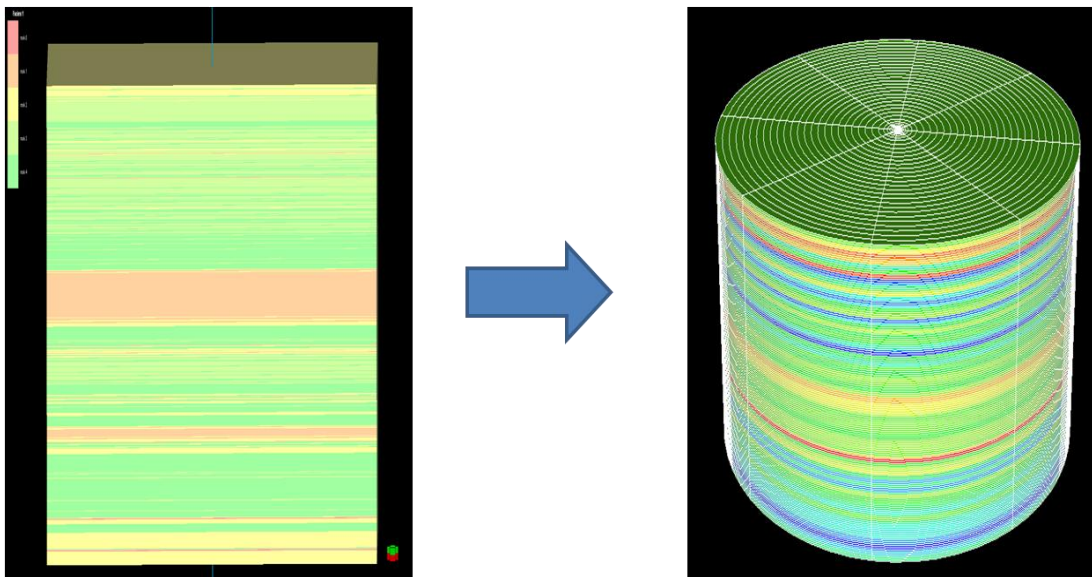


Figure 4.10: Cartesian grids single well model is converted manually to radial grids single well model.

Figures 4.11, 4.12 and 4.13 show grid configurations of three zones of interest to represent laminated reservoirs used in this study.

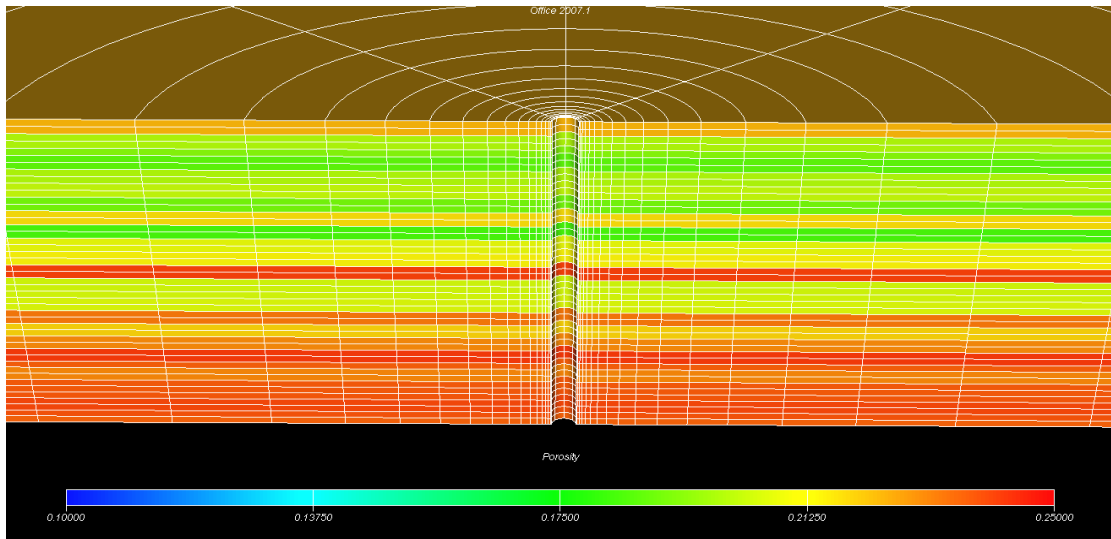


Figure 4.11: Reservoir model for IPTT#1.

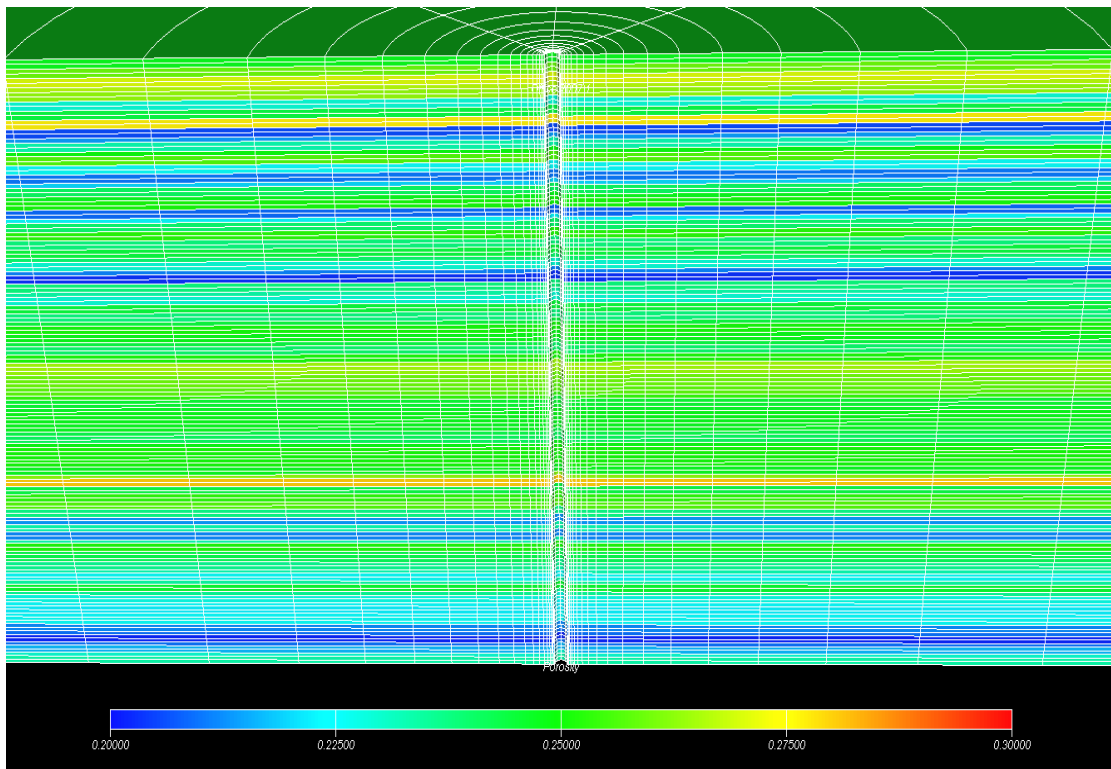


Figure 4.12: Reservoir model for IPTT#2.

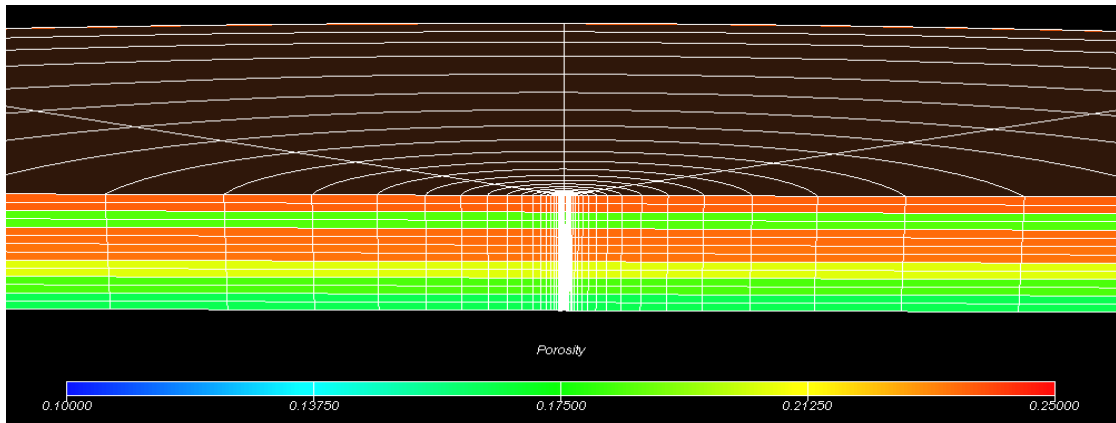


Figure 4.13: Reservoir model for IPTT#3.

4.4 Well Test Simulation

Single Well Model - NMR based method and Single Well Model – Borehole Electrical Image based method are simulated using flow rate and skin factor from the actual measurement. The pressure response simulated from the single well model was later used to estimate horizontal permeability by using Pressure Transient Analysis. Horizontal permeability results from Single Well Model – NMR based method can be obtained in this step. However, horizontal permeability from Single Well Model – Borehole Electrical Image based method needs to calibrate from horizontal permeability derived from Dual Packers WFT. The method of calibration is described in the next section.

4.5 Single Well Model Calibration

The interpreted result of horizontal permeability of an interval of the Single Well Model – Borehole Electrical Image based method was used to analyze and calibrate with the actual measurement. As a result of the calibration, the normalized coefficient from calibration process was multiplied to other k_r , k_θ and k_z of each interval of the single well model. Pressure response needs to be simulated for all intervals after the horizontal permeability was multiplied by normalized coefficient. The new pressure response was then interpreted using pressure transient analysis

technique. Figure 4.14 shows workflow of calibrated single well model – Borehole Electrical Image based method using pressure response from Dual Packers WFT.

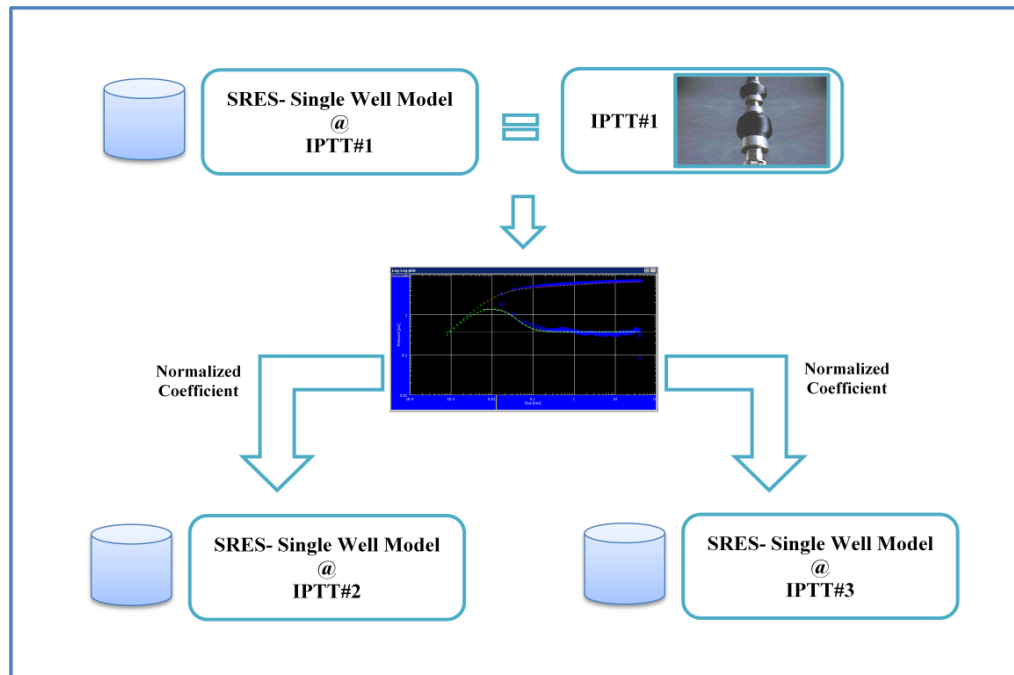


Figure 4.14: Workflow of calibrated single well model – Borehole Electrical Image based method using result from the actual measurement.

4.6 Well Productivity Prediction

After the single well model – Borehole Electrical Image based method is calibrated, if the result obtained from single well model provides the satisfying information, it can be used for predicting well productivity from the zone of interest along the wellbore. This developed methodology is described briefly as shown in Figure 4.15.

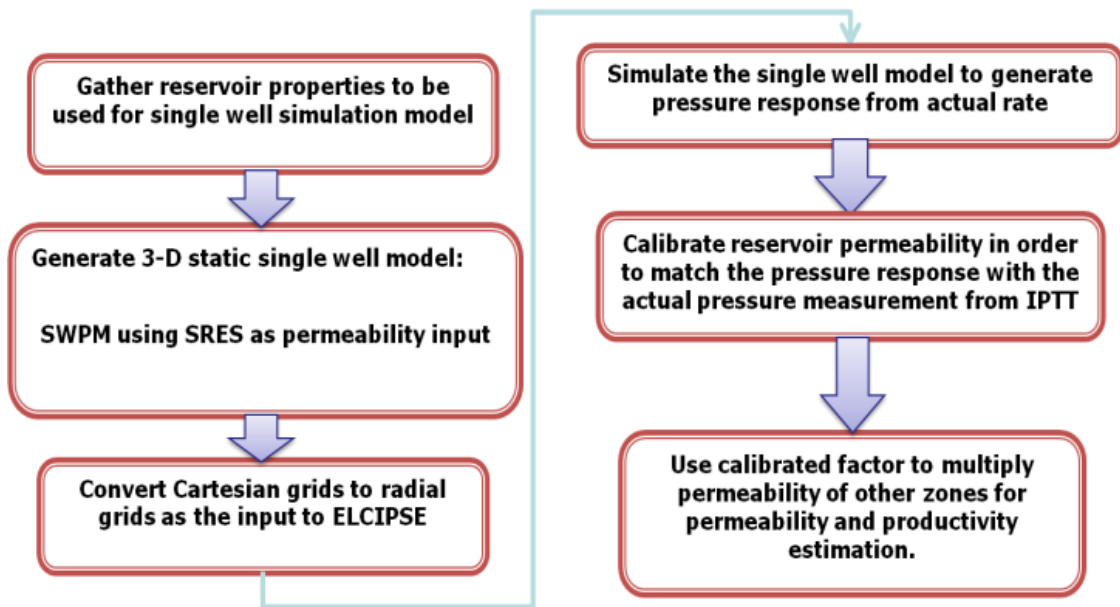


Figure 4.15: Workflow of predicting well productivity using single well model from Borehole Electrical Image.

CHAPTER V

RESULTS AND DISCUSSIONS

This chapter describes the results and analysis from pressure response and well test interpretation from both Single Well Model of NMR based method and Single Well Model of Borehole Electrical Image base method. The first single well model was chosen as a reference example by using high-resolution permeability derived from NMR logging tool. The second single well model was developed from the first single well model by using synthetic resistivity as permeability input from borehole electrical image instead of NMR permeability. The results were discussed in term of the horizontal permeability between single well model simulation and measurement from Interval Pressure Transient Test (IPTT).

Single Well Predictive Model (SWPM) is interactive wizard software to provide the user with the tools to simply and efficiently build 1D and 3D static models from wellbore data. A reservoir simulator, ELIPSE E100, was used to simulate pressure transient responses from the dual packer wireline formation tester. Then, pressure transient analysis software, called Saphir, was used to estimate reservoir parameters. The estimated reservoir parameters obtained from Pressure Transient Analysis Technique were then compared with the actual input used in the simulation.

For the well chosen for this study, IPTT has been performed for three intervals entitled as IPTT#1, IPTT#2 and IPTT#3 as can be seen in Table 4.3 and Figure 4.1 in Chapter IV.

5.1 Single Well Model of NMR based method

The first scenario was run using Single Well Model NMR based method. The numerical simulation was performed by building 3D model using petrophysical analysis with high-resolution permeability derived from NMR logging tool. The objective of this study is to investigate the interpreted result of horizontal permeability

which was estimated using pressure transient analysis software for comparison between actual measurements and simulated results. Three intervals of the single well model, namely, NMR-IPTT#1, NMR-IPTT#2 and NMR-IPTT#3 correspond to IPTT#1, IPTT#2 and IPTT#3, respectively.

5.1.1 NMR-IPTT#1

This case compares results from actual measurement and simulation model of IPTT#1 interval by using permeability derived from NMR logging tool. Figure 5.1 illustrates well schematic and borehole image available in the right track to illustrate vertical heterogeneity of the formation for NMR-IPTT#1 case.

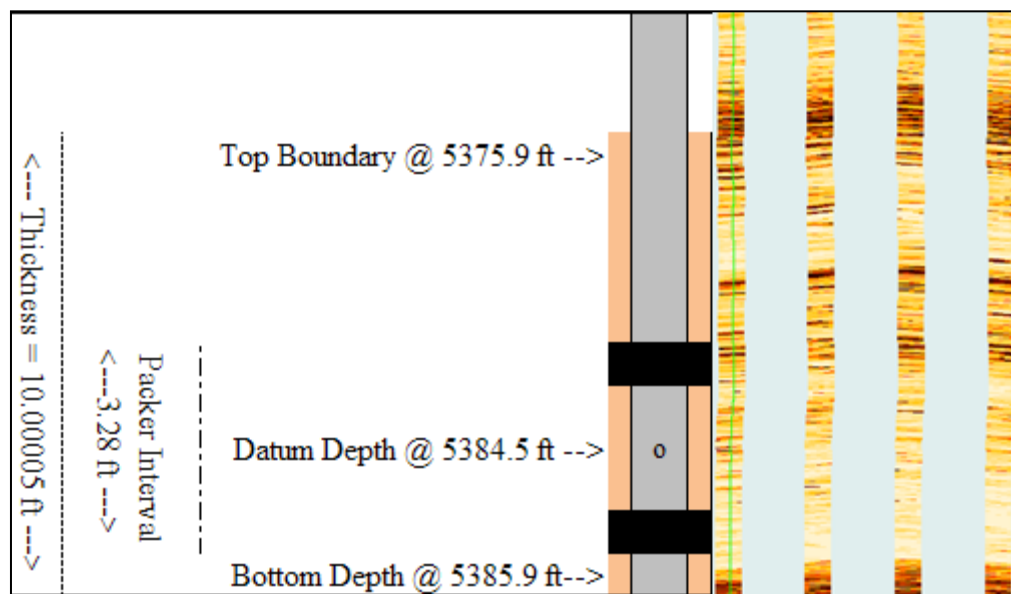


Figure 5.1: Well schematic for IPTT#1 interval.

In this NMR-IPTT#1 case, two buildups were performed with several downhole rates. The first buildup (BU#1) was performed for about 42.5 minutes while the second buildup (BU#2) was performed for 9.5 minutes as illustrated in Figure 5.4. The pressure transient test from the first buildup shows clearer behavior of Infinite Acting Radial Flow (IARF) than the second buildup. Hence, the first buildup is used for interpretation of pressure transient analysis for both actual measurement and simulation model of IPTT#1. Since the formation thickness is larger than the interval

of dual packers WFT, the pressure derivative from simulated result shows behavior of spherical flow (negative half slope) similar to the actual measurement. Figures 5.2, 5.3 and 5.4 illustrate log-log plot, semi-log plot and history plot, respectively. Blue points represent actual measurement from interval pressure transient test. Green points represent the simulated result from the single well model. Each line is the analysis to obtain reservoir parameters from the simulation result. Pressure responses from simulation result very well match with the actual measurements.

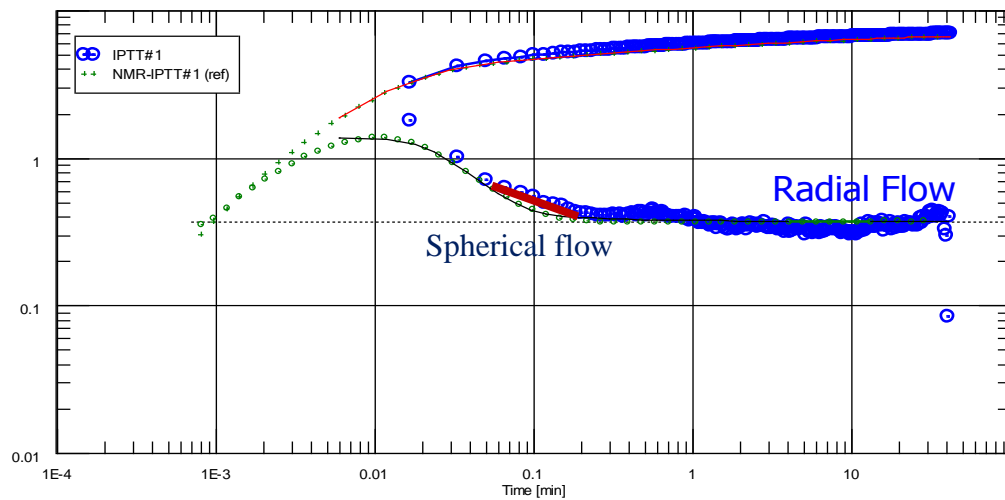


Figure 5.2: Log-log plot of NMR-IPTT#1.

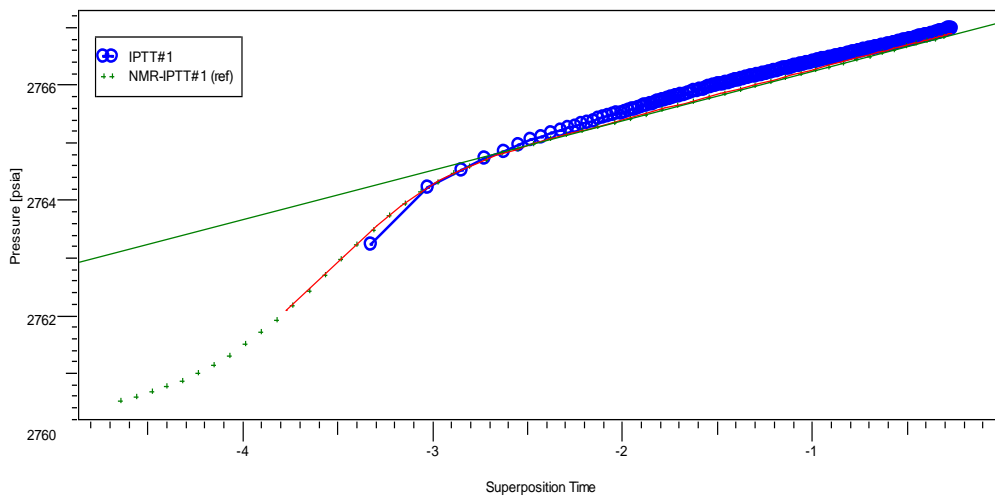


Figure 5.3: Semi-log plot of NMR-IPTT#1.

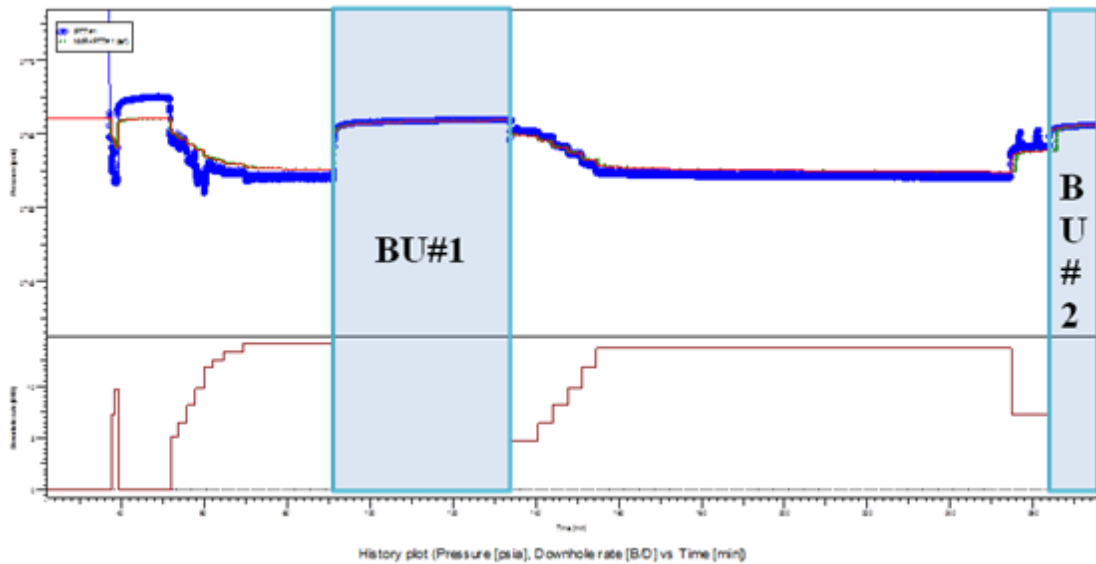


Figure 5.4: History plot of NMR-IPTT#1.

5.1.2 NMR-IPTT#2

This case compares results from actual measurement and simulation model of IPTT#2 interval by using permeability derived from NMR logging tool. Figure 5.5 illustrates well schematic and borehole image available in the right track to illustrate vertical heterogeneity of the formation for NMR-IPTT#2 case.

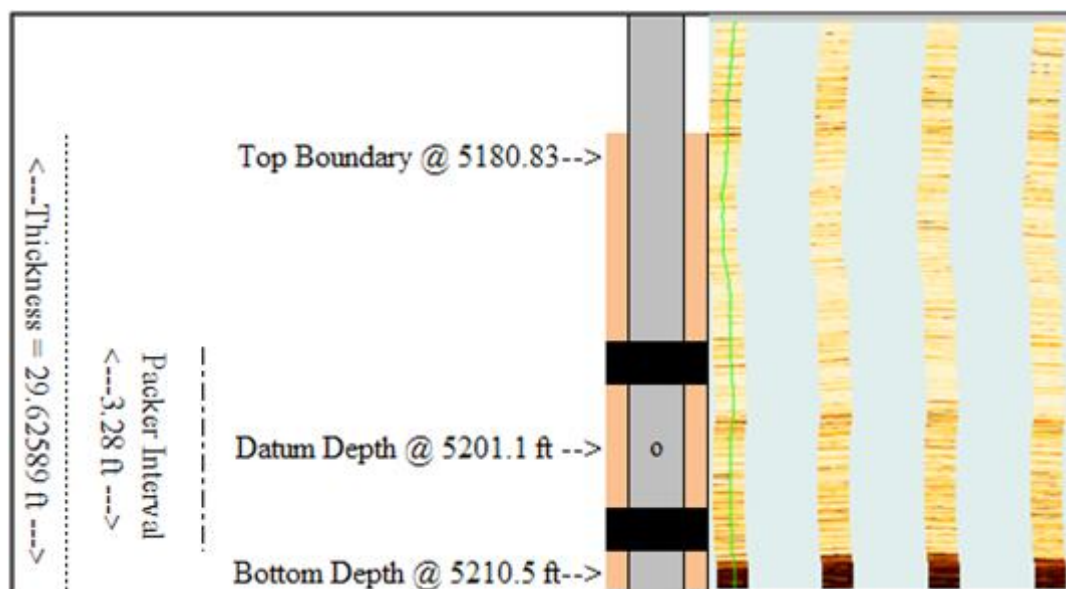


Figure 5.5: Well schematic for IPTT#2 interval.

In this NMR-IPTT#2 case, two buildups were performed with several downhole rates. The first buildup (BU#1) was performed for about 39 minutes while the second buildup (BU#2) was performed for 26.5 minutes as illustrated in Figure 5.8. The pressure transient test from both buildups shows behavior of Infinite Acting Radial Flow (IARF). The second buildup is selected for analysis because the pressure measurements in the first buildup were scattered while withdrawing fluid from the formation, due to the effect of pumping mud filtrate out from the formation. Since the formation thickness is larger than the interval of dual packers WFT, The pressure derivative from simulated result shows behavior of spherical flow (negative half slope) similar to the actual measurement. Figures 5.6, 5.7 and 5.8 illustrate log-log plot, semi-log plot and history plot, respectively. Blue points represent actual measurement from interval pressure transient test. Green points represent the simulated result from the single well model. Each line is the analysis to obtain reservoir parameters from the simulation result. Pressure responses from simulation result very well match with the actual measurements.

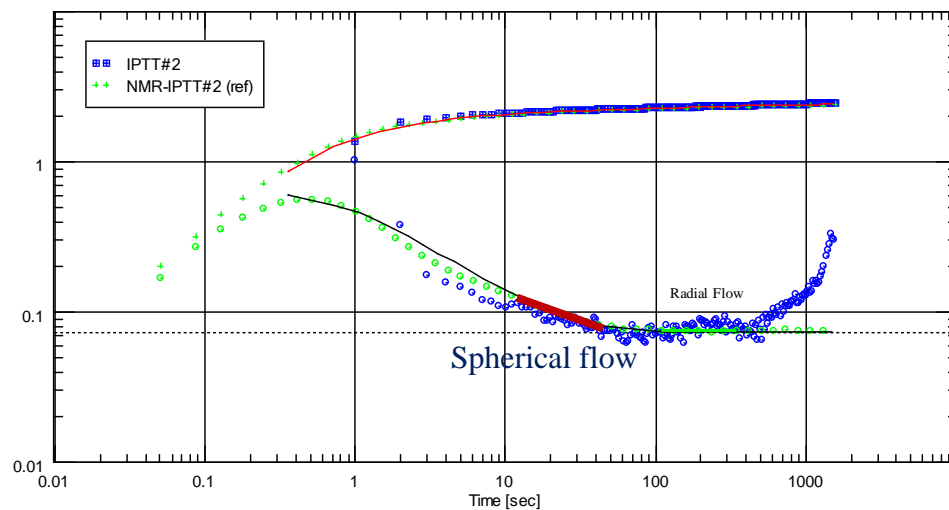


Figure 5.6: Log-log plot of NMR-IPTT#2.

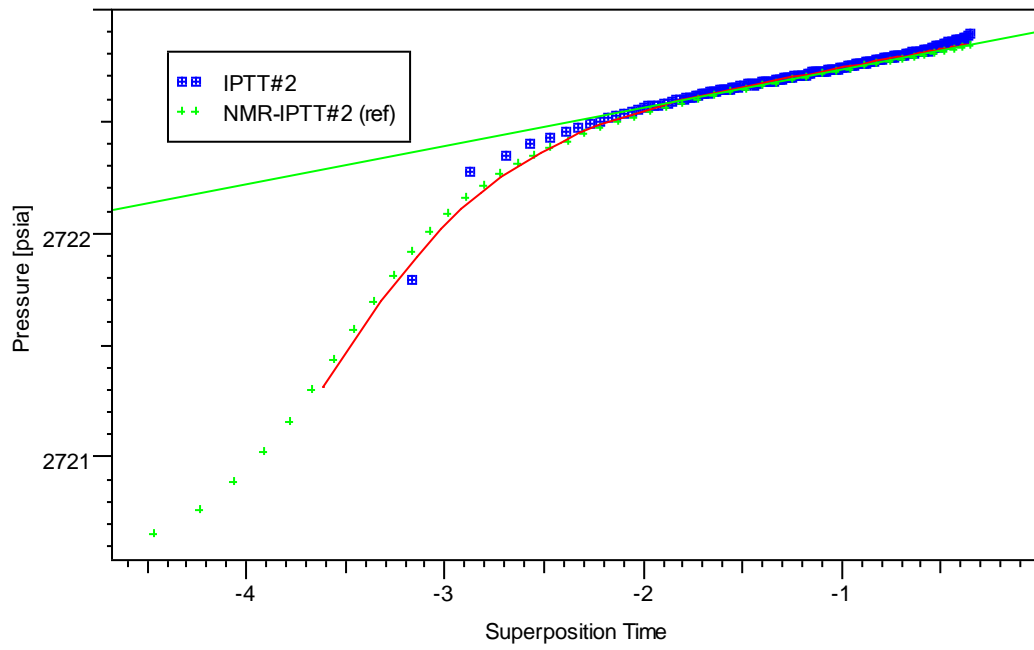


Figure 5.7: Semi-log plot of NMR-IPTT#2.

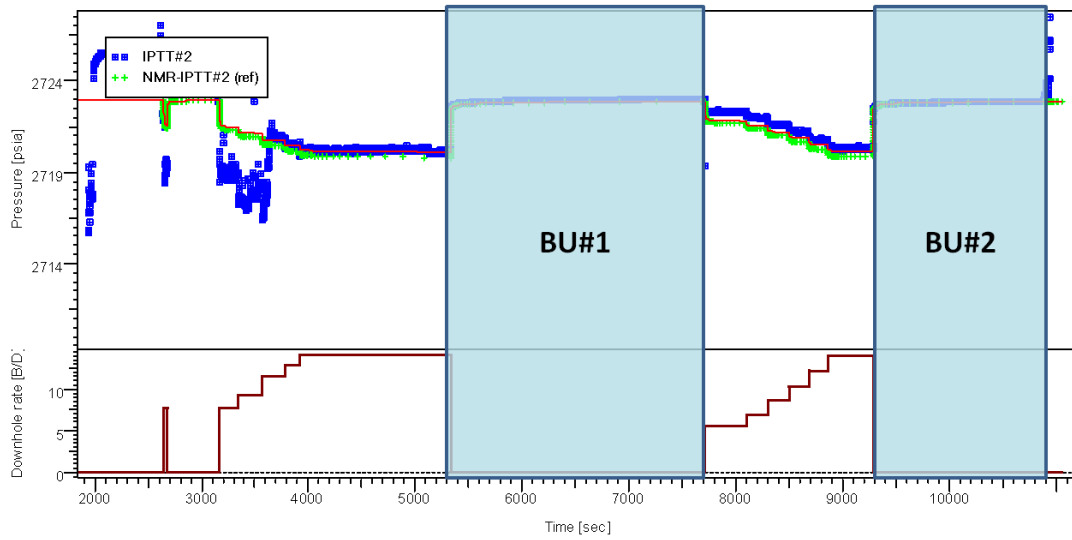


Figure 5.8: History plot of NMR-IPTT#2.

5.1.3 NMR-IPTT#3

This case compares results from actual measurement and simulation model of IPTT#3 interval by using permeability derived from NMR logging tool. Figure 5.9 illustrates well schematic and borehole image available in the right track to illustrate vertical heterogeneity of the formation for NMR-IPTT#3 case.

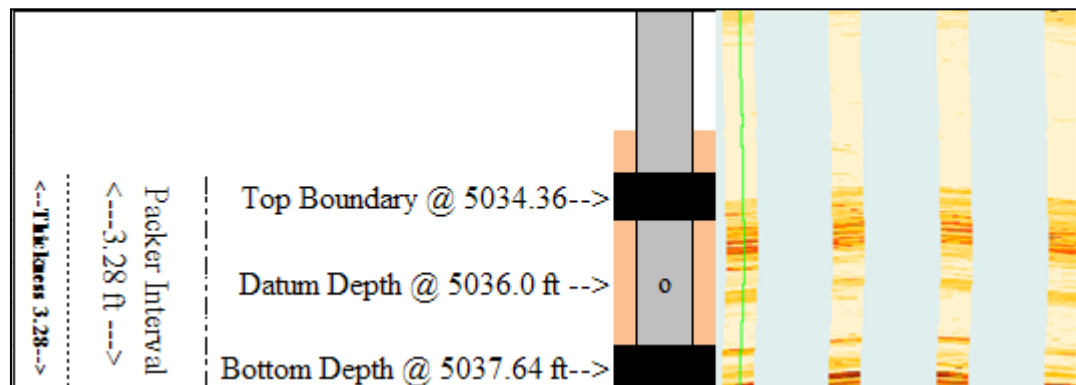


Figure 5.9: Well schematic for IPTT#3 interval.

In this NMR-IPTT#3 case, only one build up was performed with several downhole rates. The buildup (BU#1) was performed for about 34.5 minutes as illustrated in Figure 5.12. The pressure transient test shows clearly behavior of Infinite Acting Radial Flow (IARF). Since the formation thickness is equal to the interval of dual packers WFT, the spherical flow (negative half slope) cannot be seen clearly in the derivative plot as in the case of IPTT#1 and IPTT#2. Figures 5.10, 5.11 and 5.12 illustrate log-log plot, semi-log plot and history plot, respectively. Blue points represent actual measurement from interval pressure transient test. Green points represent the simulated result from the single well model. Each line is the analysis to obtain reservoir parameters from the simulation result. The results of pressure response from actual measurement and simulation were slightly deviated.

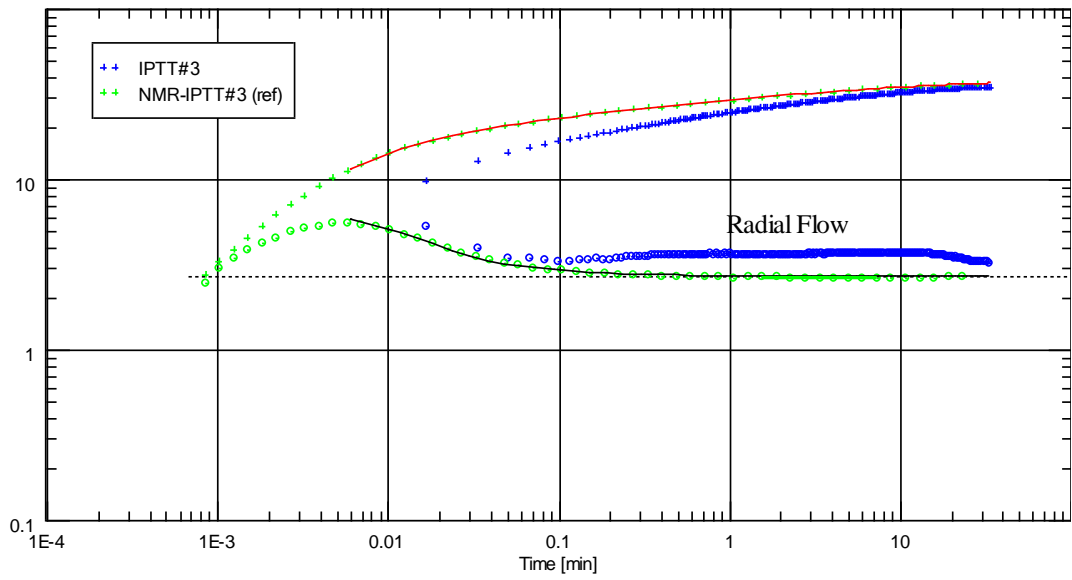


Figure 5.10: Log-log plot of NMR-IPTT#3.

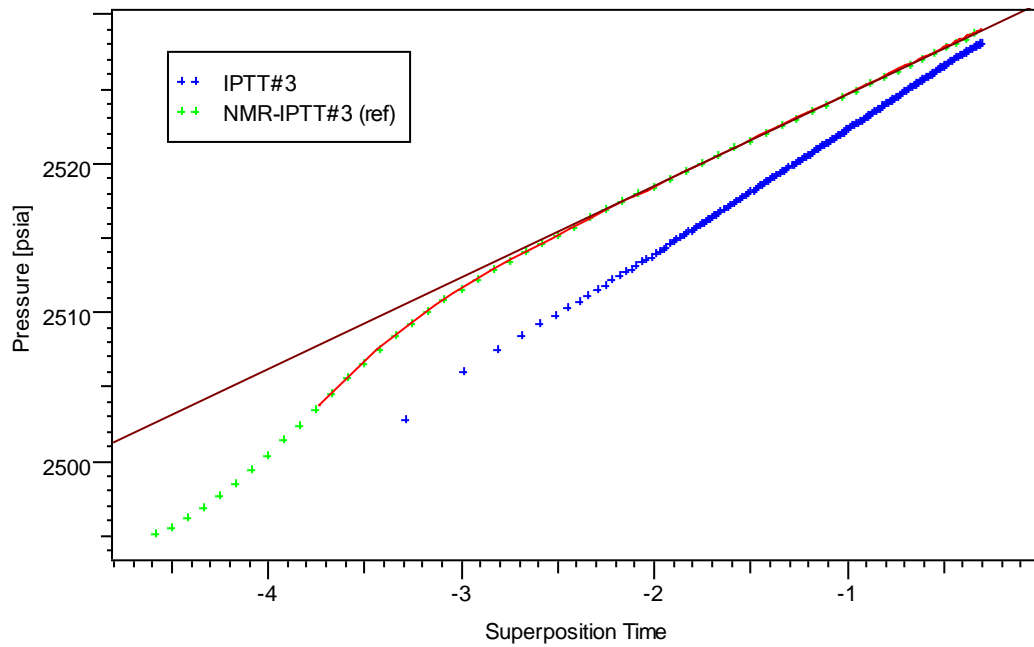


Figure 5.11: Semi-log Plot of NMR-IPTT#3.

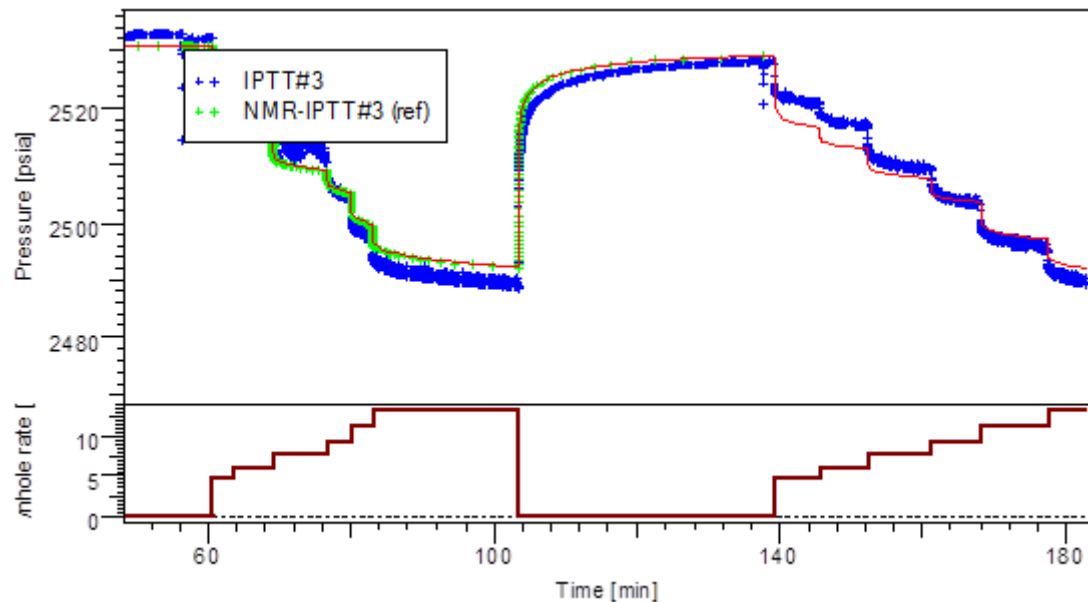


Figure 5.12: History log plot of NMR-IPTT#3.

5.1.4 Discussion

Table 5.1 shows the comparison between interpretation results of horizontal permeability from actual measurement and pressure response from Single Well Model of NMR based method. The estimated horizontal permeabilities from all intervals are consistent with less than 15% deviation from the actual measurement value except the result from this Single Well Model at IPTT#3 interval which has highest degree of lamination. Therefore, error from the measurement and single well model can cause from the degree of lamination which vertical resolution of NMR logging tool cannot detect from the formation. This single well model can be improved using advance petrophysical analysis to increase the vertical resolution from borehole electrical image log called SHARP which several papers related on this kind of processing already published to the Society of Petroleum Engineer (SPE). However these results confirm that the estimated horizontal permeabilities derived from Single Well Model of NMR based method response are reliable and benefitable to perform well productivity prediction.

Table 5.1: The comparison of interpreted k_h from the measurement of Interval Pressure Transient Tests and Single Well Model of NMR based method.

Interval	k_h (md)		Error (%)
	Measurement	Single Well Model NMR based method	
IPTT#1	116.92	102.00	12.76
IPTT#2	175.86	176.00	0.08
IPTT#3	29.54	40.70	37.77

5.2 Single Well Model of Borehole Electrical Image Based Method

The second scenario was run using Single Well Model of Borehole Electrical Image based method. The numerical simulation was performed by building 3D model using petrophysical analysis with synthetic resistivity as permeability input derived from borehole electrical image tool. The interpreted result of horizontal permeability of an interval of the single well model was used to analyze and calibrate with the actual measurement. As a result of the calibration, the normalized coefficient from calibration process was multiplied to other k_r, k_θ and k_z of each interval of the single well model. The objective of this study is to investigate the pressure behavior and value of horizontal permeability that was estimated using pressure transient analysis software for comparison between actual measurements and simulated results after applying calibration to each interval of single well model. Table 5.2 illustrates the interpreted permeability results derived from well test equation for all IPTT that were performed for the chosen well.

Table 5.2: Interpreted horizontal permeability from Interval Pressure Transient Tests

Interpreted k_h from Interval Pressure Transient Tests (IPTT)			
	IPTT#1	IPTT#2	IPTT#3
$k.h$ (mD.ft)	1170.00	5210.00	96.90
h (ft)	10.01	29.63	3.28
k (mD)	116.92	175.86	29.54

To investigate the pressure behavior and value of horizontal permeability from the single well model in this method, three simulation cases are designed as follows:

Case SRES-IPTT#1: Matching both single well model and the measurement from IPTT#1 interval in order to investigate the use of the normalized coefficient to calibrate other intervals.

Case SRES-IPTT#2: Matching both single well model and the measurement from IPTT#2 interval in order to investigate the use of the normalized coefficient to calibrate other intervals.

Case SRES-IPTT#3: Matching both single well model and the measurement from IPTT#3 interval in order to investigate the use of the normalized coefficient to calibrate other intervals.

5.2.1 SRES-IPTT#1

The objective of this case is to match the pressure response from single well model and a measurement of IPTT#1 interval in order to investigate the use of the normalized coefficient to calibrate to other intervals. Additionally, comparison between actual measurements and simulation responses calibrated from IPTT#1 by using synthetic resistivity as permeability input derived from borehole electrical image tool is made. The description of process in Figure 5.13 is listed as follows:

1. Interpret horizontal permeability from the pressure derivative of uncalibrated single well model and the measurement.
2. Obtain calibration coefficient from equalizing horizontal permeability between uncalibrated single well model and the measurement.
3. Multiply calibration coefficient multiplier to the horizontal permeability in the single well model of other IPTT intervals.
4. Re-simulate the pressure response.
5. Interpret horizontal permeability from the simulated pressure response.
6. Compare permeability estimates obtained from simulated pressure and actual pressure measurement.

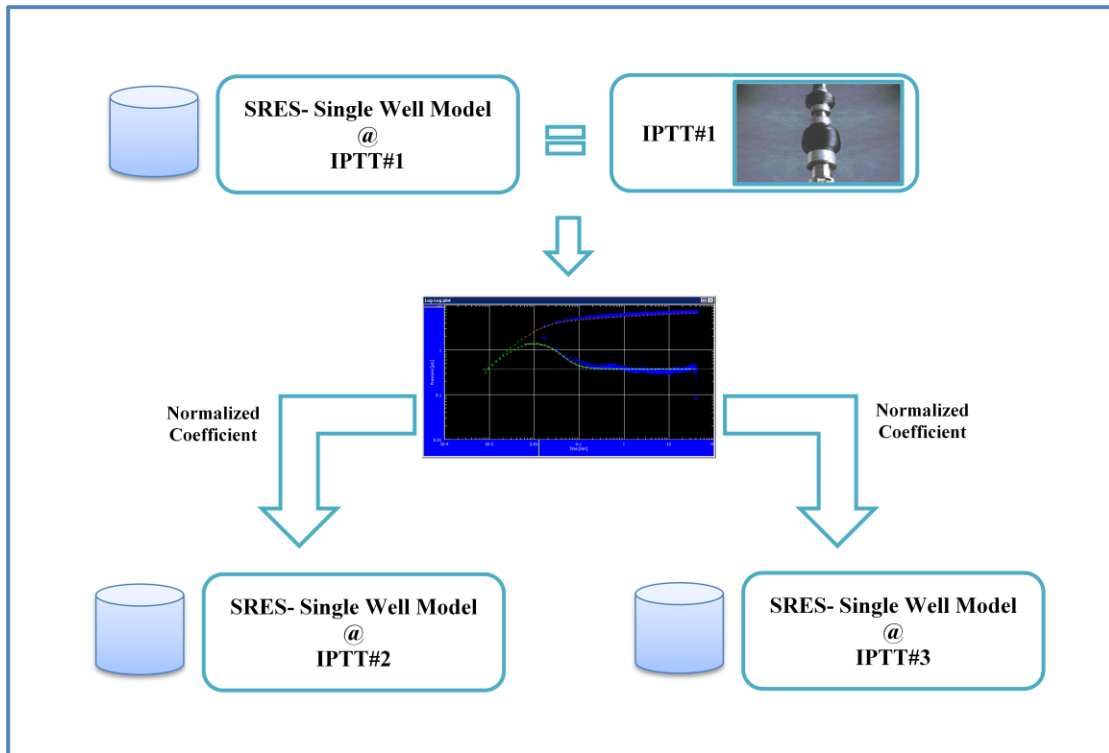


Figure 5.13: Process of case SRES-IPTT#1.

The uncalibrated model of this interval needs to be simulated in order to interpret for horizontal permeability as shown in Figure 5.14.

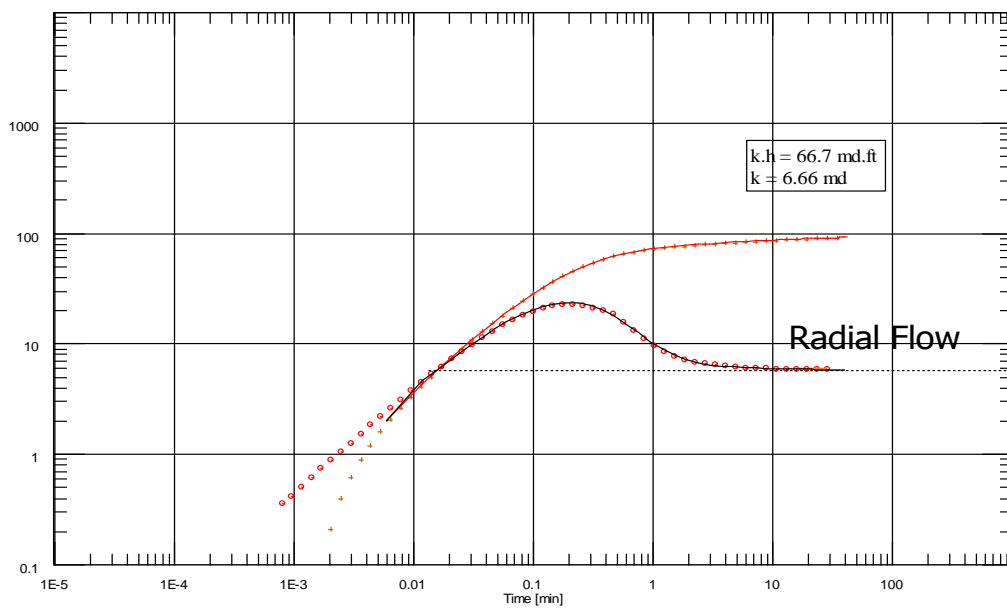


Figure 5.14: Log-log plot of uncalibrated model for IPTT#1 interval.

As illustrated in Figure 5.14, uncalibrated horizontal permeability of this SRES-IPTT#1 model equals 6.66 mD, or permeability thickness equals 66.7 mD.ft. However, from the actual measurement of this interval, the interpreted horizontal permeability equals 116.92 mD, or permeability thickness equals 1170 mD.ft. Therefore,

$$\begin{aligned}
 k_{\text{measurement(IPTT\#1)}} &= c \cdot k_{\text{SRES-IPTT\#1}} \\
 c_{\text{IPTT\#1}} &= k_{\text{measurement(IPTT\#1)}}/k_{\text{SRES-IPTT\#1}} \\
 c_{\text{IPTT\#1}} &= 116.92/6.66 \approx 17.56
 \end{aligned}$$

where

$$\begin{aligned}
 k_{\text{measurement(IPTT\#1)}} &= \text{permeability derived from the measurement at IPTT\#1} \\
 k_{\text{SRES-IPTT\#1}} &= \text{permeability derived from uncalibrated model at IPTT\#1} \\
 c_{\text{IPTT\#1}} &= \text{calibration coefficient of IPTT\#1}
 \end{aligned}$$

Figures 5.15, 5.16, 5.17 show matching results after the calibration coefficient of IPTT#1 was multiplied to k_r, k_θ and k_z of the original model. Blue points represent the actual acquisition data; green points represent the simulated result from the single well model; and line is the analysis to obtain reservoir parameters from the simulation result.

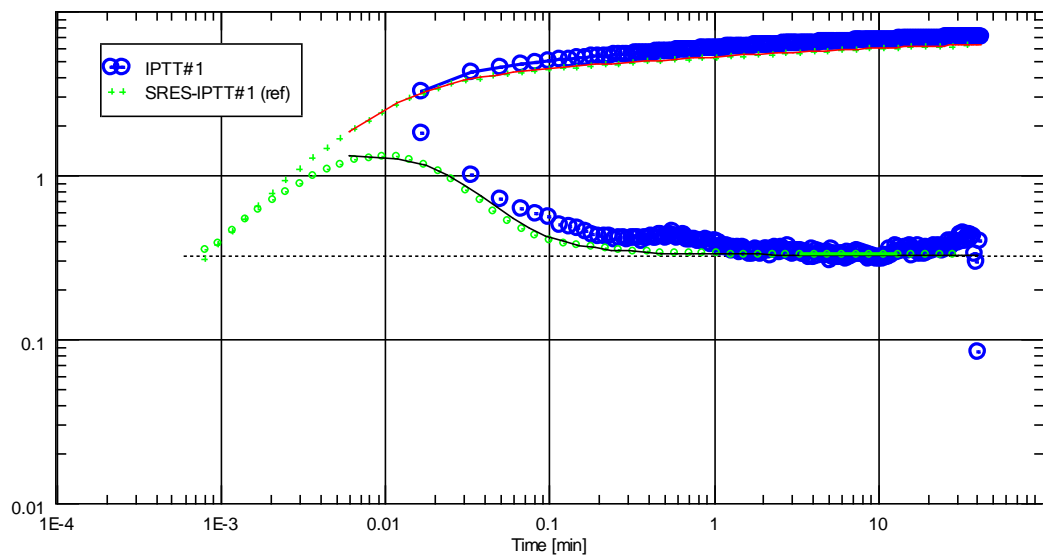


Figure 5.15: Log-log plot of actual data and calibrated single well model for IPTT#1.

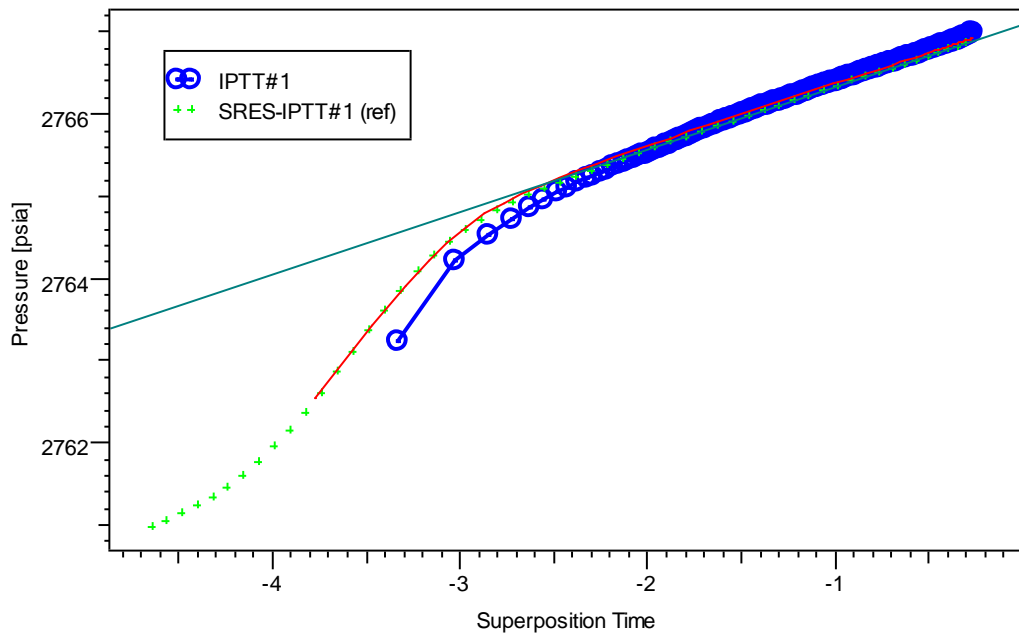


Figure 5.16: Semi-log plot of actual data and calibrated single well model for IPTT#1.

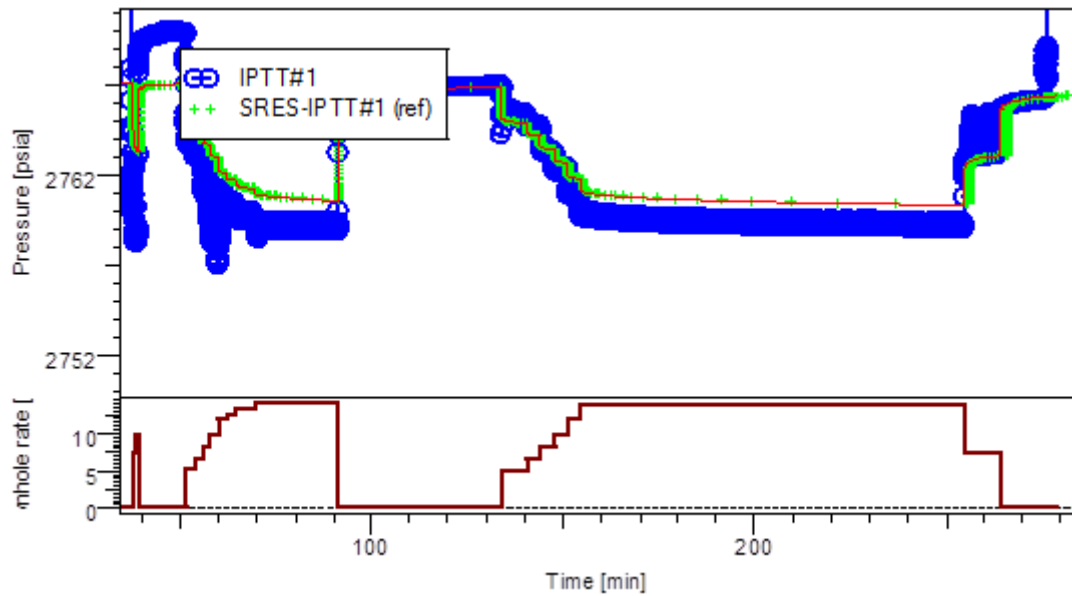


Figure 5.17: History plot of actual data and calibrated single well model for IPTT#1.

The calibration coefficient derived from the simulated pressure response of IPTT#1 interval was also multiplied to $k_r k_\theta$ and k_z of IPTT#2 and IPTT#3. Since the calibration coefficient was calibrated from a interval which has a thickness of 10.01 ft, it needs to be normalized based on the thickness of each interval before being multiplied to $k_r k_\theta$ and k_z of other intervals. The value of $c_{IPTT\#1}$ (17.56) was divided

by 10.01 to obtain the normalized coefficient of 1.75 per ft of thickness. This normalized coefficient was adjusted based on thickness of each interval before it was used as a multiplier as shown in Table 5.3.

Table 5.3: Coefficients of intervals using normalized coefficient result from IPTT#1.

Interval	Thickness (ft)	Normalized coefficient	Calibration coefficient
IPTT#1	10.01	1.75	17.56
IPTT#2	29.63	1.75	51.97
IPTT#3	3.28	1.75	5.74

After each calibration coefficient was applied to each simulation model of IPTT#2 and IPTT#3 according to Table 5.3, the results of matching pressure from calibration coefficients are illustrated in Figures 5.18, 5.19 and 5.20 for IPTT#2 interval and Figures 5.21, 5.22 and 5.23 for IPTT#3 interval.

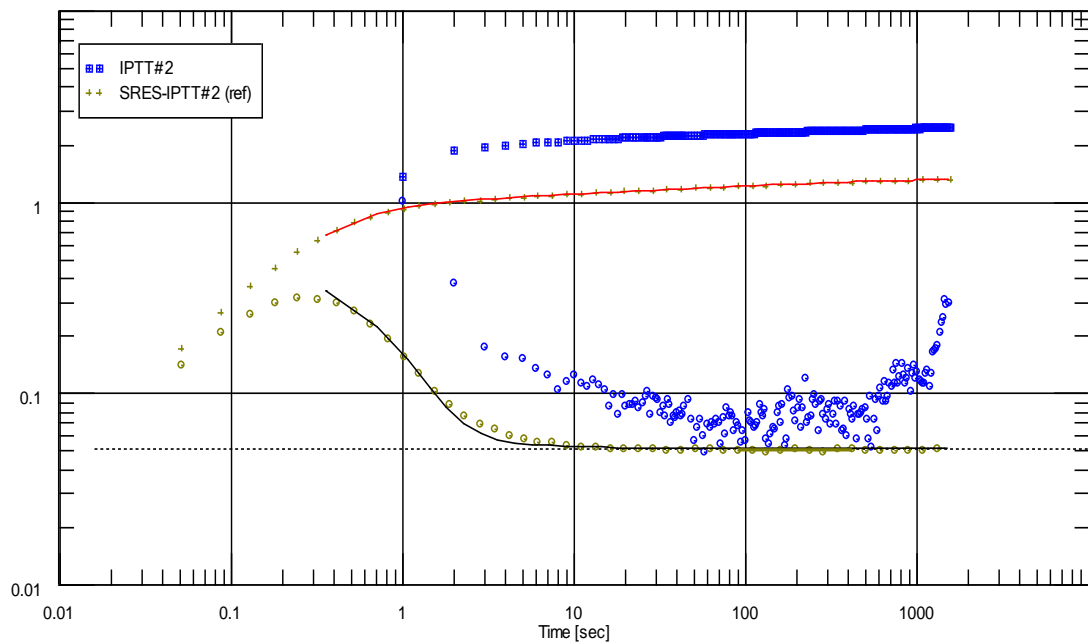


Figure 5.18: Log-log plot of actual data and calibrated single well model for IPTT#2.

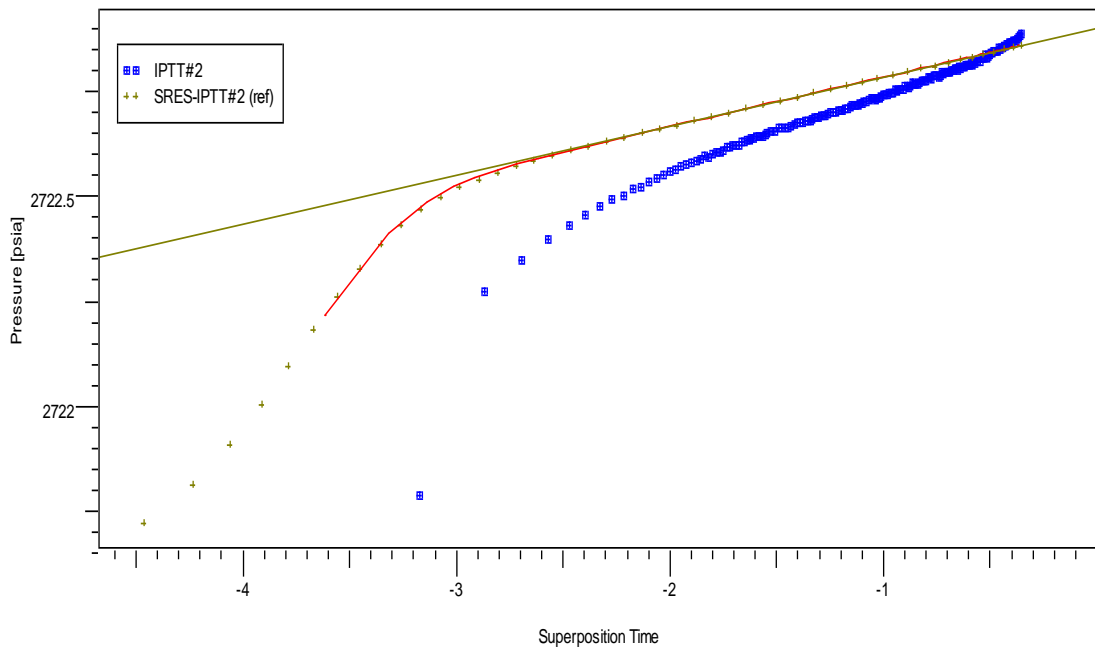


Figure 5.19: Semi-log plot of actual data and calibrated single well model for IPTT#2.

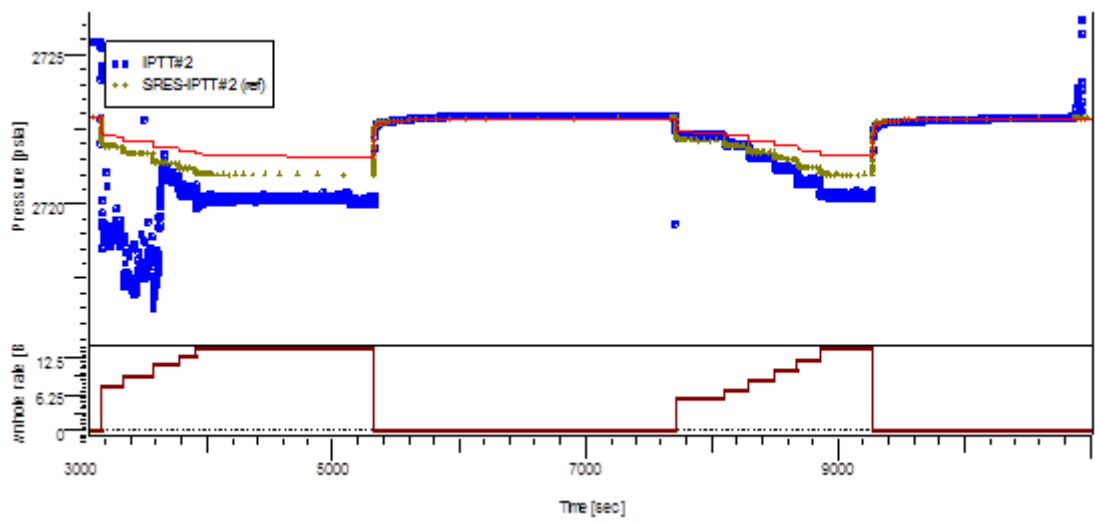


Figure 5.20: History plot of actual data and calibrated single well model for IPTT#2.

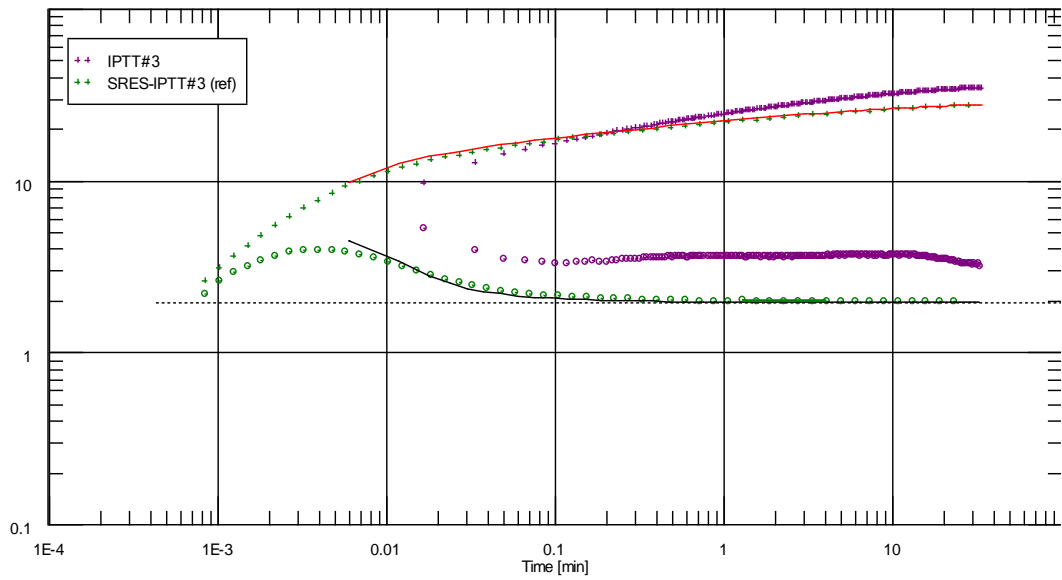


Figure 5.21: Log-log plot of actual data and calibrated single well model for IPTT#3.

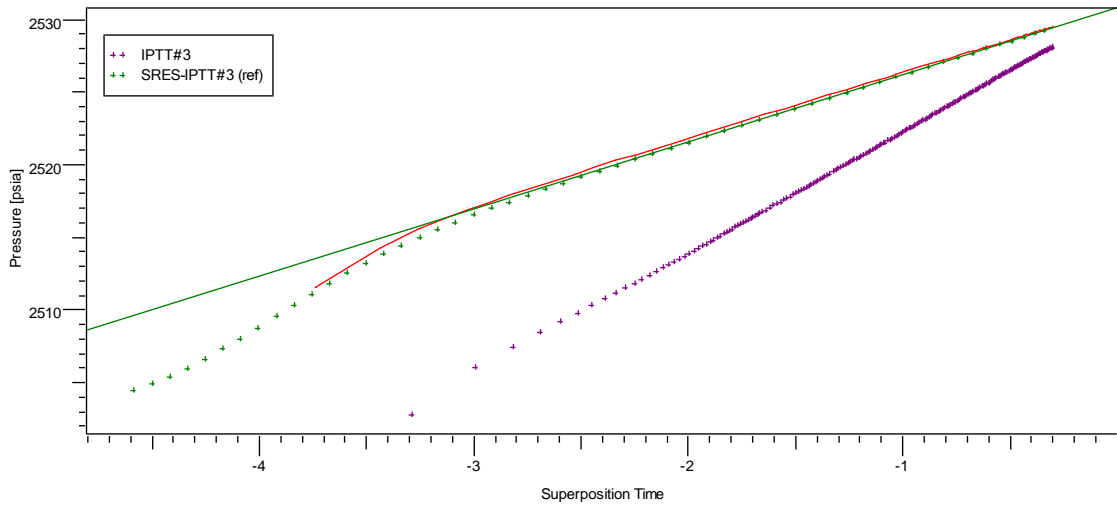


Figure 5.22: Semi-log plot of actual data and calibrated single well model for IPTT#3.

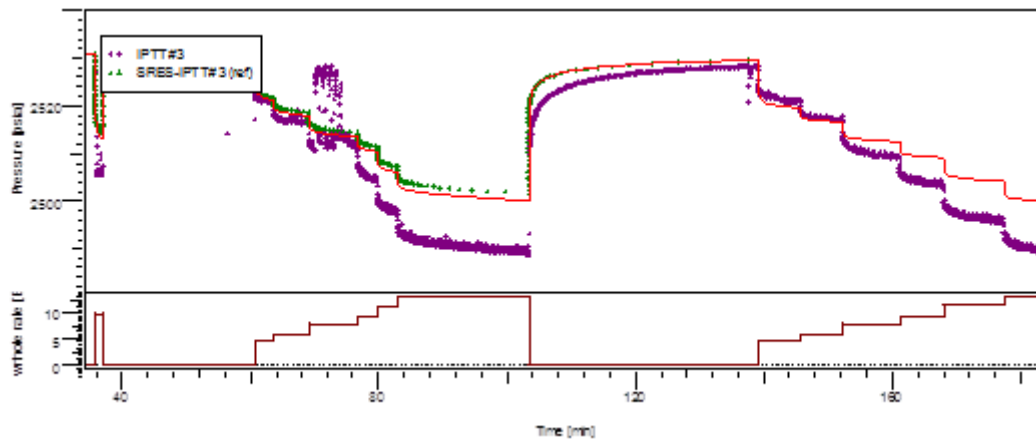


Figure 5.23: History plot of actual data and calibrated single well model for IPTT#3.

5.2.2 SRES-IPTT#2

The objective of this case is to match the pressure response from single well model and a measurement of IPTT#2 interval in order to investigate the use of the normalized coefficient to calibrate to other intervals. Additionally, comparison between actual measurements and simulation responses calibrated from IPTT#2 by using synthetic resistivity as permeability input derived from borehole electrical image tool is made. The description of process in Figure 5.24 is listed as follows:

1. Interpret horizontal permeability from the pressure derivative of uncalibrated single well model and the measurement.
2. Obtain calibration coefficient from equalizing horizontal permeability between uncalibrated single well model and the measurement.
3. Multiply calibration coefficient multiplier to the horizontal permeability in the single well model of other IPTT intervals.
4. Re-simulate the pressure response.
5. Interpret horizontal permeability from the simulated pressure response.
6. Compare permeability estimates obtained from simulated pressure and actual pressure measurement.

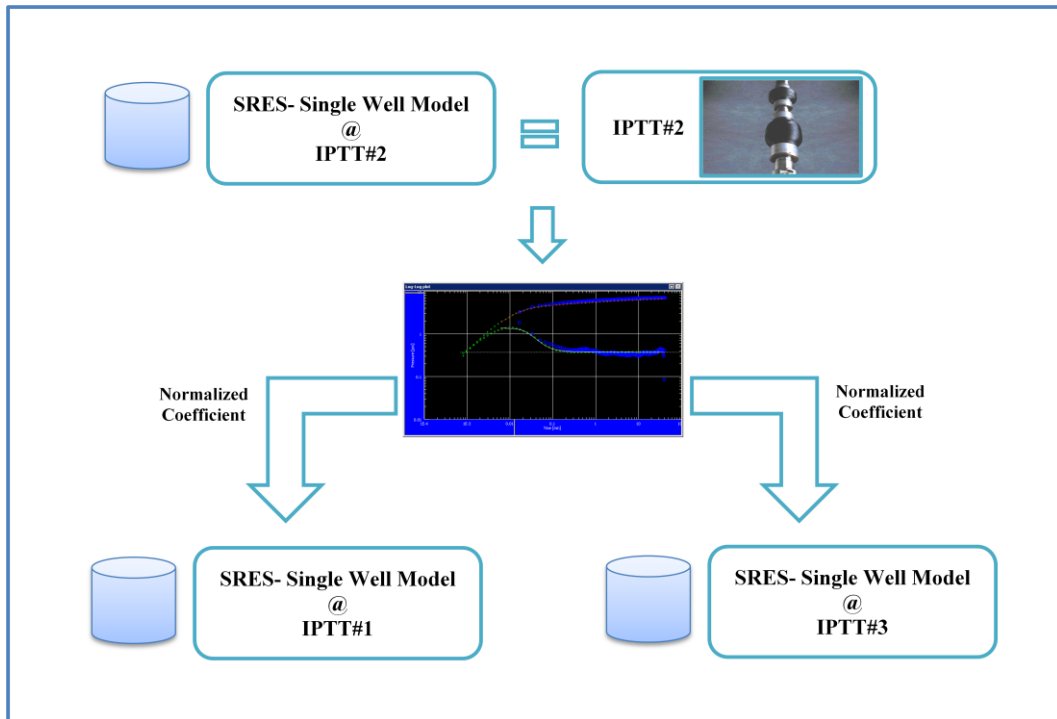


Figure 5.24: Process of case SRES-IPTT#2.

The uncalibrated model of this interval needs to be simulated in order to interpret for horizontal permeability as shown in Figure 5.25.

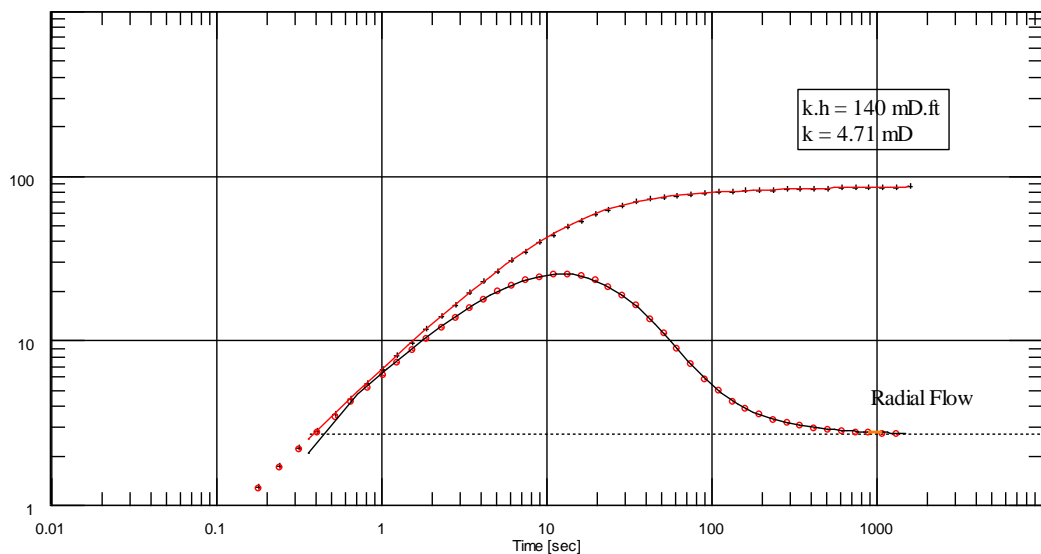


Figure 5.25: Log-log plot of uncalibrated model for IPTT#2 interval.

As illustrated in Figure 5.25, uncalibrated horizontal permeability of this SRES-IPTT#1 model equals 4.71 mD, or permeability thickness equals 140 mD.ft.

However, from the actual measurement of this interval, the interpreted horizontal permeability equals 176 mD, or permeability thickness equals 5210 mD.ft. Therefore,

$$\begin{aligned}
 k_{\text{measurement(IPTT\#2)}} &= c \cdot k_{\text{SRES-IPTT\#2}} \\
 c_{\text{IPTT\#2}} &= k_{\text{measurement(IPTT\#2)}}/k_{\text{SRES-IPTT\#2}} \\
 c_{\text{IPTT\#2}} &= 176/4.71 \approx 37.367
 \end{aligned}$$

where

$$\begin{aligned}
 k_{\text{measurement(IPTT\#2)}} &= \text{permeability derived from the measurement at IPTT\#2} \\
 k_{\text{SRES-IPTT\#2}} &= \text{permeability derived from uncalibrated model at IPTT\#2} \\
 c_{\text{IPTT\#2}} &= \text{calibration coefficient of IPTT\#2}
 \end{aligned}$$

Figures 5.26, 5.27, 5.28 show matching results after the calibration coefficient of IPTT#2 was multiplied to k_r, k_θ and k_z of the original model. Blue points represent the actual acquisition data; green points represent the simulated result from the single well model; and line is the analysis to obtain reservoir parameters from the simulation result.

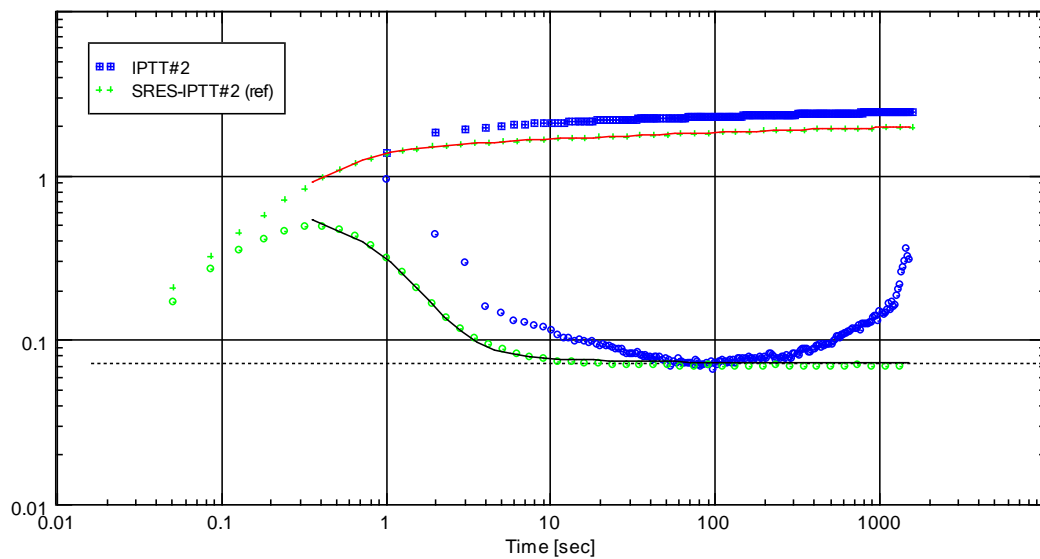


Figure 5.26: Log-log plot of actual data and calibrated single well model for IPTT#2.

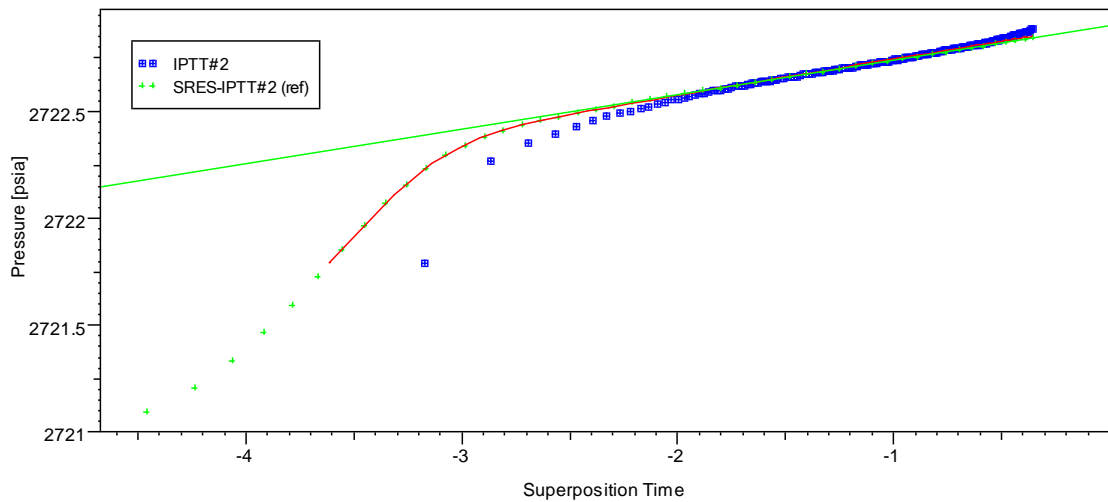


Figure 5.27: Semi-log plot of actual data and calibrated single well model for IPTT#2.

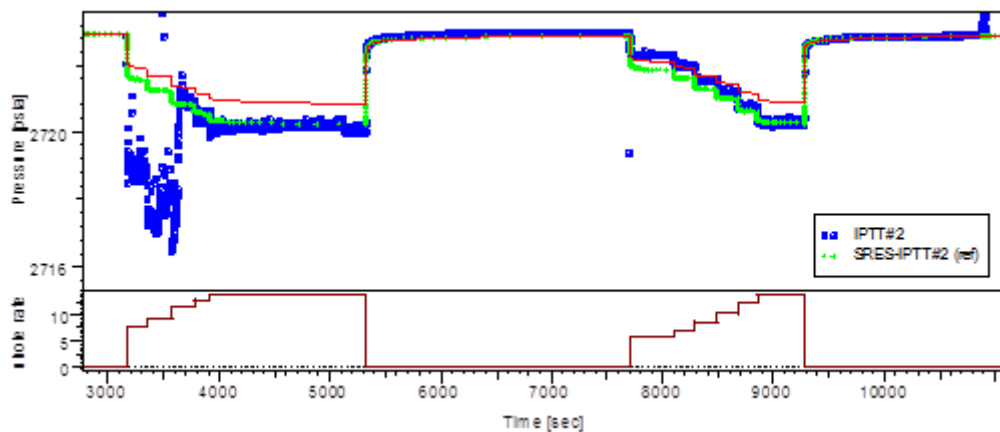


Figure 5.28: History plot of actual data and calibrated single well model for IPTT#2.

The calibration coefficient derived from the simulated pressure response of IPTT#2 interval was also multiplied to k_r, k_θ and k_z of IPTT#1 and IPTT#3. Since the calibration coefficient was calibrated from a interval which has a thickness of 29.63 ft, it needs to be normalized based on the thickness of each interval before being multiplied to k_r, k_θ and k_z of other intervals. The value of $c_{IPTT\#2}$ (37.367) was divided by 29.63 to obtain the normalized coefficient of 1.26 per ft of thickness. This normalized coefficient was adjusted based on thickness of each interval before it was used as a multiplier as shown in Table 5.4.

Table 5.4: Coefficients of intervals using normalized coefficient result from IPTT#2.

Interval	Thickness (ft)	Normalized coefficient	Calibration coefficient
IPTT#1	10.01	1.26	12.61
IPTT#2	29.63	1.26	37.34
IPTT#3	3.28	1.26	4.13

After each calibration coefficient was applied to each simulation model of IPTT#1 and IPTT#3 according to Table 5.4, the results of matching pressure from calibration coefficients are illustrated in Figures 5.29, 5.30 and 5.31 for IPTT#1 interval and Figures 5.32, 5.33 and 5.34 for IPTT#3 interval.

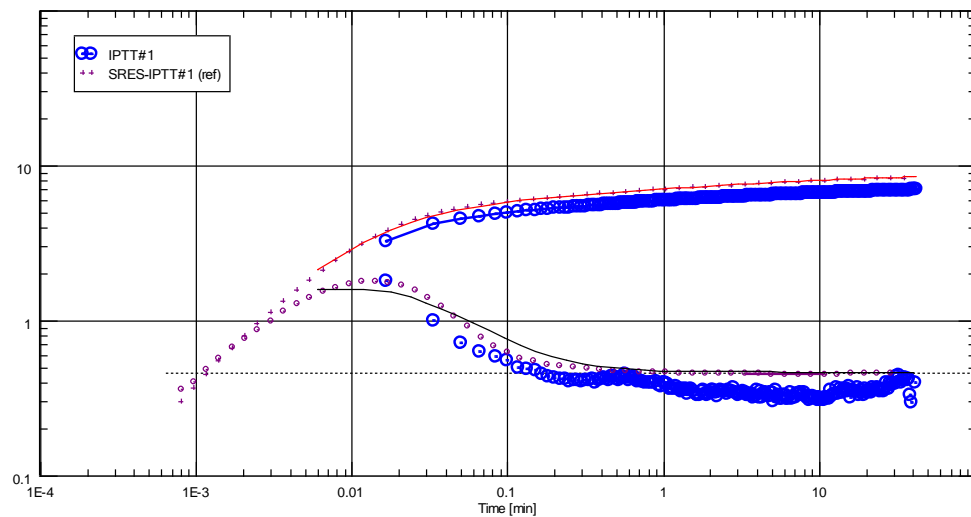


Figure 5.29: Log-log Plot of actual data and calibrated single well model for IPTT#1.

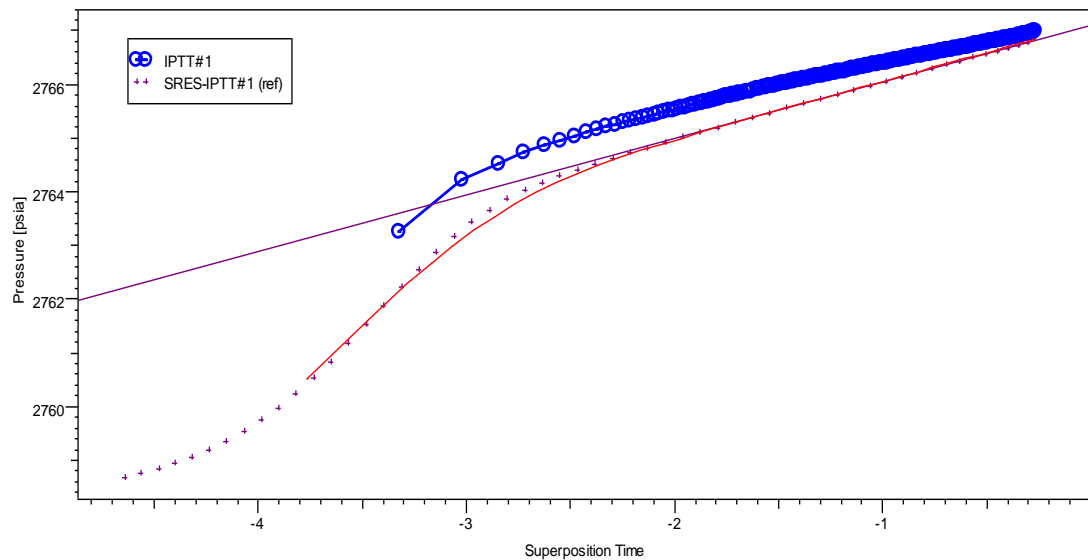


Figure 5.30: Semi-log plot of actual data and calibrated single well model for IPTT#1.

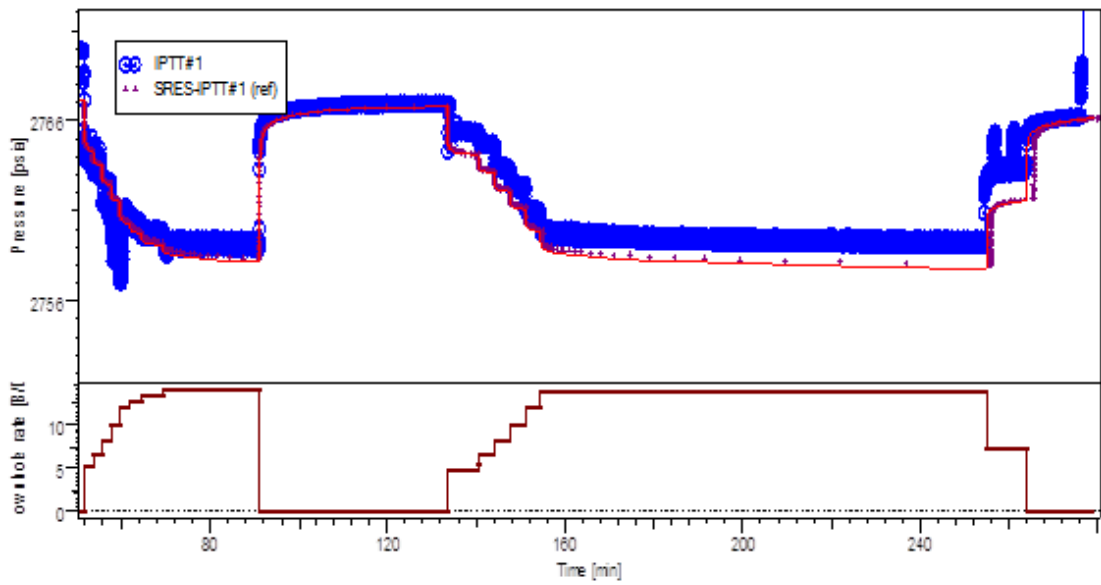


Figure 5.31: History plot of actual data and calibrated single well model for IPTT#1.

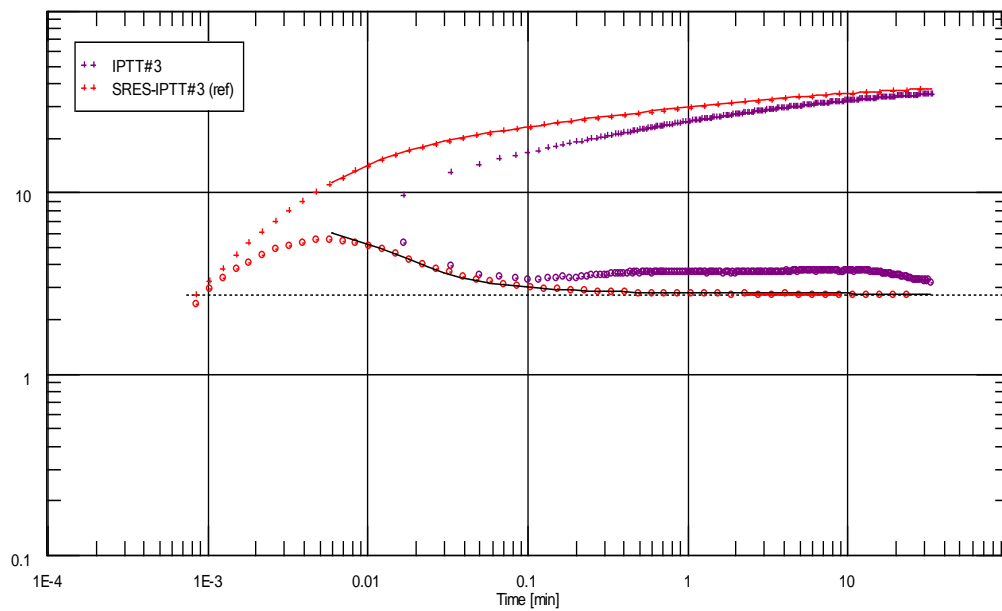


Figure 5.32: Log-log plot of actual data and calibrated single well model for IPTT#3.

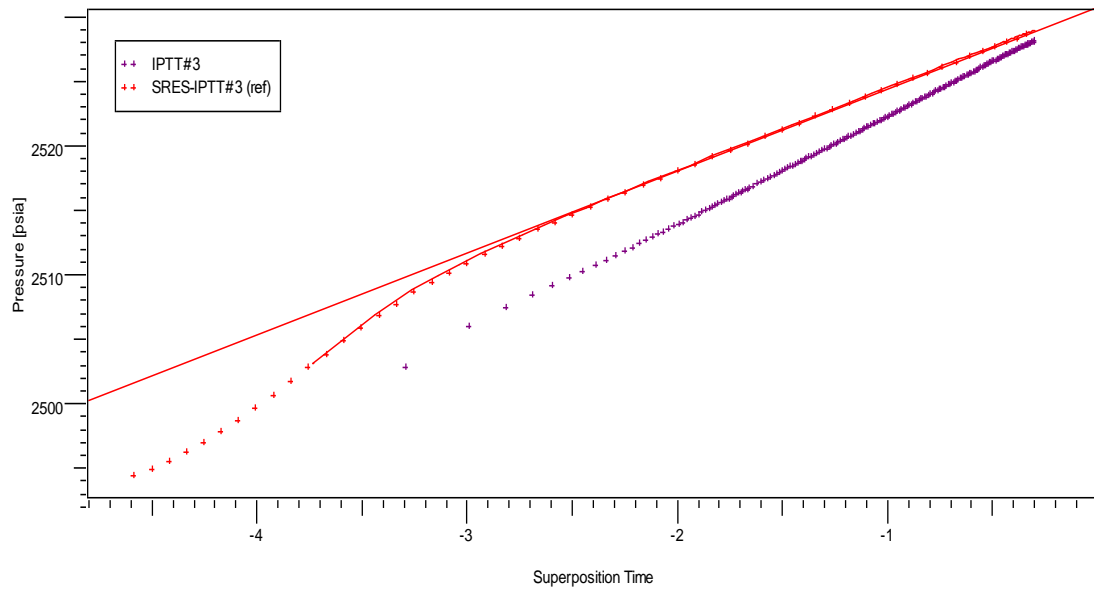


Figure 5.33: Semi-log plot of actual data and calibrated single well model for IPTT#3.

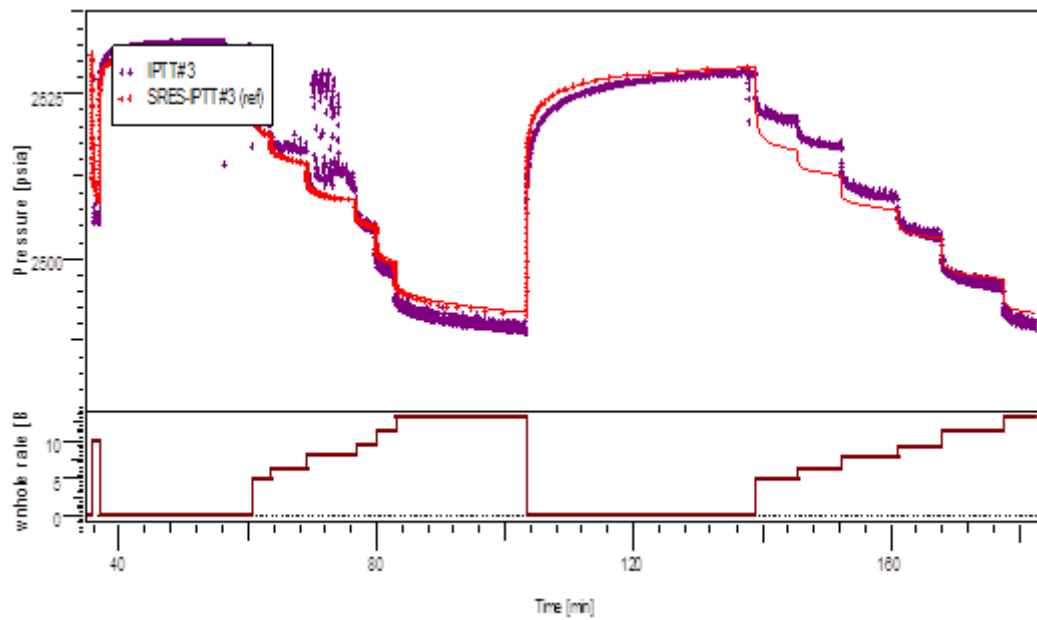


Figure 5.34: History plot of actual data and calibrated single well model for IPTT#3.

5.2.3 SRES-IPTT#3

The objective of this case is to match the pressure response from single well model and a measurement of IPTT#3 interval in order to investigate the use of the normalized coefficient to calibrate to other intervals. Additionally, comparison between actual measurements and simulation responses calibrated from IPTT#3 by using synthetic resistivity as permeability input derived from borehole electrical image tool is made. The description of process in Figure 5.35 is listed as follows:

1. Interpret horizontal permeability from the pressure derivative of uncalibrated single well model and the measurement.
2. Obtain calibration coefficient from equalizing horizontal permeability between uncalibrated single well model and the measurement.
3. Multiply calibration coefficient multiplier to the horizontal permeability in the single well model of other IPTT intervals.
4. Re-simulate the pressure response.
5. Interpret horizontal permeability from the simulated pressure response.
6. Compare permeability estimates obtained from simulated pressure and actual pressure measurement.

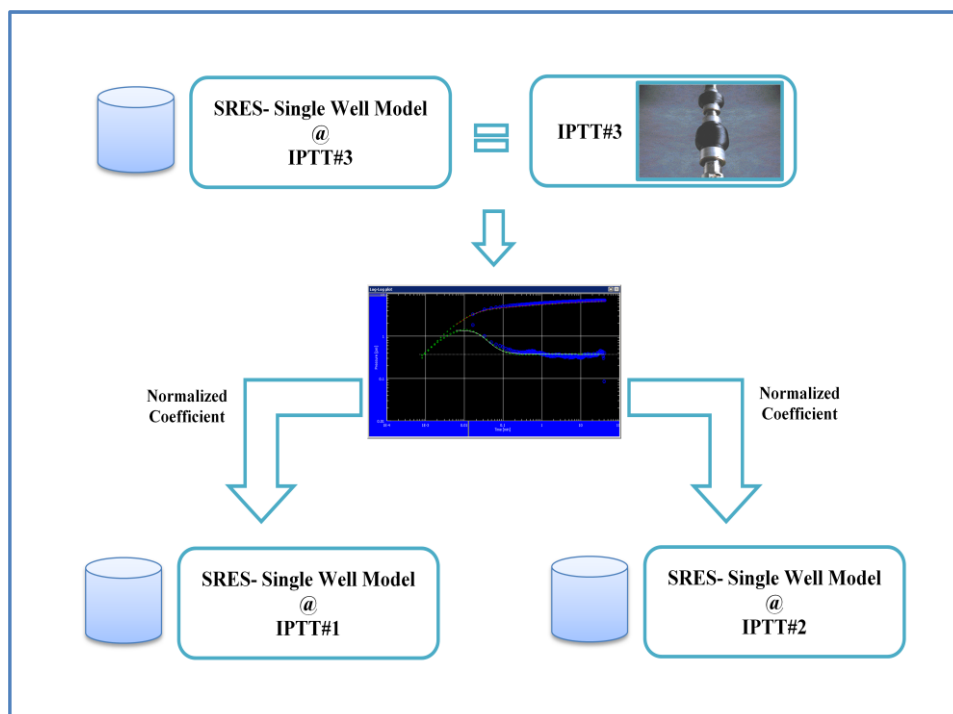


Figure 5.35: Process of case SRES-IPTT#3.

The uncalibrated model of this interval needs to be simulated in order to interpret for horizontal permeability as shown in Figure 5.36.

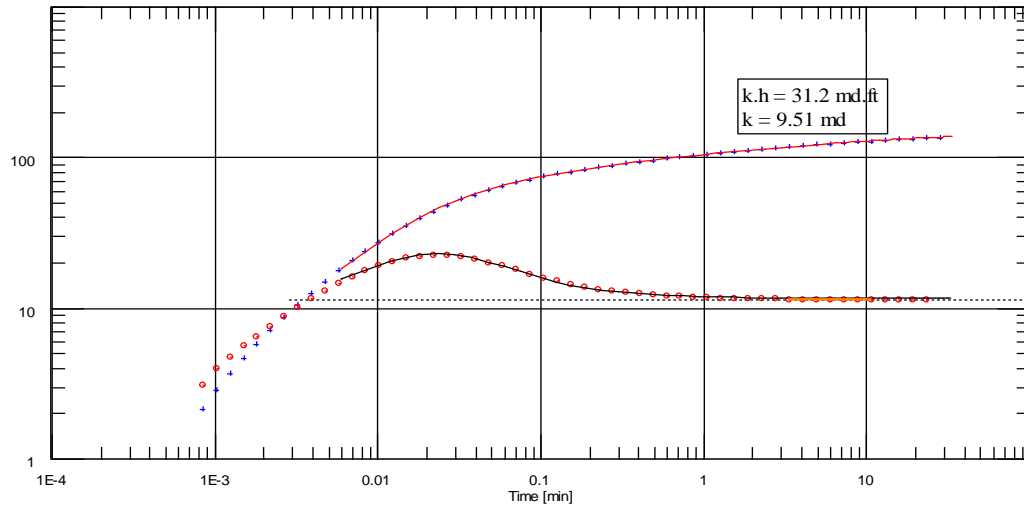


Figure 5.36: Log-log plot of uncalibrated model for IPTT#3 interval.

As illustrated in Figure 5.36, uncalibrated horizontal permeability of this SRES-IPTT#1 model equals 9.51 mD, or permeability thickness equals 31.2 mD.ft. However, from the actual measurement of this interval, the interpreted horizontal permeability equals 32.5 mD, or permeability thickness equals 109 mD.ft. Therefore,

$$\begin{aligned}
 k_{\text{measurement(IPTT\#3)}} &= c \cdot k_{\text{SRES-IPTT\#3}} \\
 c_{\text{IPTT\#3}} &= k_{\text{measurement(IPTT\#3)}} / k_{\text{SRES-IPTT\#3}} \\
 c_{\text{IPTT\#3}} &= 29.54 / 9.51 \approx 3.11
 \end{aligned}$$

where

$$\begin{aligned}
 k_{\text{measurement(IPTT\#3)}} &= \text{permeability derived from the measurement at IPTT\#3} \\
 k_{\text{SRES-IPTT\#3}} &= \text{permeability derived from uncalibrated model at IPTT\#3} \\
 c_{\text{IPTT\#3}} &= \text{calibration coefficient of IPTT\#3}
 \end{aligned}$$

Figures 5.37, 5.38, 5.39 show matching results after the calibration coefficient of IPTT#2 was multiplied to k_r, k_θ and k_z of the original model. Blue points represent the actual acquisition data; green points represent the simulated result from the single well model; and line is the analysis to obtain reservoir parameters from the simulation result.

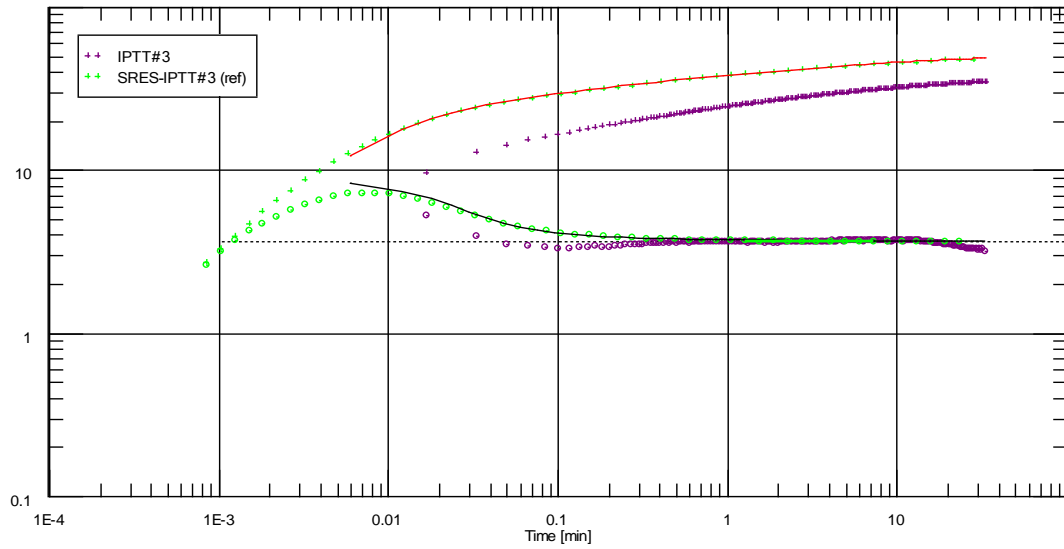


Figure 5.37: Log-log plot of calibrated model for IPTT#3 interval.

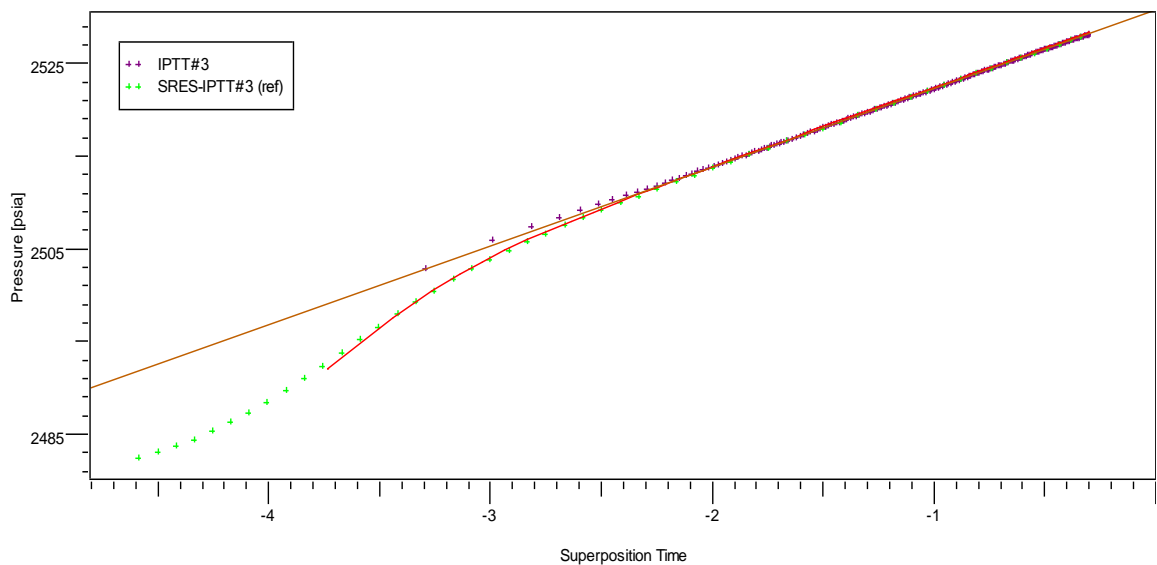


Figure 5.38: Semi-log plot of calibrated model for IPTT#3 interval.

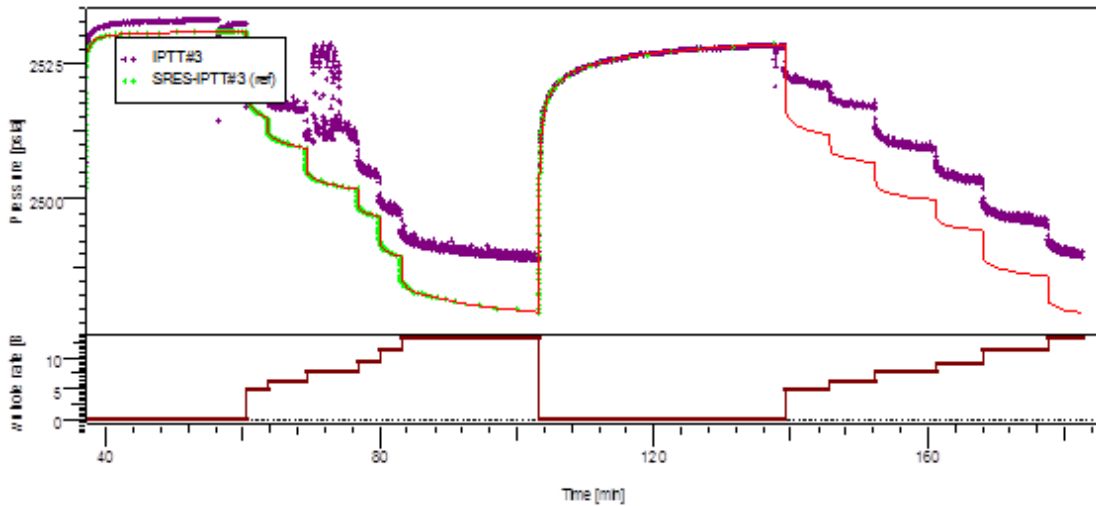


Figure 5.39: History plot of calibrated model for IPTT#3 interval.

The calibration coefficient derived from the simulated pressure response of IPTT#3 interval was also multiplied to k_r, k_θ and k_z of IPTT#1 and IPTT#2. Since the calibration coefficient was calibrated from a interval which has a thickness of 3.28 ft, it needs to be normalized based on the thickness of each interval before being multiplied to k_r, k_θ and k_z of other intervals. The value of $c_{IPTT\#3}$ (3.11) was divided by 3.28 to obtain the normalized coefficient of 0.95 per ft of thickness. This normalized coefficient was adjusted based on thickness of each interval before it was used as a multiplier as shown in Table 5.5.

Table 5.5: Coefficients of intervals using normalized coefficient result from IPTT#3.

Interval	Thickness (ft)	Normalized coefficient	Calibration coefficient
IPTT#1	10.01	0.95	9.50
IPTT#2	29.63	0.95	28.15
IPTT#3	3.28	0.95	3.11

After each calibration coefficient was applied to each simulation model of IPTT#1 and IPTT#2 according to Table 5.5, the results of matching pressure from calibration coefficients are illustrated in Figures 5.40, 5.41 and 5.42 for IPTT#1 interval and Figures 5.43, 5.44 and 5.45 for IPTT#2 interval.

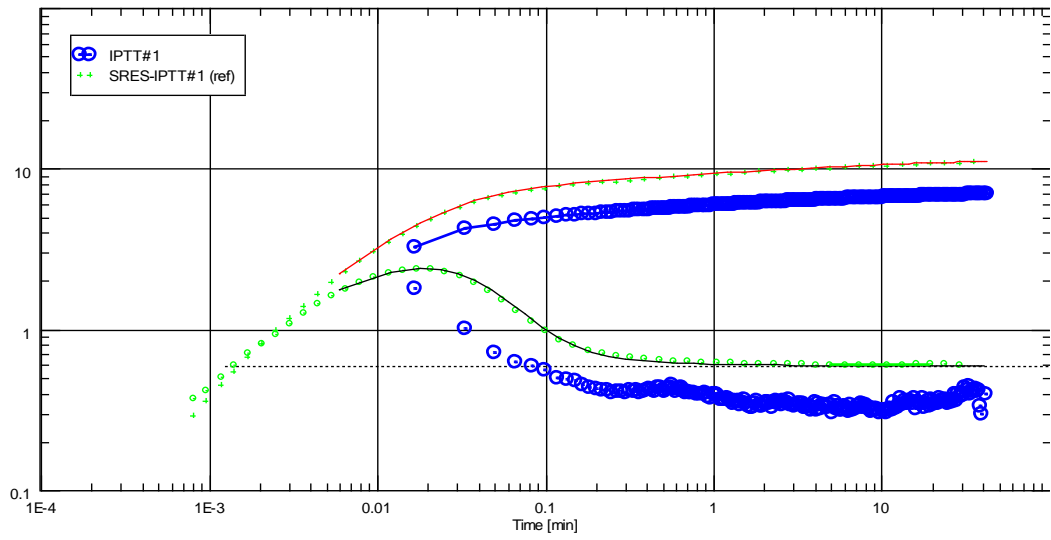


Figure 5.40: Log-log plot of calibrated model for IPTT#1 interval.

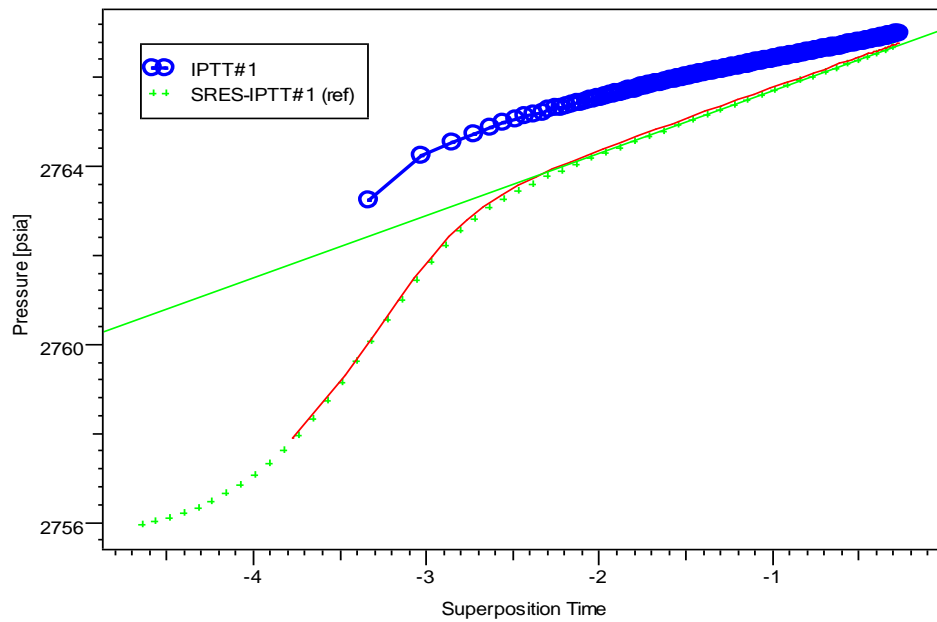


Figure 5.41: Semi-log plot of calibrated model for IPTT#1 interval.

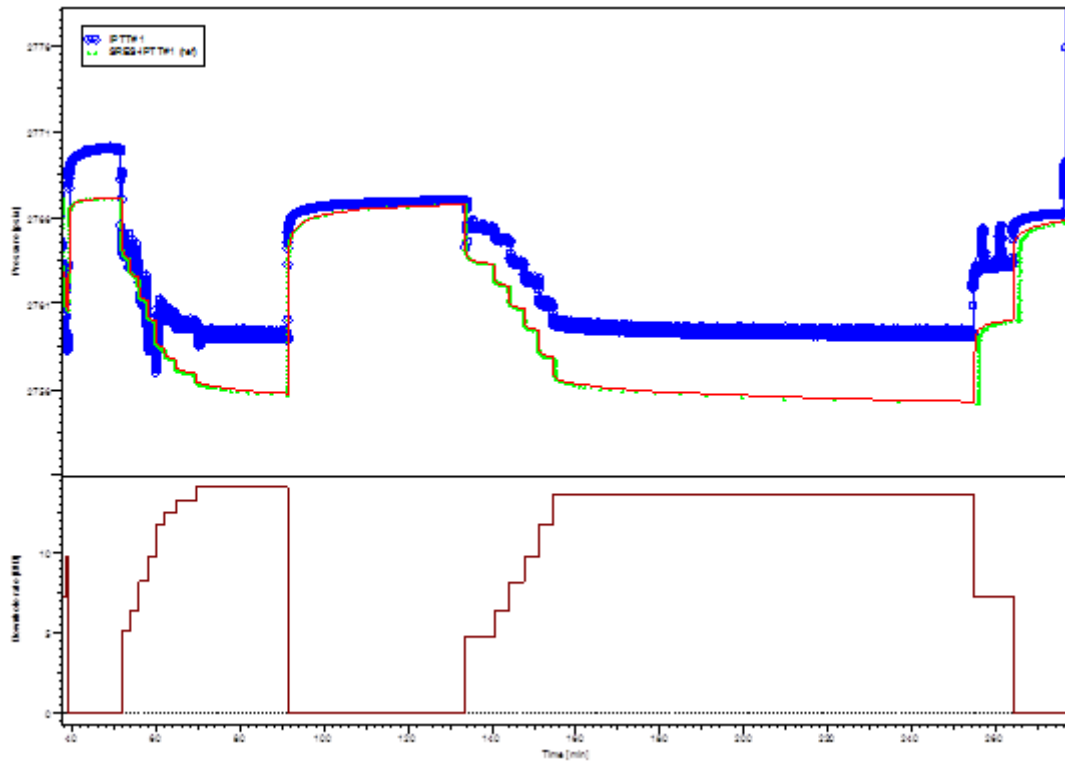


Figure 5.42: History plot of calibrated model for IPTT#1 interval.

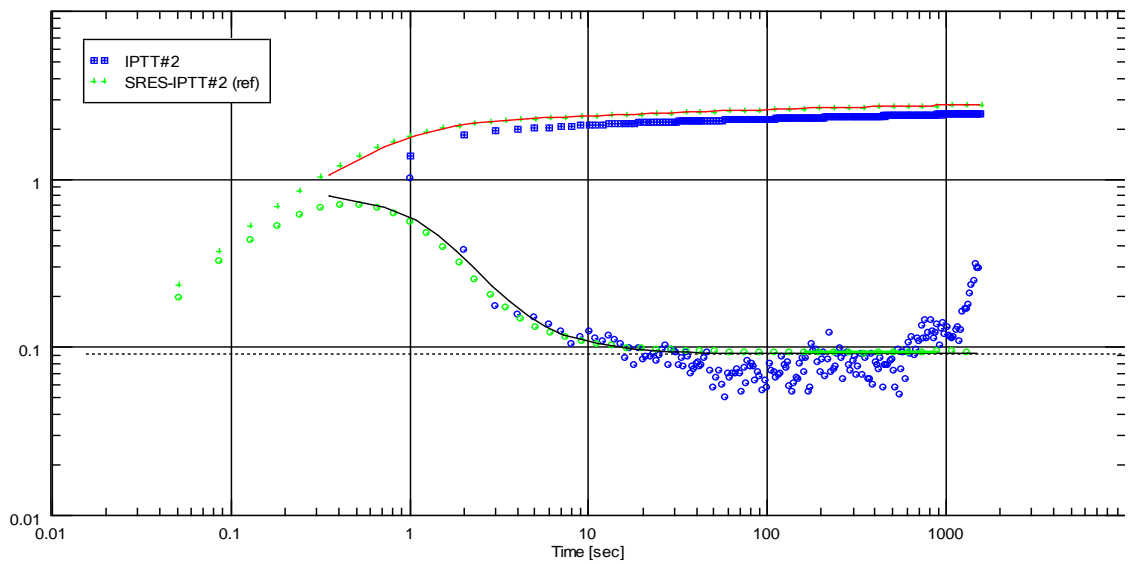


Figure 5.43: Log-log plot of calibrated model for IPTT#2 interval.

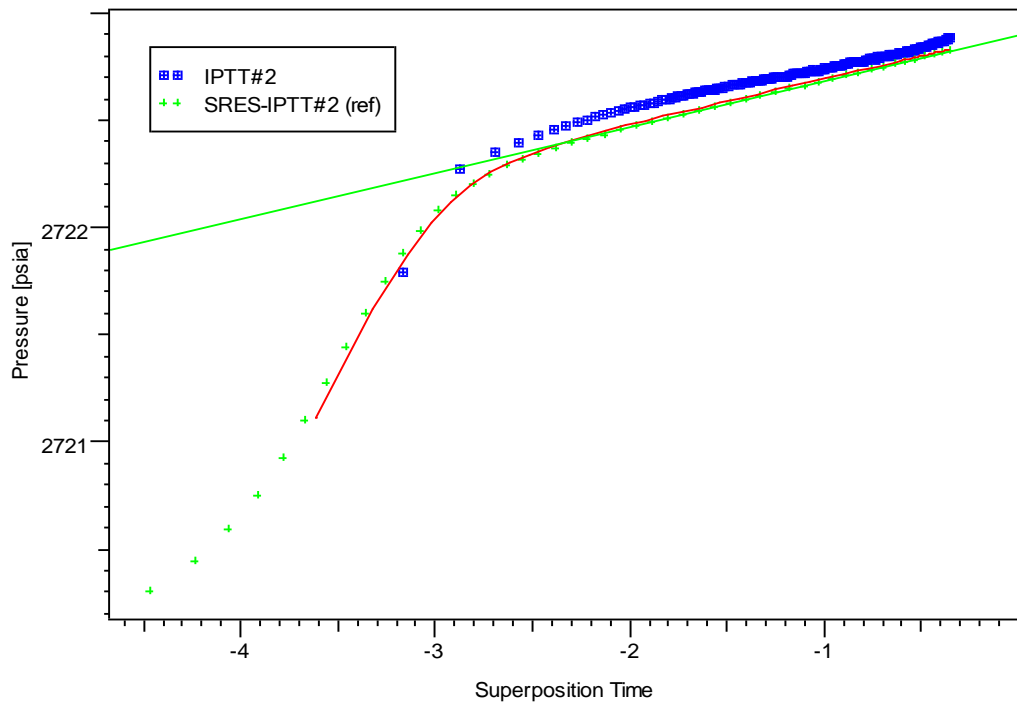


Figure 5.44: Semi-log plot of calibrated model for IPTT#2 interval.

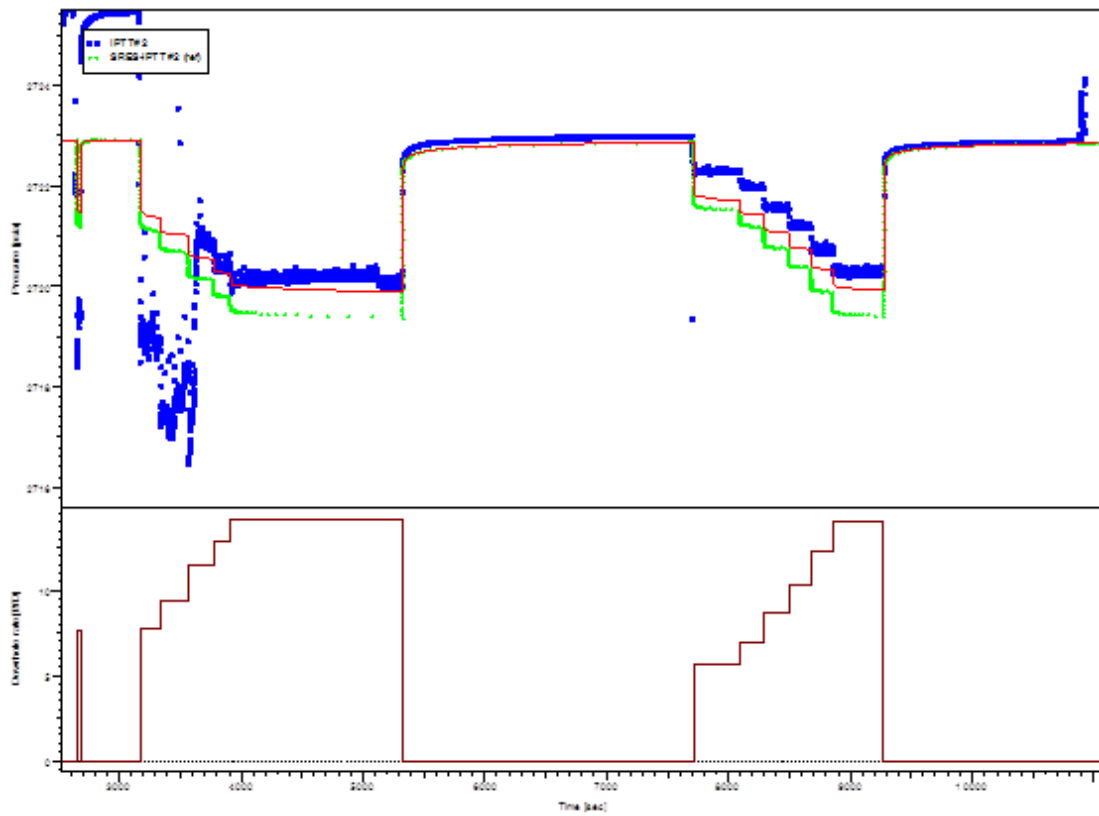


Figure 5.45: History plot of calibrated model for IPTT#2 interval.

5.2.4 Discussion

Table 5.6 compares the horizontal permeabilities from WFT measurements and horizontal permeabilities from pressure response of single well models according to SRES-IPTT#1, SRES-IPTT#2 and SRES-IPTT#3 .

Table 5.6: Horizontal permeability from WFT and all single well models.

Calibrated Model	WFT Measurement	SRES-IPTT#1	Error	SRES-IPTT#2	Error	SRES-IPTT#3	Error
	k_h (mD)	k_h (mD)	(%)	k_h (mD)	(%)	k_h (mD)	(%)
SRES-IPTT#1	116.92	116.92	0	250.12	42.23	55.79	88.86
SRES-IPTT#2	176	81.75	30.08	176	0	39.63	34.16
SRES-IPTT#3	29.54	64.06	45.24	138.73	21.11	29.76	0.75

The case of using calibrated model from SRES-IPTT#1 and SRES-IPTT#3 are looked over. Since the single well model has an error value up to 88.86%, interpretation result from the WFT measurement at IPTT#1 and 45.24% interpretation result from the WFT measurement at IPTT#3 intervals. They were investigated and found that the derivatives in the log-log plot indicate that there are possibility of two radial flows as illustrated in Figure 5.46 and Figure 47. The new interpretation, the first radial flow yields a permeability-thickness of 910 mD.ft, and the second radial flow gives permeability-thickness of 1170 mD.ft. for IPTT#1 and the first radial flow yields a permeability-thickness of 109 mD.ft, and the second radial flow gives permeability-thickness of 97.5 mD.ft for IPTT#3.

The multipliers from IPTT#1 and IPTT#3 were referred to permeability-thickness of the second radial flow. From well test principle, the radius of investigation of the second radial flow is higher than that of the first radial flow. Since borehole electrical image measurement has very shallow depth of investigation (a few inch always from the borehole), the first radial flow should be the right response instead of the second one. Therefore, the reservoir model should be changed from homogenous infinite-acting model to radial composite model. Reservoir behavior of radial composite model is illustrated in Figure 5.48. However, the single

well model in this studied was assumed as homogenous infinite model. The permeability-thickness of first radial flow was assumed that thickness remains constant and permeability can be various in order to simplify the single model simulation. The modified SRES-IPTT#1 and SRES-IPTT#3 cases from the analysis above, this single well model entitled as MODIFIED-SRES-IPTT#1 and MODIFIED-SRES-IPTT#3 cases in Sections 5.2.5 and 5.2.6 respectively.

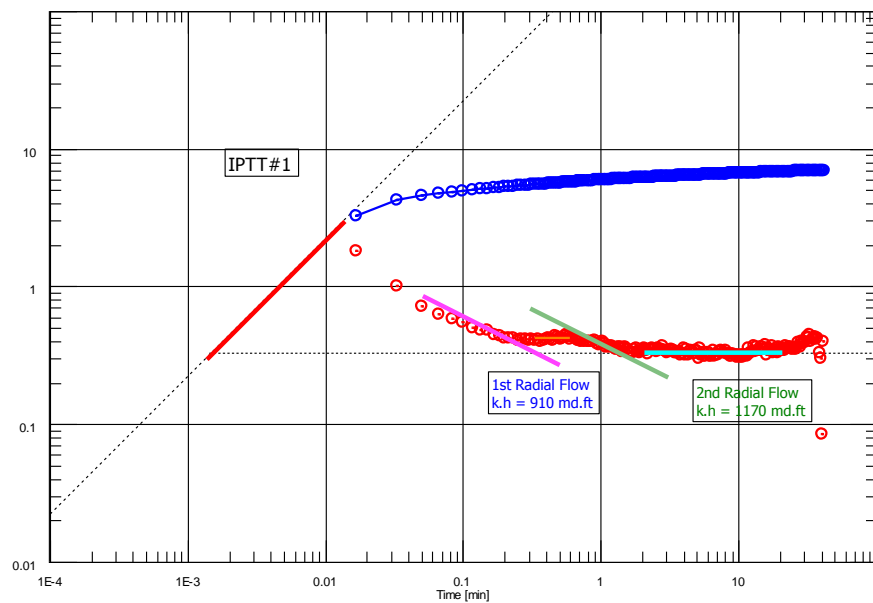


Figure 5.46: Modified Log-log plot of WFT measurement at IPTT#1 interval.

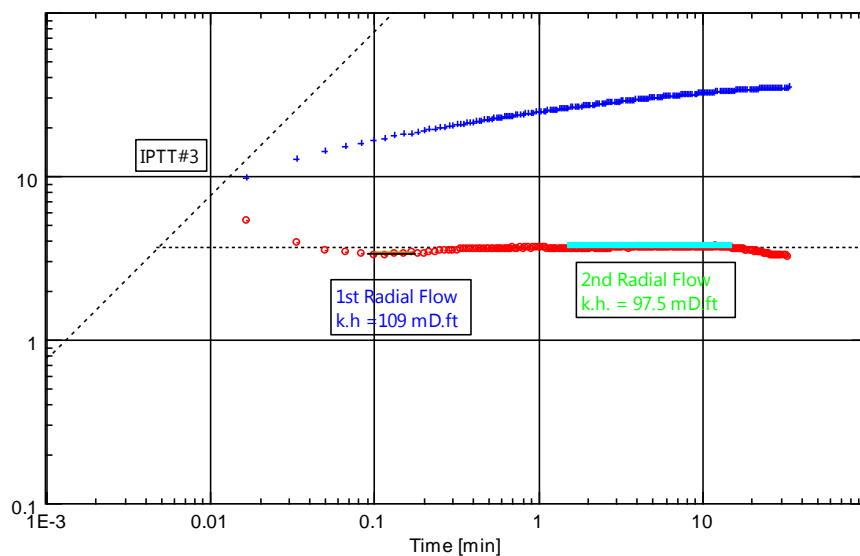


Figure 5.47: Modified Log-log plot of WFT measurement at IPTT#3 interval.

Figures 5.49, 5.50, 5.51 show matching results after the calibration coefficient of IPTT#1 was multiplied to k_r, k_{θ} and k_z of the original model. Blue points represent the actual acquisition data; green points represent the simulated result from the single well model; and line is the analysis to obtain reservoir parameters from the simulation result.

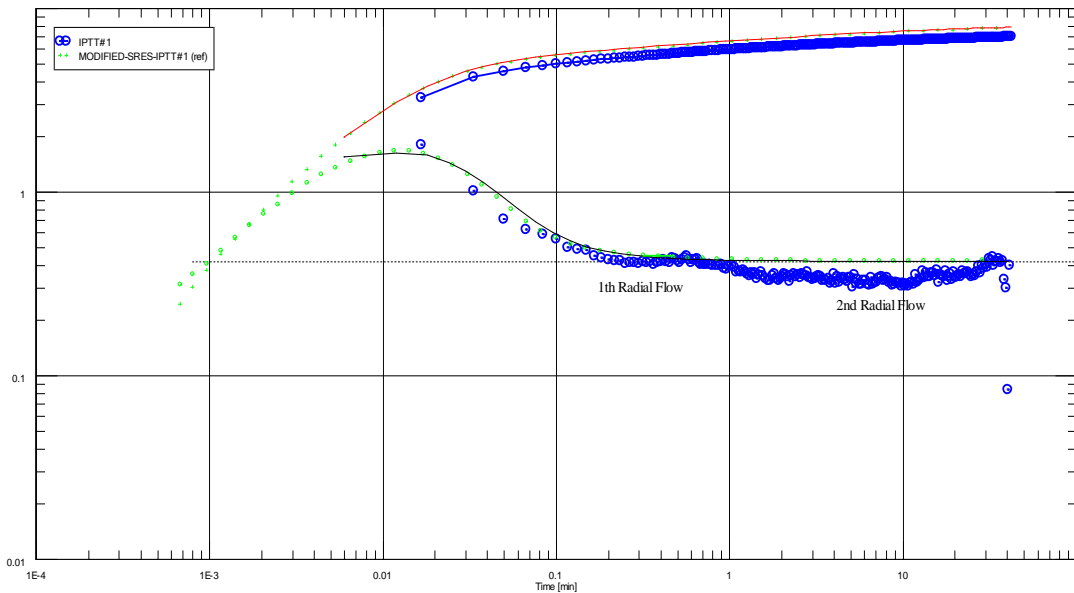


Figure 5.49: Log-log plot of actual data and calibrated single well model for IPTT#1.

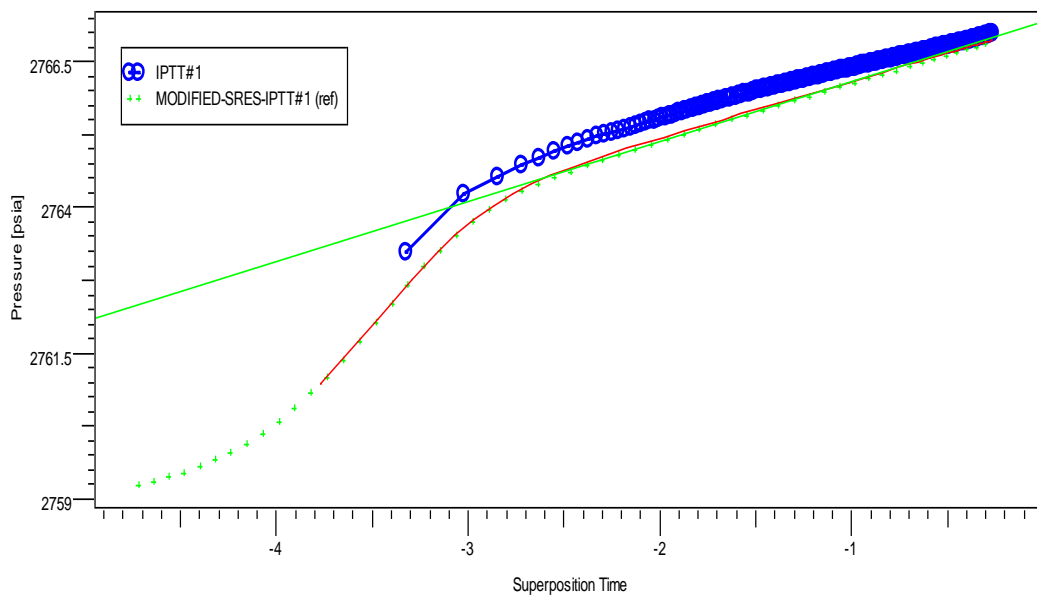


Figure 5.50: Semi-log plot of actual data and calibrated single well model for IPTT#1.

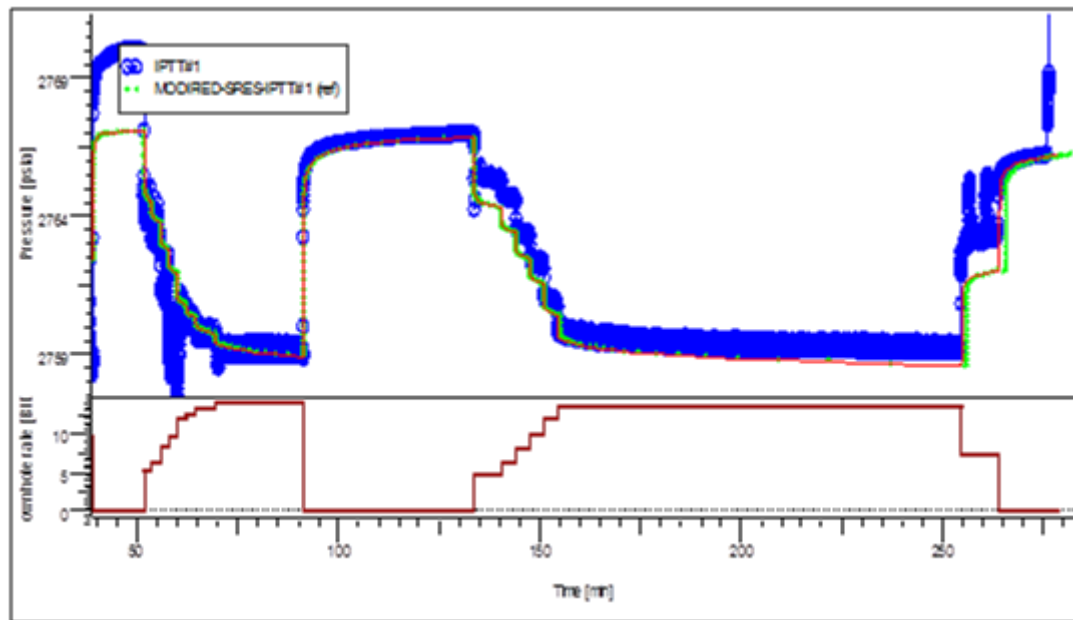


Figure 5.51: History plot of actual data and calibrated single well model for IPTT#1.

The calibration coefficient derived from the simulated pressure response of IPTT#1 interval was also multiplied to k_r, k_θ and k_z of IPTT#2 and IPTT#3. Since the calibration coefficient was calibrated from a interval which has a thickness of 10.01 ft, it needs to be normalized based on the thickness of each interval before being multiplied to k_r, k_θ and k_z of other intervals. The value of $c_{\text{MODIFIED-IPTT\#1}}$ (13.66) was divided by 10.01 to obtain the normalized coefficient of 1.365 per ft of thickness. This normalized coefficient was adjusted based on thickness of each interval before it was used as a multiplier as shown in Table 5.7.

Table 5.7: Coefficients of intervals using normalized coefficient result from IPTT#1.

Interval	Thickness (ft)	Normalized coefficient	Calibration coefficient
IPTT#1	10.01	1.365	13.66
IPTT#2	29.63	1.365	40.45
IPTT#3	3.28	1.365	4.48

After each calibration coefficient was applied to each simulation model of IPTT#2 and IPTT#3 according to Table 5.7, the results of matching pressure from calibration coefficients are illustrated in Figures 5.52, 5.53 and 5.54 for IPTT#2 interval and Figures 5.55, 5.56 and 5.57 for IPTT#3 interval.

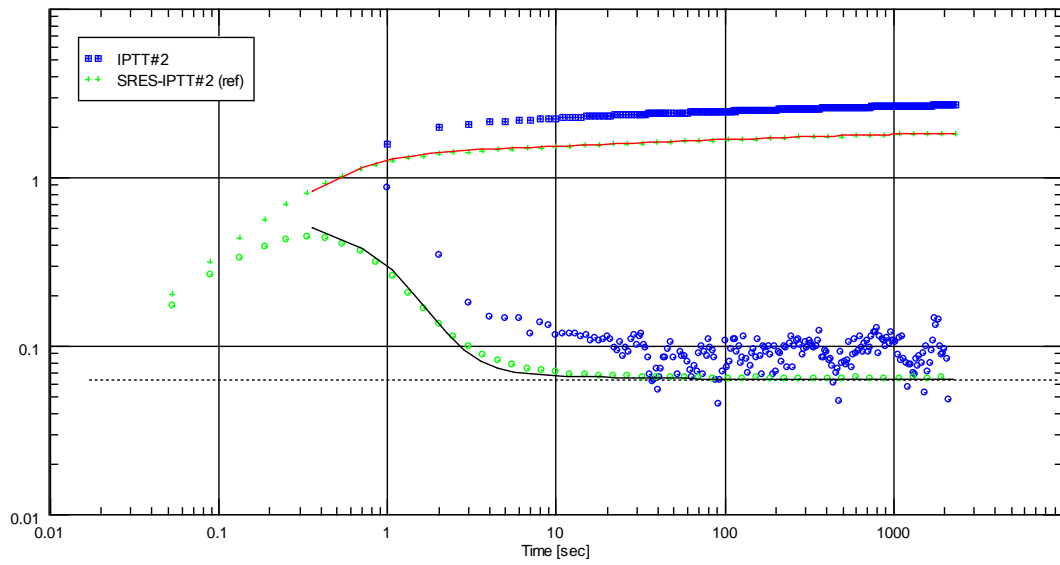


Figure 5.52: Log-log plot of actual data and calibrated single well model for IPTT#2.

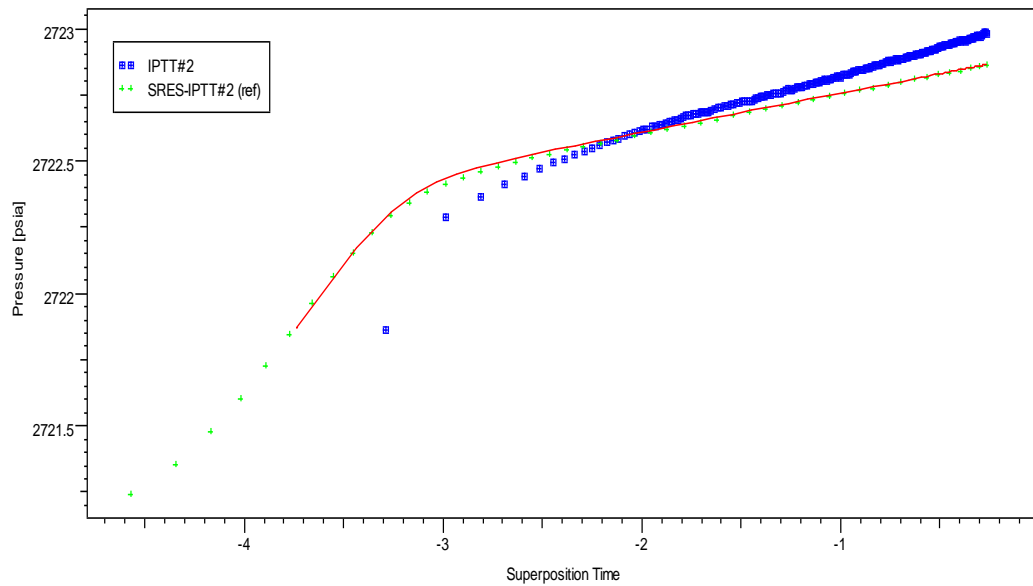


Figure 5.53: Semi-log plot of actual data and calibrated single well model for IPTT#2.

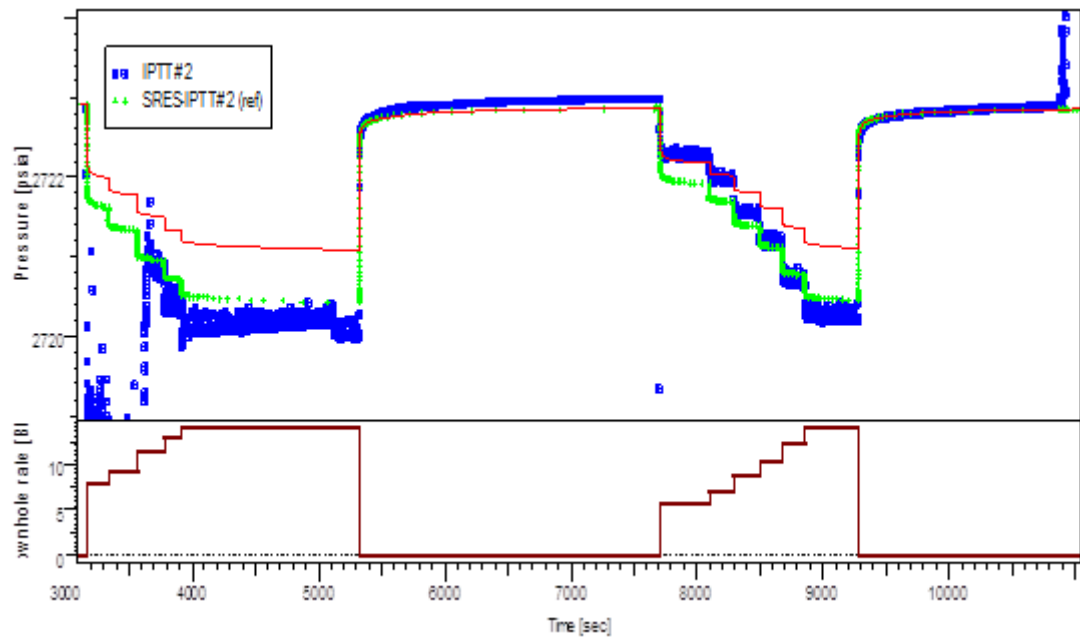


Figure 5.54: History plot of actual data and calibrated single well model for IPTT#2.

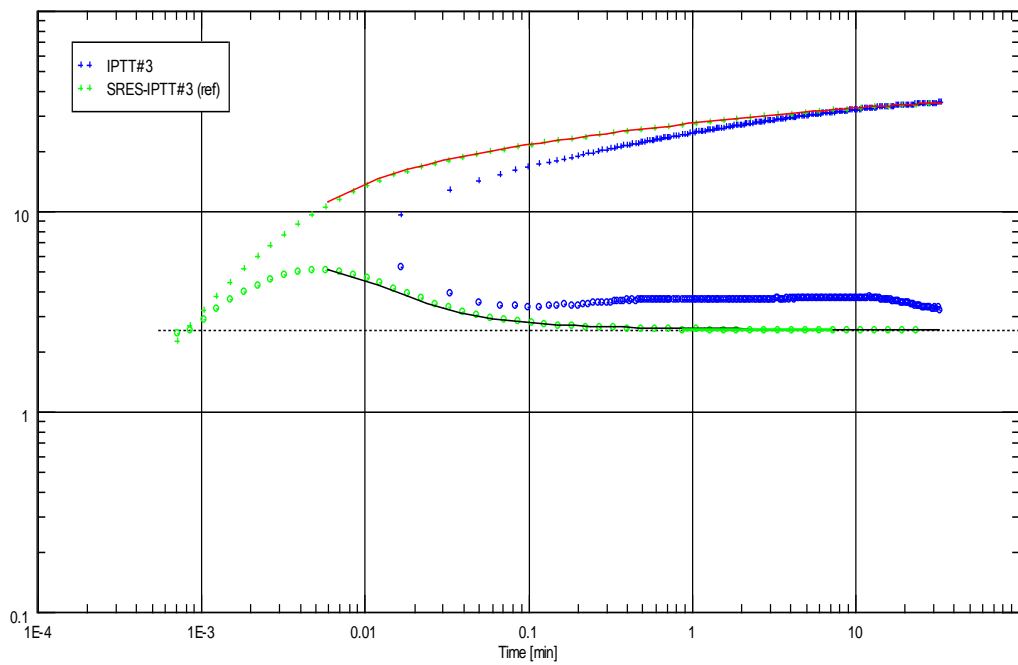


Figure 5.55: Log-log plot of actual data and calibrated single well model for IPTT#3.

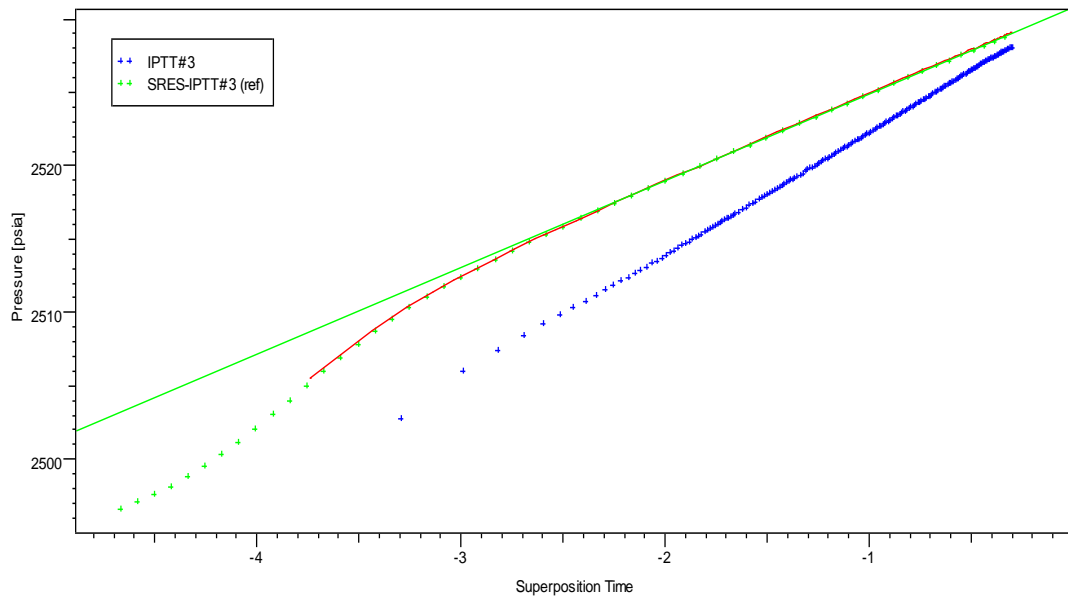


Figure 5.56: Semi-log Plot of actual data and calibrated single well model for IPTT#3.

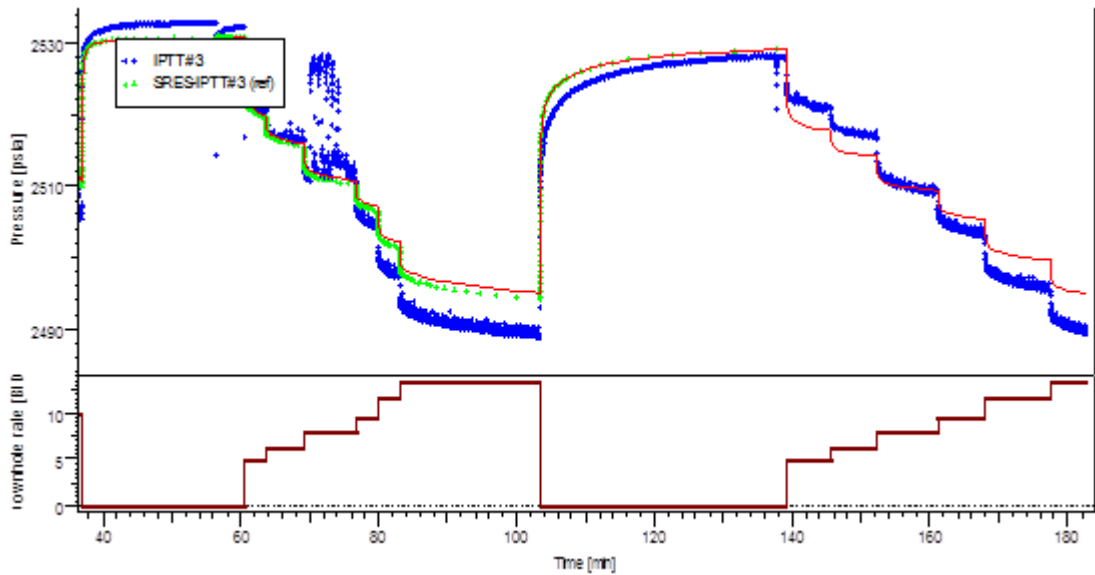


Figure 5.57: History plot of actual data and calibrated single well model for IPTT#3.

5.2.6 MODIFIED-SRES-IPTT#3

In the previous section, SRES-IPTT#3 case was referred to permeability thickness of the first radial flow with the constant thickness. As illustrated in Figure 5.36, uncalibrated horizontal permeability of this SRES-IPTT#3 model equals 9.51 mD, or permeability thickness equals 31.19 mD.ft. However, from the first radial flow

of this interval, the interpreted horizontal permeability equals 32.5 mD, or permeability thickness equals 109 mD.ft. Therefore,

$$\begin{aligned}
 k_{\text{measurement(MODIFIED-IPTT\#3)}} &= c \cdot k_{\text{(MODIFIED-SRES-IPTT\#3)}} \\
 C_{\text{(MODIFIED-IPTT\#3)}} &= k_{\text{measurement(MODIFIED-IPTT\#3)}}/k_{\text{(MODIFIED-SRES-IPTT\#3)}} \\
 C_{\text{(MODIFIED-IPTT\#3)}} &= 32.5/9.51 \approx 3.42
 \end{aligned}$$

where

$$\begin{aligned}
 k_{\text{measurement(MODIFIED-IPTT\#3)}} &= \text{permeability derived from the} \\
 &\quad \text{measurement at IPTT\#3} \\
 k_{\text{(MODIFIED-SRES-IPTT\#3)}} &= \text{permeability derived from uncalibrated} \\
 &\quad \text{model at IPTT\#3} \\
 C_{\text{(MODIFIED-IPTT\#3)}} &= \text{calibration coefficient of IPTT\#3}
 \end{aligned}$$

Figures 5.58, 5.59, 5.60 show matching results after the calibration coefficient of IPTT#3 was multiplied to k_r, k_θ and k_z of the original model. Blue points represent the actual acquisition data; green points represent the simulated result from the single well model; and line is the analysis to obtain reservoir parameters from the simulation result.

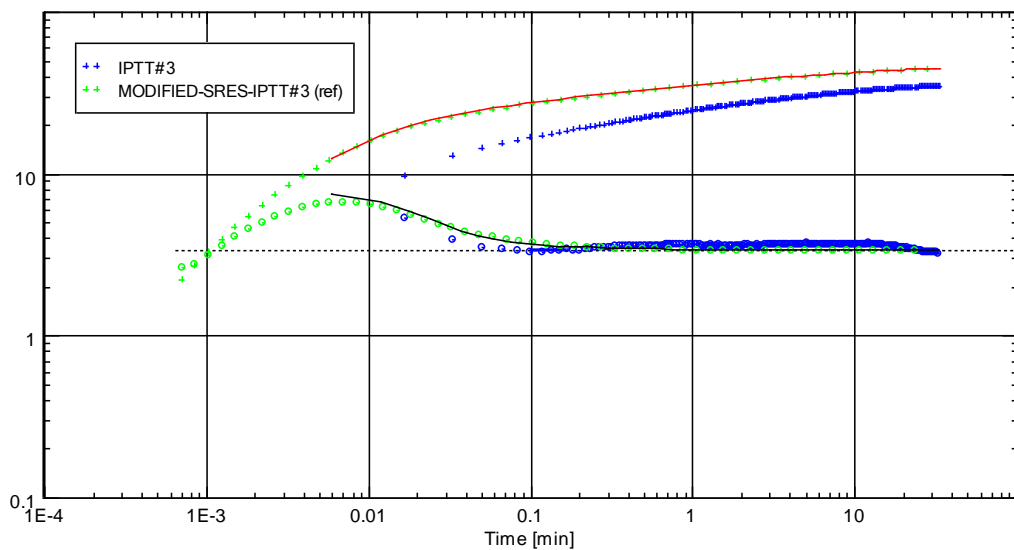


Figure 5.58: Log-log plot of actual data and calibrated single well model for IPTT#3.

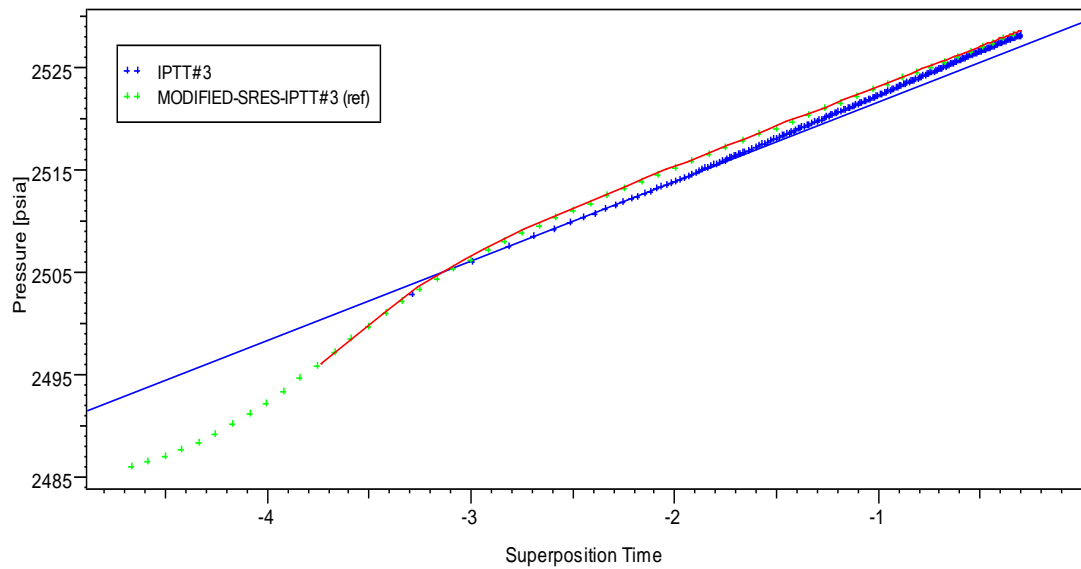


Figure 5.59: Semi-log plot of actual data and calibrated single well model for IPTT#3.

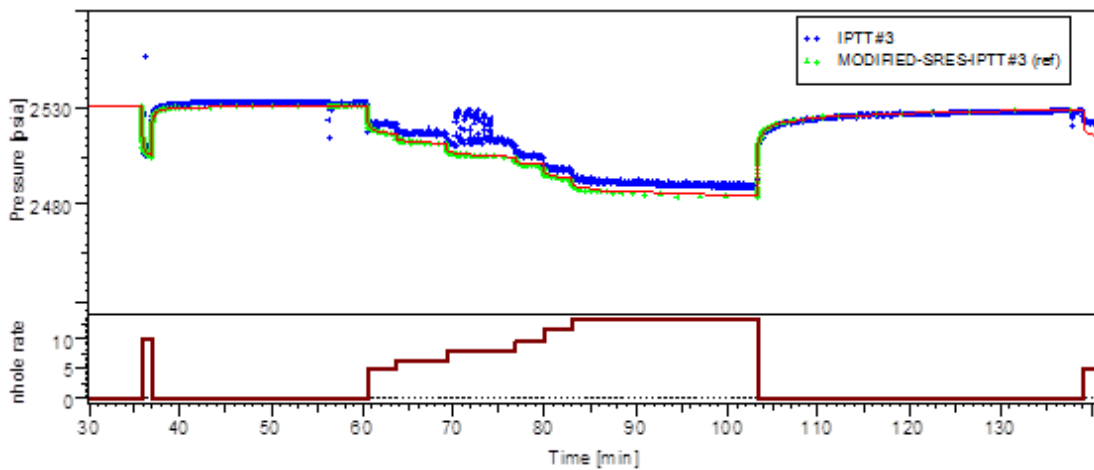


Figure 5.60: History plot of actual data and calibrated single well model for IPTT#3.

The calibration coefficient derived from the simulated pressure response of IPTT#3 interval was also multiplied to k_r, k_θ and k_z of IPTT#1 and IPTT#2. Since the calibration coefficient was calibrated from a interval which has a thickness of 3.28 ft, it needs to be normalized based on the thickness of each interval before being multiplied to k_r, k_θ and k_z of other intervals. The value of $c_{\text{MODIFIED-IPTT\#3}}$ (3.42) was divided by 3.28 to obtain the normalized coefficient of 1.043 per ft of thickness. This normalized coefficient was adjusted based on thickness of each interval before it was used as a multiplier as shown in Table 5.8.

Table 5.8: Coefficients of intervals using normalized coefficient result from IPTT#3.

Interval	Thickness (ft)	Normalized coefficient	Calibration coefficient
IPTT#1	10.01	1.043	10.44
IPTT#2	29.63	1.043	30.90
IPTT#3	3.28	1.043	3.42

After each calibration coefficient was applied to each simulation model of IPTT#1 and IPTT#2 according to Table 5.8, the results of matching pressure from calibration coefficients are illustrated in Figures 5.61, 5.62 and 5.63 for IPTT#1 interval and Figures 5.64, 5.65 and 5.66 for IPTT#2 interval.

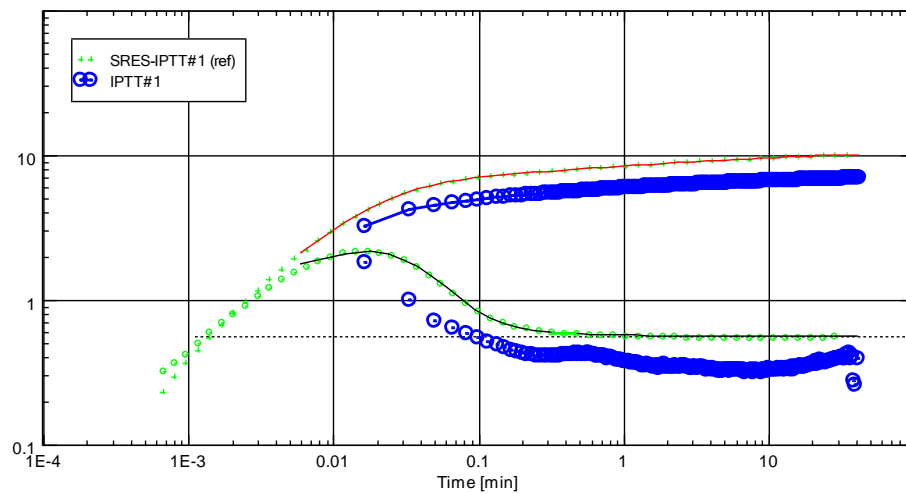


Figure 5.61: Log-log plot of actual data and calibrated single well model for IPTT#1.

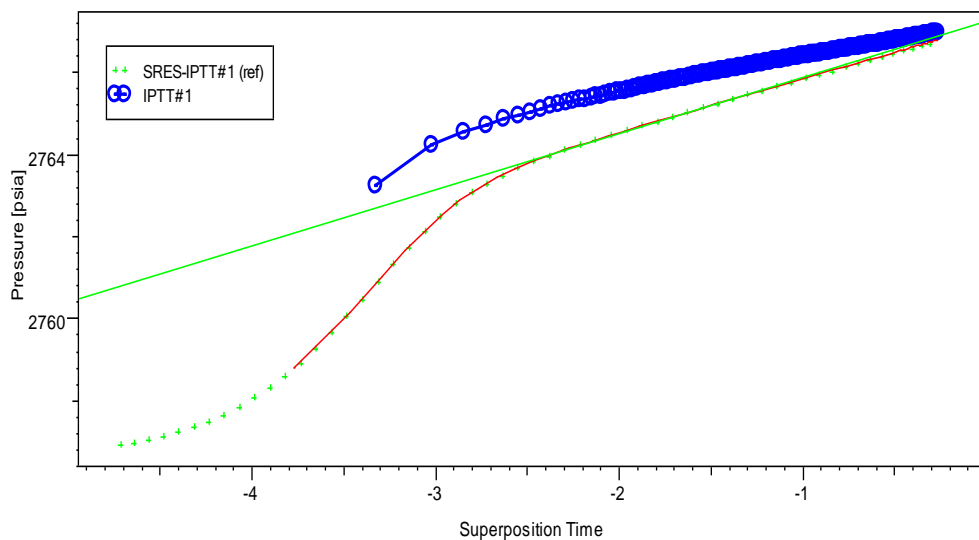


Figure 5.62: Semi-log plot of actual data and calibrated single well model for IPTT#1.

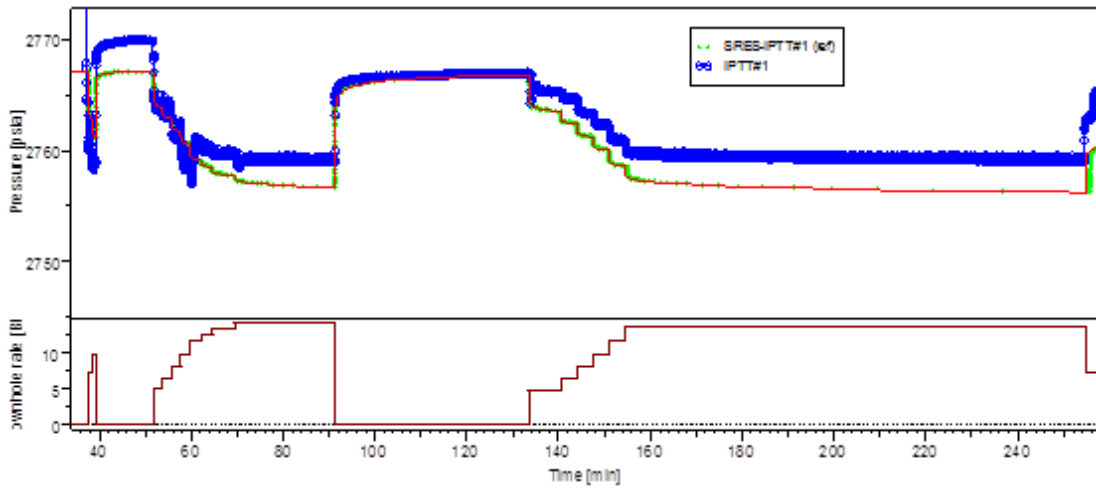


Figure 5.63: History plot of actual data and calibrated single well model for IPTT#1.

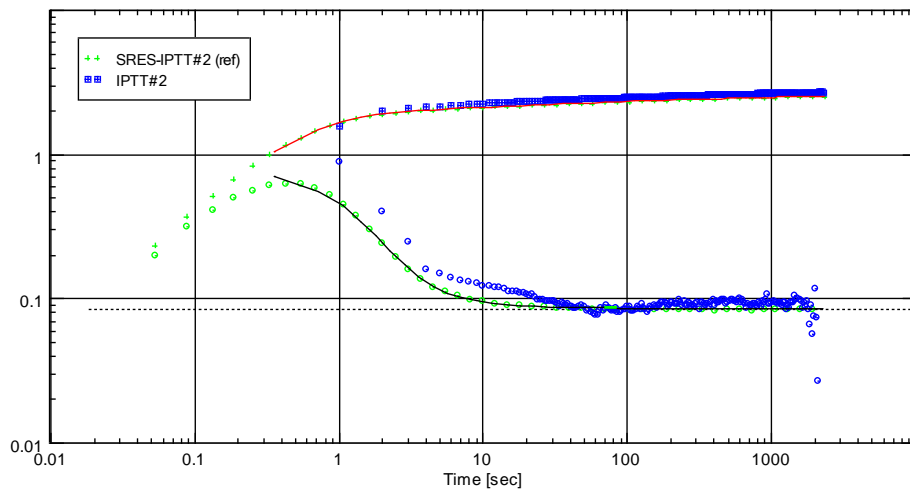


Figure 5.64: Log-log plot of actual data and calibrated single well model for IPTT#2.

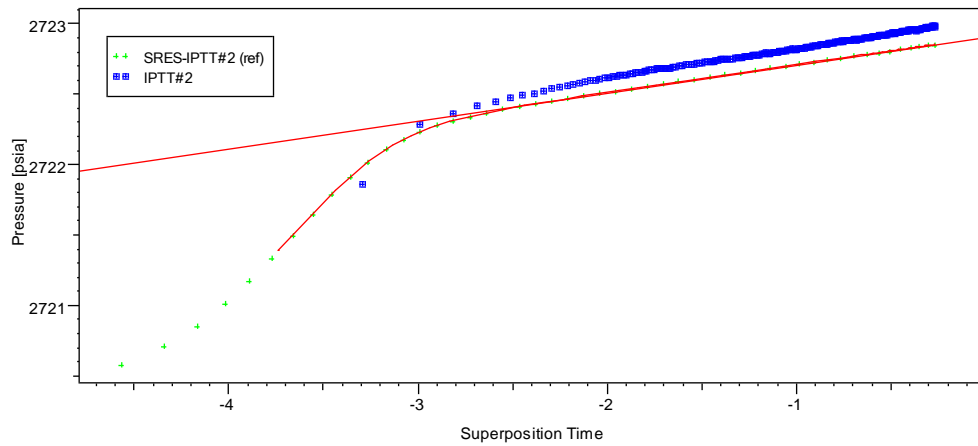


Figure 5.65: Semi-log plot of actual data and calibrated single well model for IPTT#2.

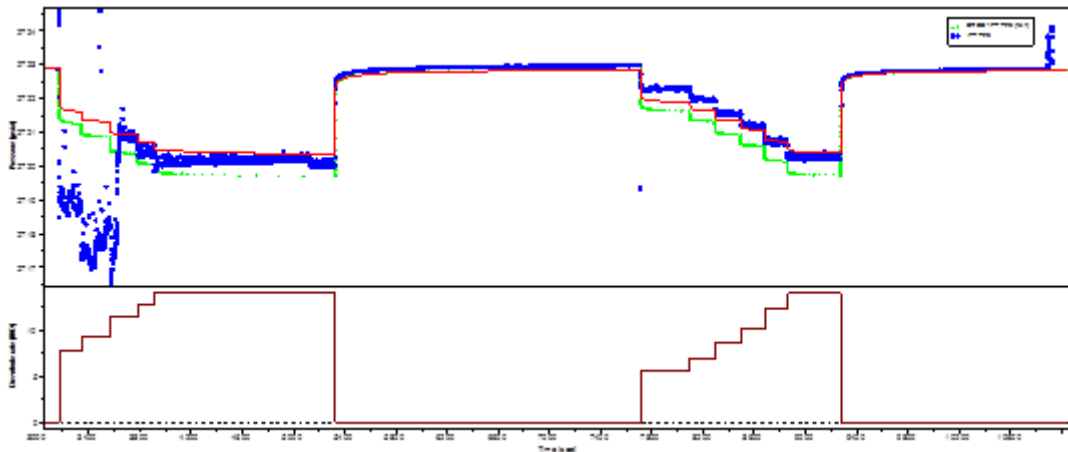


Figure 5.66: History plot of actual data and calibrated single well model for IPTT#2.

After SRES-IPTT#1 and SRES-IPTT#3 were revised as MODIFIED-SRES-IPTT#1 and MODIFIED-SRES-IPTT#3, normalized coefficients were applied to other intervals, the horizontal permeability error between actual measurements and single well model of other intervals decreased significantly. The error for SRES-IPTT#2 decreased from 42.23% to 14.20%, and that for SRES-IPTT#3 decreased from 88.86% to 43.87% from MODIFIED-SRES-IPTT#1. The error for SRES-IPTT#1 decreased from 29.60% to 25.16%, and that for SRES-IPTT#2 decreased from 21.11% to 14.20% from MODIFIED-SRES-IPTT#3. The result is illustrated in Table 5.9.

Table 5.9: k_h from the measurements and all modified single well models.

Calibrated Model	WFT Measurement	Normalized Coefficient	IPTT#1	Error	IPTT#2	Error	IPTT#3	Error
	k_h (md)	c	k_h (md)	(%)	k_h (md)	(%)	k_h (md)	(%)
MODIFIED -SRES-IPTT#1	91	1.365	91	0	201	14.30	42.5	43.87
SRES-IPTT#2	176	1.260	81.75	10.16	176	0	39.63	34.16
MODIFIED -SRES-IPTT#3	32.5	1.043	68.10	25.16	151	14.20	29.76	0.75

5.3 Result Comparison

From Sections 5.1 and 5.2, the summary of horizontal permeability from both single well models is shown in Table 5.10. The horizontal permeabilities from two single well models were derived from different types of indirect measurement. The fundamental of NMR logging tool response for the fluid in the pore space and is used to measure lithology-independent effective porosity, pore size distribution, bound and movable fluid saturation, and permeability. On the other hand, SRES is derived from the formation conductivity which is measured from several micro-resistivity sensors from borehole electrical image tool. Therefore, permeability derived from NMR shows that it provides better horizontal permeability than Borehole Electrical Image. However, permeability from NMR is derived from Equation 3.1 in Chapter III, in which the constant “ a ” needs appropriate adjustment in order to match with other permeability measurement before being used as input in the single well model.

Table 5.10: Horizontal permeabilities from the measurements and single well models.

Single Well Model	IPTT#1	Error	IPTT#2	Error	IPTT#3	Error
	k_h (mD)	(%)	k_h (mD)	(%)	k_h (mD)	(%)
WFT	91		175.86		29.54	
NMR	102	12.08	176	0.08	40.70	37.77
MODIFIED-SRES-IPTT#1	91	0.00	201	14.30	42.50	43.87
SRES-IPTT#2	81.75	30.08	176	0.00	39.63	34.16
MODIFIED-SRES-IPTT#3	68.1	25.16	151	14.20	29.76	0.75

5.4 Well Productivity Prediction

Inflow Performance Relationship (IPR) is a mathematical tool used in production engineering to assess well productivity by plotting the well production rate against the flowing bottomhole pressure (BHP). The data required to create the IPR are obtained by measuring the production rates under various drawdown pressures. In this studied was using flowing bottomhole pressure and well production rate from

history plot of all intervals from the actual measurements and history plot of all intervals from simulation results of borehole electrical image single well model. Productivity Index (PI) is usually stated as the production volume delivered per psi of drawdown at the sandface (bbl/day/psi). Absolute Open Flow Potential (AOFP) is the maximum flow rate a well could theoretically deliver with zero pressure.

PI and AOFP estimations from the actual measurement are illustrated as IPR plots in Figures 5.67, 5.68 and 5.69 for IPTT#1, IPTT#2 and IPTT#3 respectively.

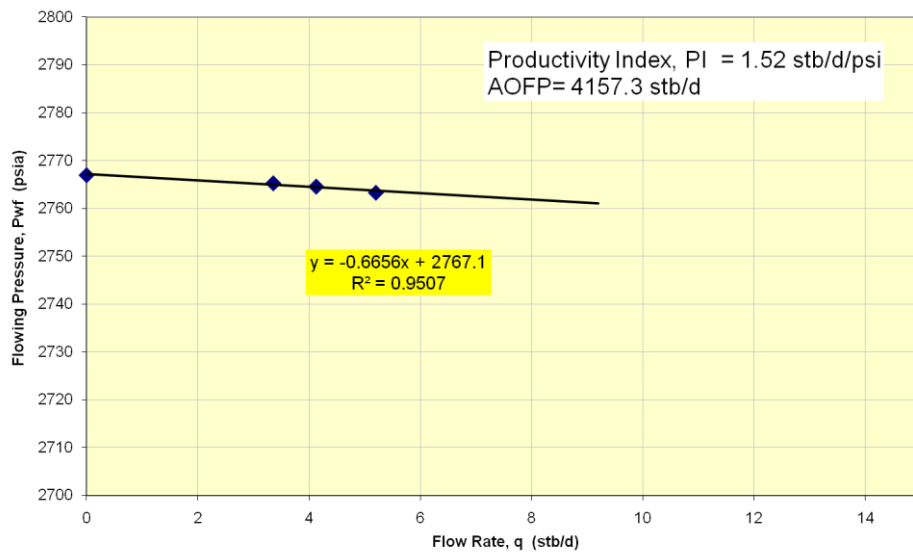


Figure 5.67: IPR plot from actual measurement of IPTT#1.

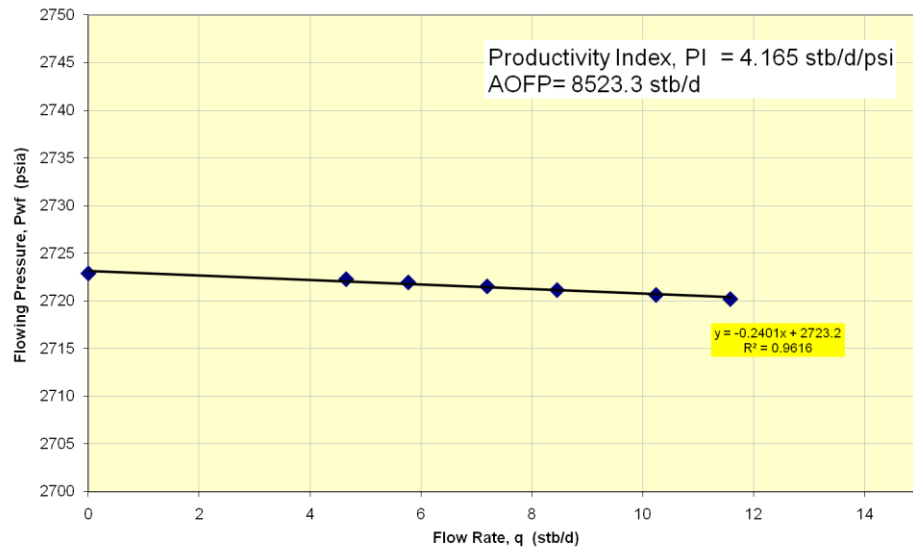


Figure 5.68: IPR plot from actual measurement of IPTT#2.

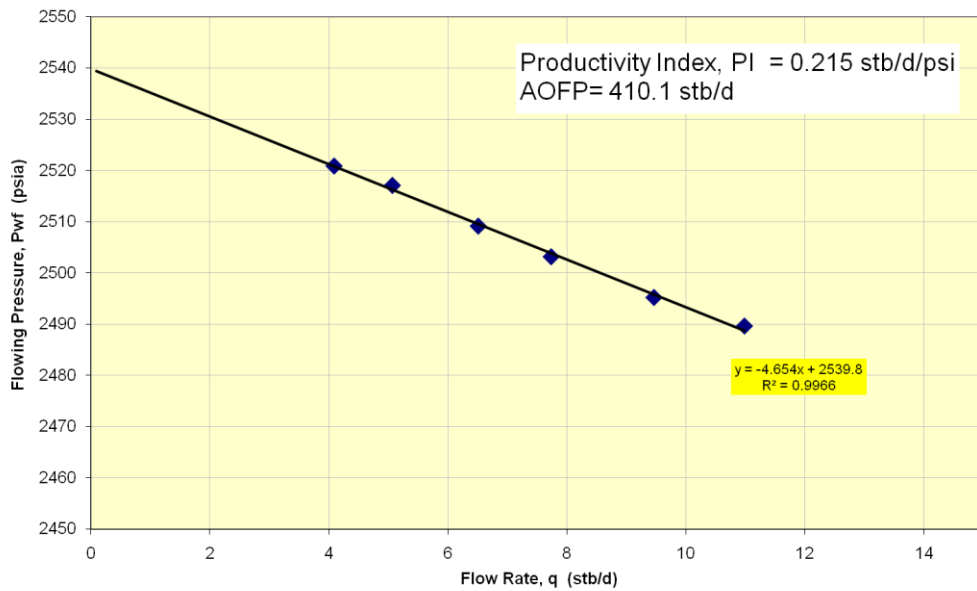


Figure 5.69: IPR plot from actual measurement of IPTT#3.

PI and AOFp estimations from the single well model of borehole electrical image based method calibrated from MODIFIED-SRES-IPTT#1 are illustrated as IPR plots in Figures 5.70, 5.71 and 5.72 for IPTT#1, IPTT#2 and IPTT#3 respectively.

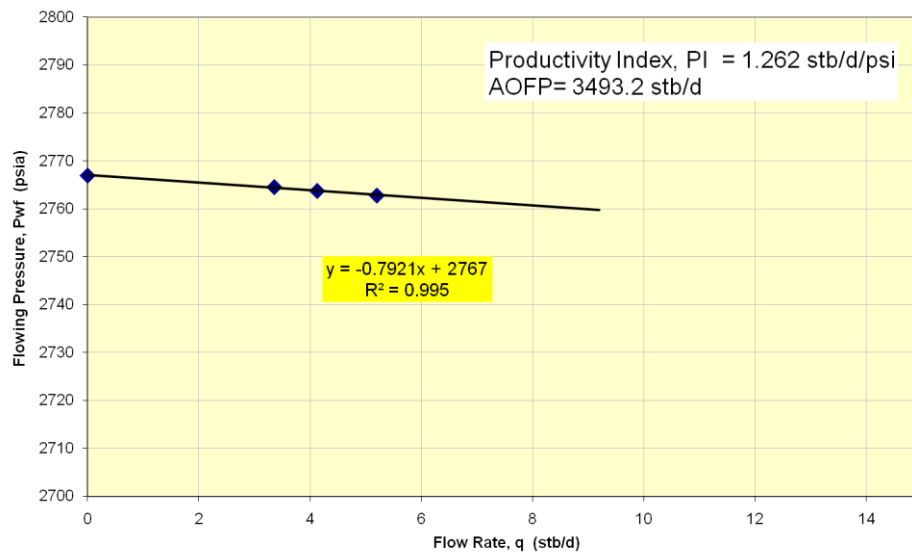


Figure 5.70: IPR plot from single well model of borehole electrical image based method calibrated from MODIFIED-SRES-IPTT#1 for IPTT#1.

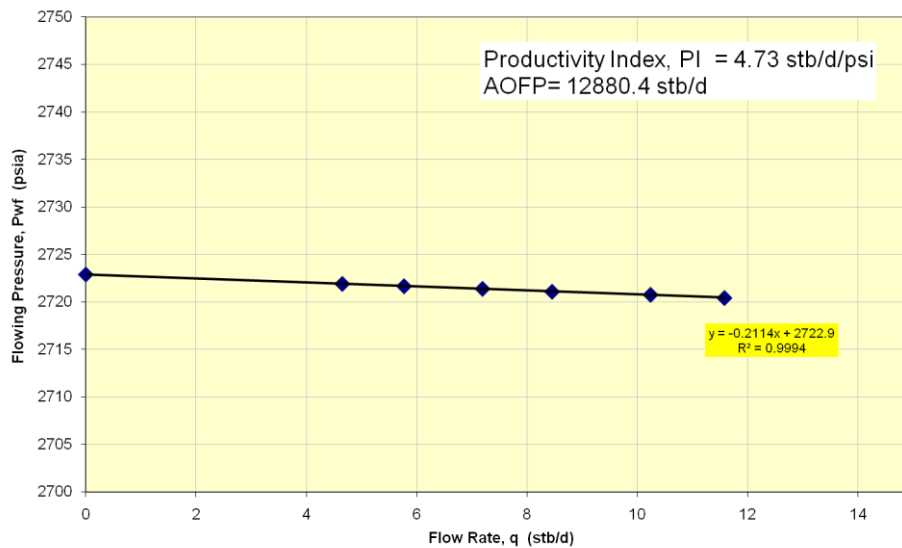


Figure 5.71: IPR plot from single well model of borehole electrical image based method calibrated from MODIFIED-SRES-IPTT#1 for IPTT#2.

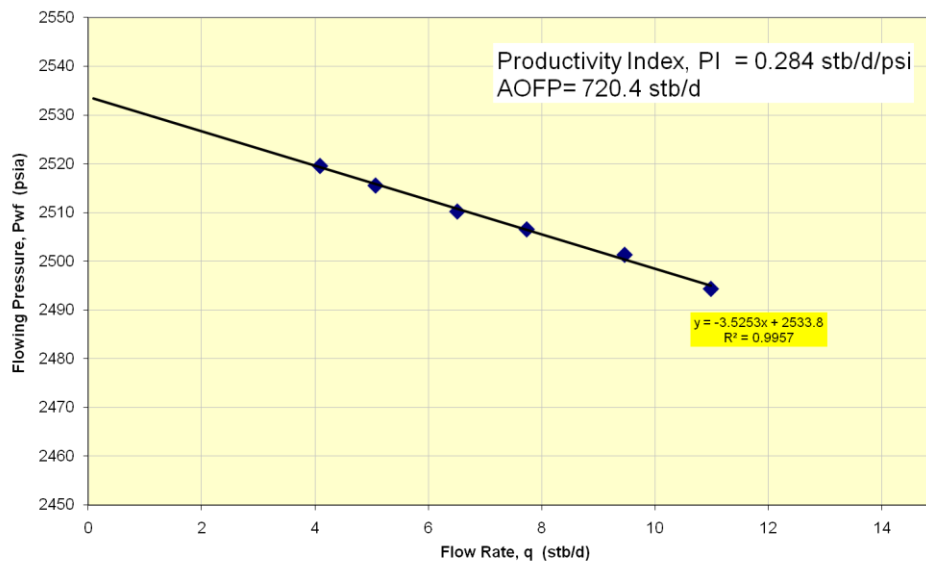


Figure 5.72: IPR plot from single well model of borehole electrical image based method calibrated from MODIFIED-SRES-IPTT#1 for IPTT#3.

PI and AOFP estimations from the single well model of borehole electrical image based method calibrated from SRES-IPTT#2 are illustrated as IPR plots in Figures 5.73, 5.74 and 5.75 for IPTT#1, IPTT#2 and IPTT#3 respectively.

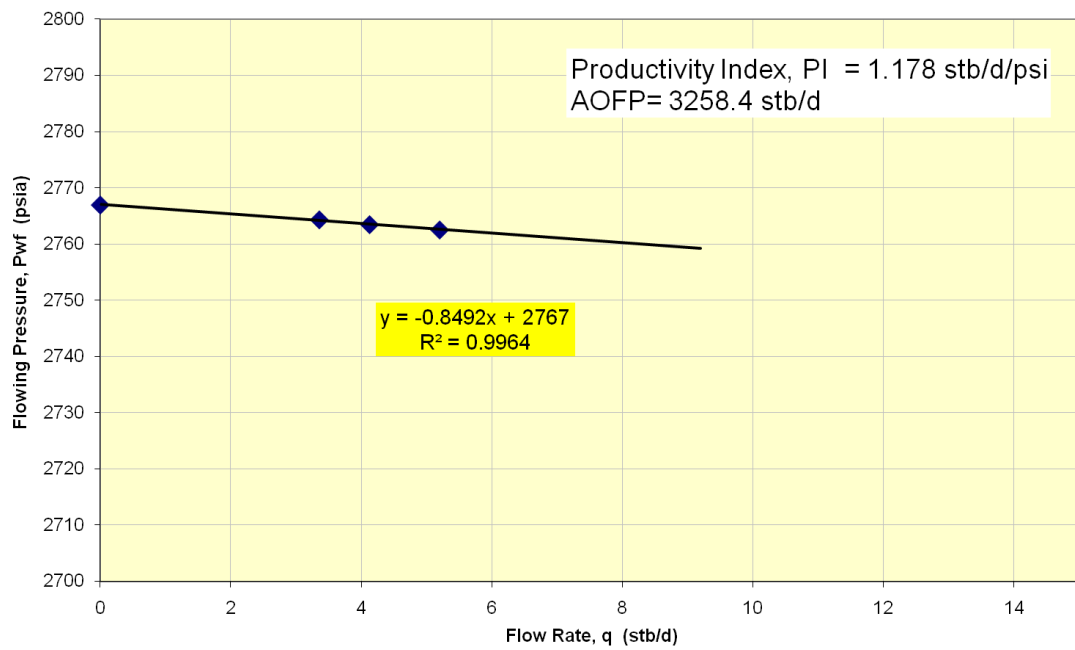


Figure 5.73: IPR plot from single well model of borehole electrical image based method calibrated from SRES-IPTT#2 for IPTT#1.

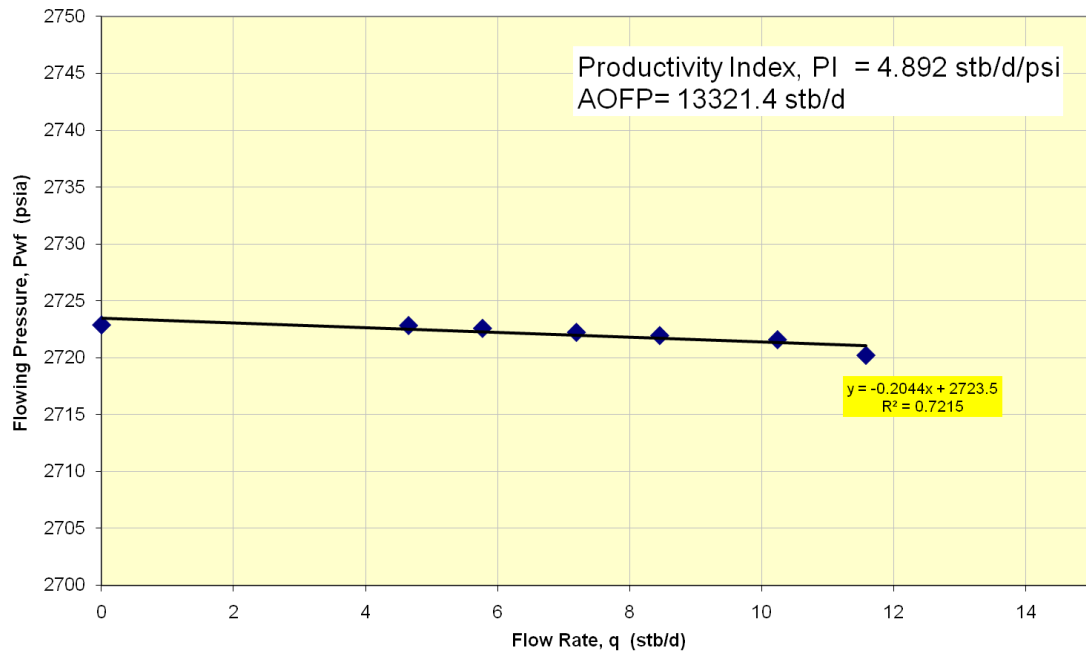


Figure 5.74: IPR plot from single well model of borehole electrical image based method calibrated from SRES-IPTT#2 for IPTT#2.

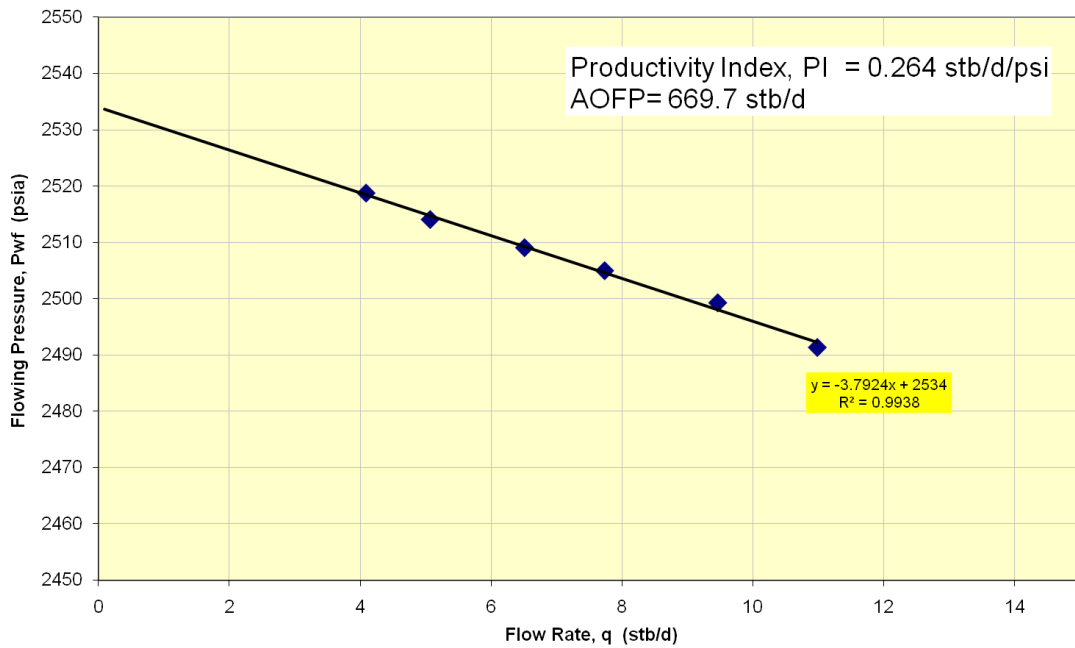


Figure 5.75: IPR plot from single well model of borehole electrical image based method calibrated from SRES-IPTT#2 for IPTT#3.

PI and AOFP estimations from the single well model of borehole electrical image based method calibrated from MODIFIED-SRES-IPTT#3 are illustrated as IPR plots in Figures 5.76, 5.77 and 5.78 for IPTT#1, IPTT#2 and IPTT#3 respectively.

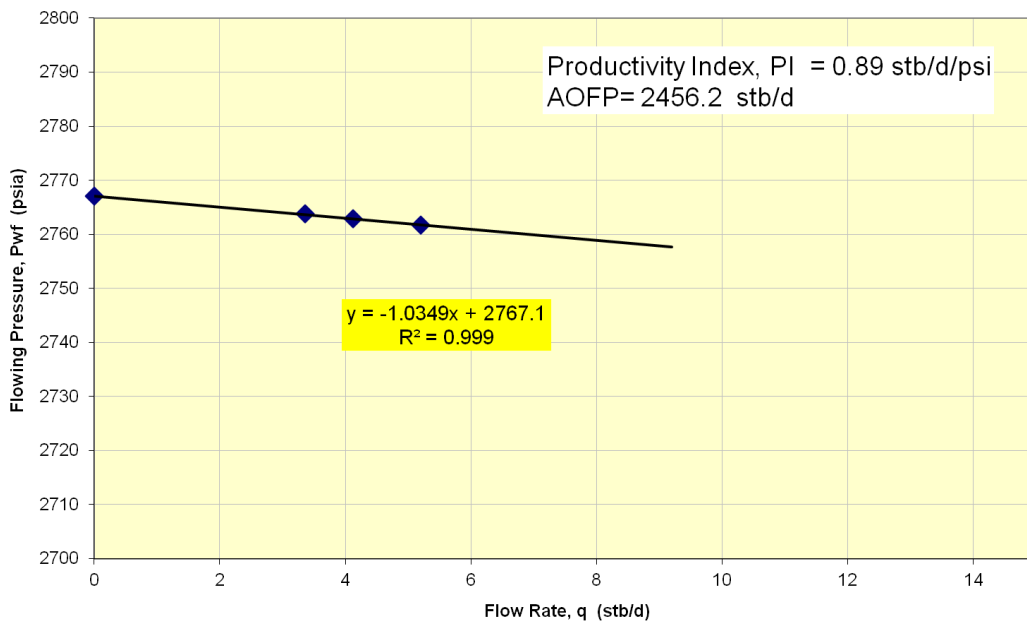


Figure 5.76: IPR plot from single well model of borehole electrical image based method calibrated from MODIFIED-SRES-IPTT#3 for IPTT#1.

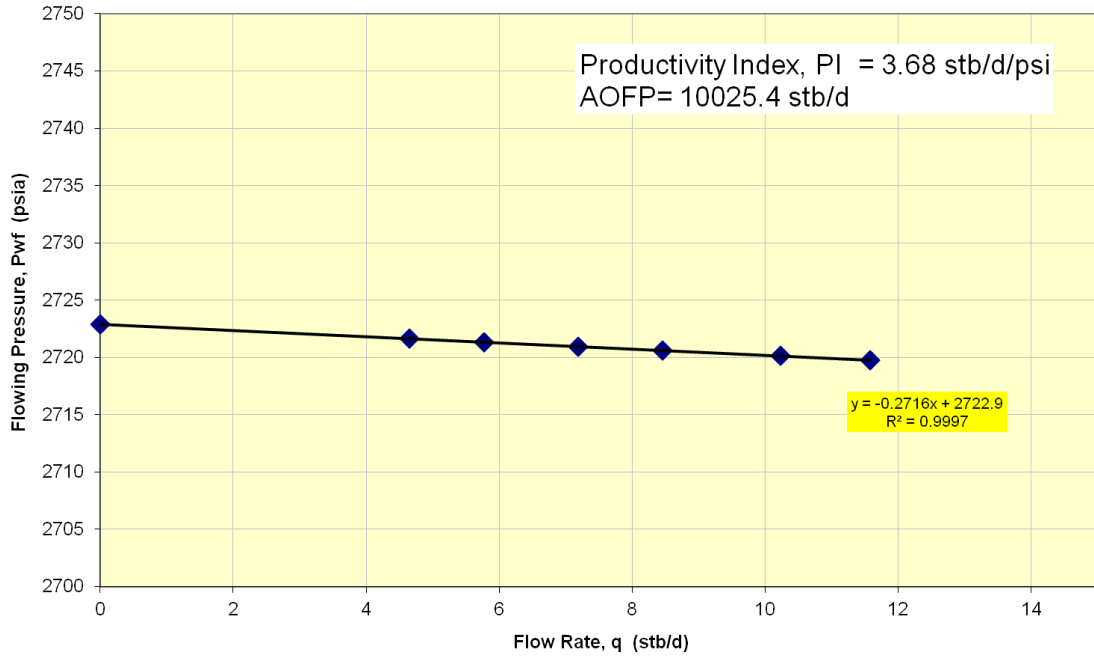


Figure 5.77: IPR plot from single well model of borehole electrical image based method calibrated from MODIFIED-SRES-IPTT#3 for IPTT#2.

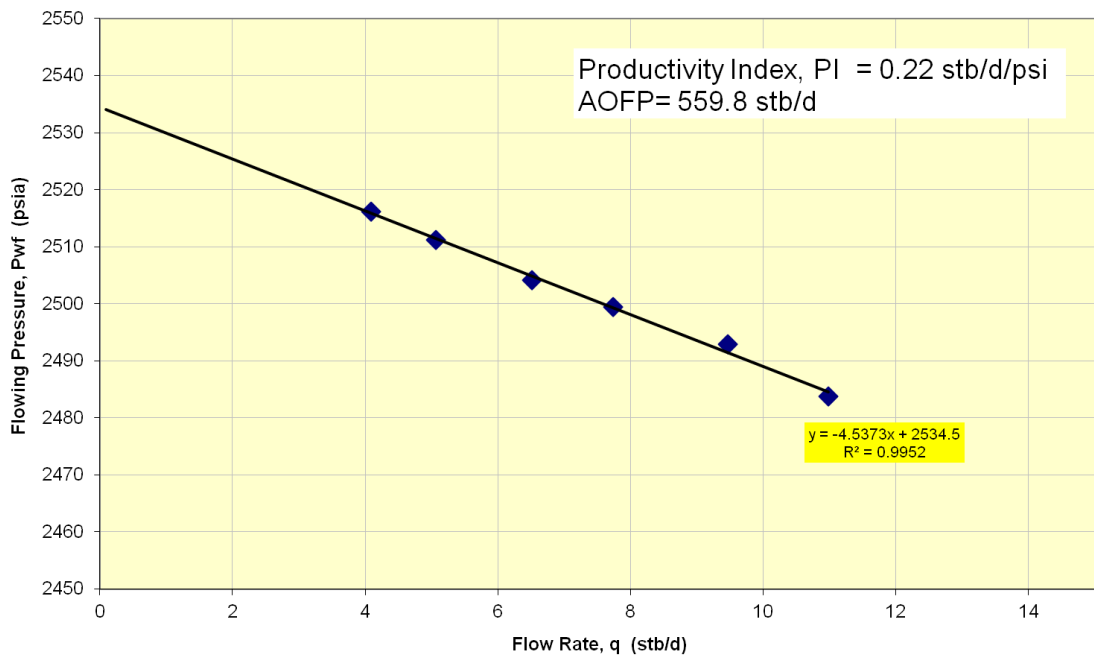


Figure 5.78: IPR plot from single well model of borehole electrical image based method calibrated from MODIFIED-SRES-IPTT#3 for IPTT#3.

Tables 5.11 and 5.12 show summary of Productivity Index (PI) and Absolute Open Flow Potential (AOFP) solved by using Inflow Performance Relationship (IPR) plots above. The result from single well model using SRES from borehole electrical image log and actual measurement are compared in these tables. From the results of single well model, PI and AOFP deviate from the actual measurement with a high value of error (up to 36.18% for PI and 75.66% for AOFP). However, one of the objectives of this study is to maximize the value of information of Borehole Electrical Image using the new workflow to generate a high resolution single well model for predicting the well productivity quantitatively.

Table 5.11: Productivity index from the measurement and single well model.

Single Well Model	IPTT#1	Error	IPTT#2	Error	IPTT#3	Error
	PI (stb/d/psi)	(%)	PI (stb/d/psi)	(%)	PI (stb/d/psi)	(%)
Dual Packers WFT	1.52		4.17		0.215	
MODIFIED-SRES-IPTT#1	1.26	16.97	4.730	13.57	0.284	32.09
SRES-IPTT#2	1.18	22.50	4.892	17.45	0.264	22.79
MODIFIED-SRES-IPTT#3	0.97	36.18	3.682	11.70	0.220	2.32

Table 5.12: AOFP from the measurement and single well model.

Single Well Model	IPTT#1	Error	IPTT#2	Error	IPTT#3	Error
	AOFP (stb/d)	(%)	AOFP (stb/d)	(%)	AOFP (stb/d)	(%)
Dual Packers WFT	4157.30	0.00	8523.30	0.00	410.10	0.00
MODIFIED-SRES-IPTT#1	3493.20	15.97	12880.40	51.12	720.40	75.66
SRES-IPTT#2	3258.40	21.62	13321.40	56.29	669.70	63.30
MODIFIED-SRES-IPTT#3	2673.90	35.53	10025.4	17.63	559.80	36.53

CHAPTER VI

CONCLUSIONS AND RECOMMENDATIONS

This chapter presents conclusions that can be drawn from estimation of horizontal permeability from both NMR based method and Borehole Electrical Image based method. In addition, discussion about limitation from this study and recommendations for future works are included.

6.1 Conclusions

In this study, a simulator was used to simulate the pressure responses from two single well models with different permeability inputs which are permeability derived from NMR logging tool and permeability derived from synthetic resistivity from Borehole Electrical Image logging tool.

This is the first attempt to develop a numerical technique to build a relationship between the synthetic resistivity derived from borehole electrical image tool with other dynamic permeability measurements such as Interval Pressure Transient Testing (IPTT) from dual packer module from wireline formation tester (WFT). Horizontal permeability result from single well model of Borehole Electrical Image based method shows good match with the actual measurement. The horizontal permeability from this single well model can be used for forecasting well productivity. From the results shown in Chapter V, it can be concluded as follows:

1. This study shows that the integration of petrophysical analysis with the proper techniques and workflows can be used to build 3D static model and run numerical simulation to estimate permeability and well productivity.
2. High-resolution permeability derived from Nuclear Magnetic Resonance (NMR) logging tool provide very good results when compared with the

actual data. However, the error between the measurement and the single well model simulation can occur from the degree of lamination which vertical resolution of NMR logging tool cannot detect from the thinly laminated formation.

3. This study shows that Synthetic Resistivity from borehole image logging tool used as permeability input provides good permeability prediction if it is calibrated with IPTT data. Calibration coefficient is used to apply to other intervals where actual measurements are not acquired. In this study, the results show that the estimated horizontal permeability of simulation results and actual results are comparable. From the predicted horizontal permeability, it can be used for predicting well productivity.
4. Synthetic Resistivity from borehole image logging tool has very shallow depth of investigation. If there is a change of mobility away from the wellbore, the first radial flow (nearby well) has to be used in the analysis.
5. When decided to use the Synthetic Resistivity from borehole image logging tool, several limitations need to be considered. Due to the fact that Synthetic Resistivity can be affected from several factors such as type of formation deposition, formation salinity, volume of shale in the formation, rock density, drilling fluid, reservoir fluid, temperature and metallic debris, we need to ensure that these factors do not change any resistivity contrast. Otherwise, the workflow from this study may not be used for predicting reservoir productivity.

6.2 Recommendations

1. There are several available techniques of using Synthetic Resistivity with numerical model for analyzing rock textures, variations of grain size, sorting index, rock facies, high-resolution porosity in clastic environment. Some of these outputs such as high-resolution porosity, grain size, and sorting index can be used to improve our workflow and accuracy of the well performance forecasting.
2. Since this study is the first attempt to develop a technique to predict well productivity using Synthetic Resistivity from borehole electrical image logging tool, there are still limited data in this study. With more data available, more conclusive results should be obtained.

REFERENCES

- [1] Reda, A., and Hashem A.H. Precise Method Using Resistivity Imaging Tool for Estimation of High Resolution Parameters Calibrated to Reservoir Description Tool and Nuclear Magnetic Resonance Data for Better Reservoir Characterization, paper SPE 126331 presented at the SPE North Africa Technical Conference and Exhibition held in Cairo, Egypt. 14-17 February, 2010.
- [2] Elarouci, F., Mokrani, N., Mouici, D.S., and Hill, P. How to Integrate Wireline Formation Tester, Logs, Core and Well Test Data to Get Hydraulic Flow Unit Permeability's: Application to Algeria Gas Field, paper SPE 134001 presented at the SPE International Oil and Gas Conference and Exhibition, Tunis, Tunisia. 8 - 10 June 2010.
- [3] Thomas, S., Corbett, P., and Jensen, J. Permeability and Permeability Anisotropy Characterisation in the Near Wellbore: A Numerical Model using the Probe Permeameter and Micro-Resistivity Image Data, paper presented at SPWLA 37th Annual Logging Symposium. June 16-19,1996
- [4] Anxionnaz, H.A., Delhomme, J.P., and De Haan, S. Reconstructing Petrophysical Borehole Images: Their Potential for Evaluating Permeability Distribution in Heterogeneous Formation, paper SPE 56786 presented at the 1999 SPE Annual Technical Conference and Exhibition held in Houston, Texas. 3-6 October 1999.
- [5] Jackson, R.R., Banerjee R., and Thambynayagam, R.K.M. An Integrated Approach to Interval Pressure Transient Test Analysis Using Analytical and Numerical Method, paper SPE 81515 presented at the SPE 13th Middle East Oil Show & Conference to be held in Bahrain. 5-8 April 2003.

- [6] Daungkaew, S., Harfoushian, J.H., Cheong, B., Akinsanmi, O., Toulekima, S., and Yeo, J. Mini-DST Applications for Shell Deepwater Malaysia, paper SPE 109279, presented at the 2007 SPE Asia Pacific Oil & Gas Conference and Exhibition held in Jakarta, Indonesia. 30 October -1 November 2007.
- [7] Haddad, S., Cribbs, M., Viro, E., Castelijn, K., and Tang, Y. So What is the Reservoir Permeability?, paper SPE 63138, presented at the 2000 SPE Annual Technical Conference and Exhibition held in Dallas, Texas. 1–4 October 2000.
- [8] Zhou, W., and Chen, J., SWPM 3.1 User Guide (Single Well Predictive Model). unpublished paper, Schlumberger.
- [9] Close, D., and Reynolds, B. Petrel and High-Resolution Micro-Resistivity Data for Efficient Analysis of Laminated Reservoirs. unpublished paper, Schlumberger.
- [10] Daungkaew, S., Claverie, M., Cheong, B., Hansen, S., Leech, R., Azam, N., Malim, E., Lasman, R., and Witjaksana, R. Forecasting the Productivity of Thinly Laminated Sands with a Single Well Predictive Model, paper SPE 116370 presented at the 2008 SPE Asia Pacific Oil & Gas Conference and Exhibition held in Perth, Australia. 20–22 October 2008.
- [11] Daungkaew, S., Prosser, D.J., Manescu, A., and Morales, M. An Illustration of the Information that can be obtained from Pressure Transient Analysis of Wireline Formation Test Data, paper SPE 88560 presented at the SPE Asia Pacific Oil and Gas Conference and Exhibition held in Perth, Australia. 18–20 October 2004.
- [12] Claverie, M., Hansen, S., Daungkaew, S., Prickett, Z., Akinsanmi, O., and Pillai, P. Applications of NMR Logs and Borehole Images to the Evaluation of Laminated Deepwater Reservoirs, paper SPE 110223 presented at the 2007

SPE Asia Pacific Oil & Gas Conference and Exhibition held in Jakarta, Indonesia. 30 October–1 November 2007.

- [13] Sheng, G.S., Jun, C., Jing, Z., Qiang, N.Y., Xiang, F.L., Hua, Y.Y., and Khong, C.K. Hydraulic Flow Unit Based Permeability Characterization and Rapid Production Prediction Workflow for an Offshore Field, South China Sea, paper SPE 131486 presented at the CPS/SPE International Oil & Gas Conference and Exhibition in China held in Beijing, China. 8–10 June 2010.
- [14] Amaefule, J.O., Altunbay, M., and Tiab, D., Kersey, D.G., and Keelan, D.K. Enhanced Reservoir Description: Using Core and Log Data to Identify Hydraulic (Flow) Units and Predict Permeability in Uncored Intervals/Wells, paper SPE 26436 presented at the 68th Annual Technical Conference and EXhibition of the Society of Petroleum Engineers held in Houston, Texas. 3-6 October 1993.
- [15] Kiatpadungkul, W., Daungkaew, S., Athichanagorn, S., Hisham, M.N., Doorn, J.V., Haddad, S. Formation Evaluation Challenges in Thin Bedded Reservoirs: How to Effectively Test This Formation?, paper SPE 133961 presented at the SPE Asia Pacific Oil & Gas Conference and Exhibition held in Brisbane, Queensland, Australia. 18–20 October 2010.
- [16] Moran, J.H. and Finklea, E.E. Theoretical Analysis of Pressure Phenomena Associated with the Wireline Formation Test Data, paper SPE 177 presented at 36th Annual Fall Meeting of SPE in Dallas, Nevada, U.S.A. 8-11 October, 1962.
- [17] Stewart, G. and Wittman, M. Interpretation of the Pressure Response of the Repeat Formation Tester, paper SPE 8362 presented at the 54th Annual Fall Conference and Exhibition, Las Vegas, Nevada, U.S.A.: 23-26 September, 1979.

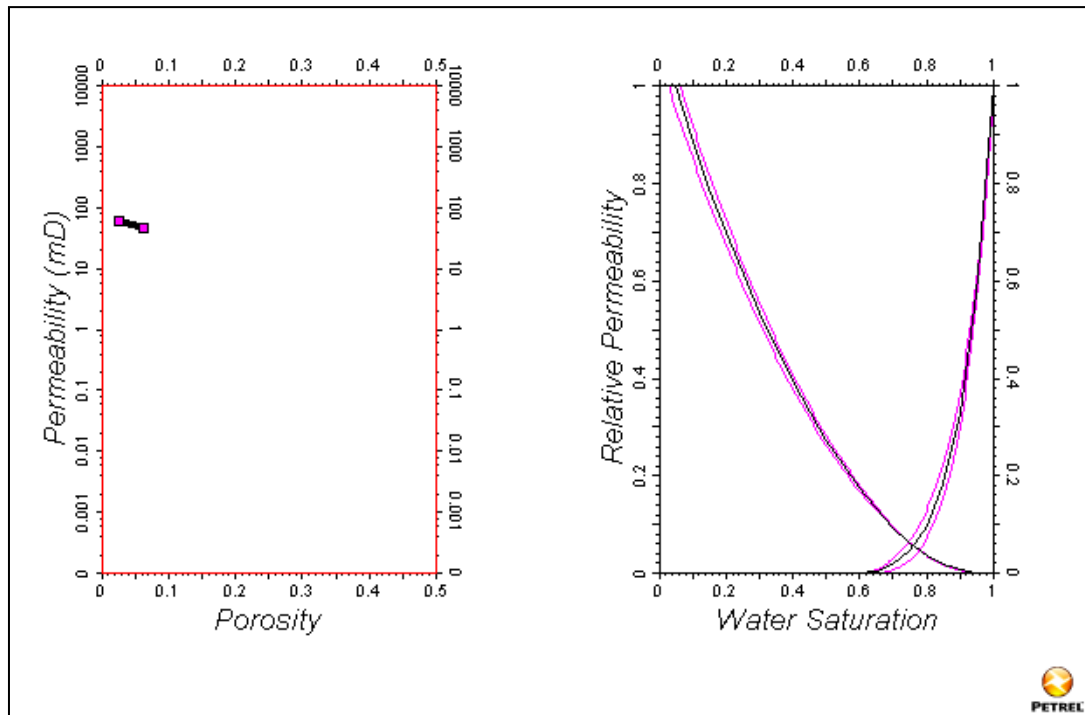
- [18] Kuchuk, F.J., Ramakrishnan, T.S., and Dave, Y., I. Interpretation of Wireline Formation Tester Packer and Probe Pressures, paper SPE 28404 presented at the 69th Annual Technical Conference and Exhibition, New Orleans, Louisiana, U.S.A.: 25-28 September, 1994.
- [19] Gunter, G.W., Finneran, J.M., Hartmann, D.J., and Miller, J.D. Early Determination of Reservoir Flow Units Using an Integrated Petrophysical Method, paper SPE 38679 presented at 1997 Annual Technical Conference and Exhibition, San Antonio, Texas, U.S.A.: 5-8 October, 1997.
- [20] McClain, D. MDT Basic Tool String Training Manual: Schlumberger, July 31, 1996.
- [21] Wireline Formation Testing and Sampling. Schlumberger Wireline & Testing. Schlumberger : 1996.
- [22] Horne, R.N. Modern Well Test Analysis: A Computer-Aided Approach. U.S.A.: Petroway, 1998.
- [23] Schlumberger. Fundamentals of Formation Testing. Texas: Schlumberger Marketing Communications, 2006.
- [24] Well Test Interpretation. Schlumberger : 2002.
- [25] MDT Overview general. Schlumberger Wireline. Schlumberger : 2009.
- [26] Mattar, P, and Dean, L., RESERVOIR ENGINEERING FOR GEOLOGISTS, Fekete Associates Inc. 2008
- [27] ECLIPSE Technical Description Manual [Computer file]. Schlumberger, 2006.

APPENDICES

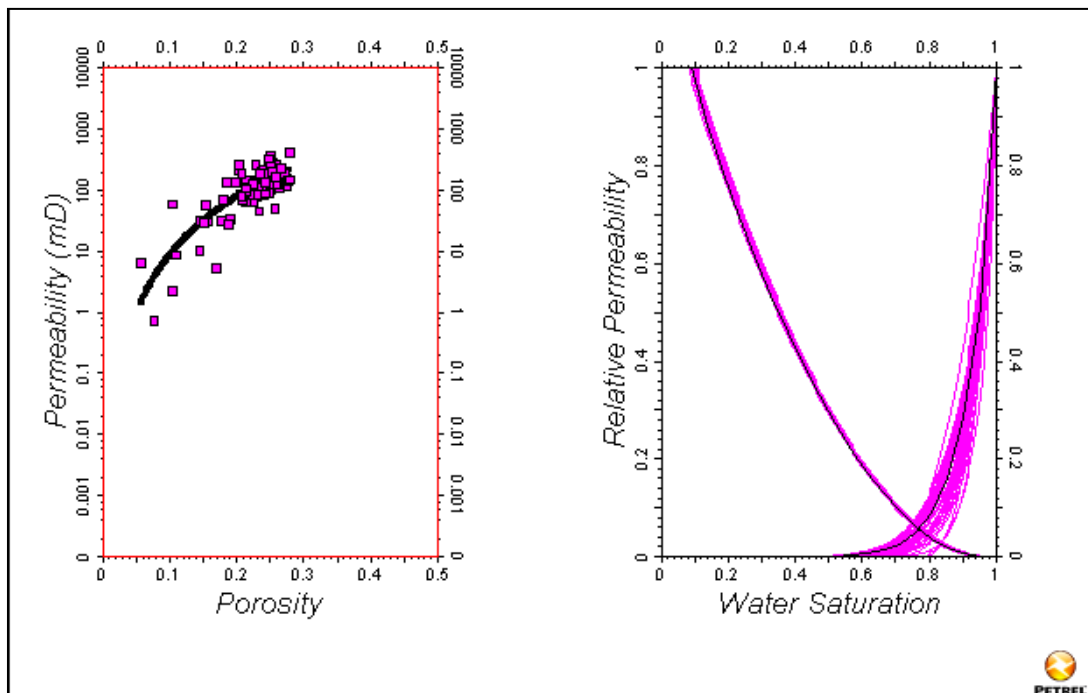
APPENDIX A

Hydraulics Flow Units (HFUs) of Single Well Model of NMR based method.

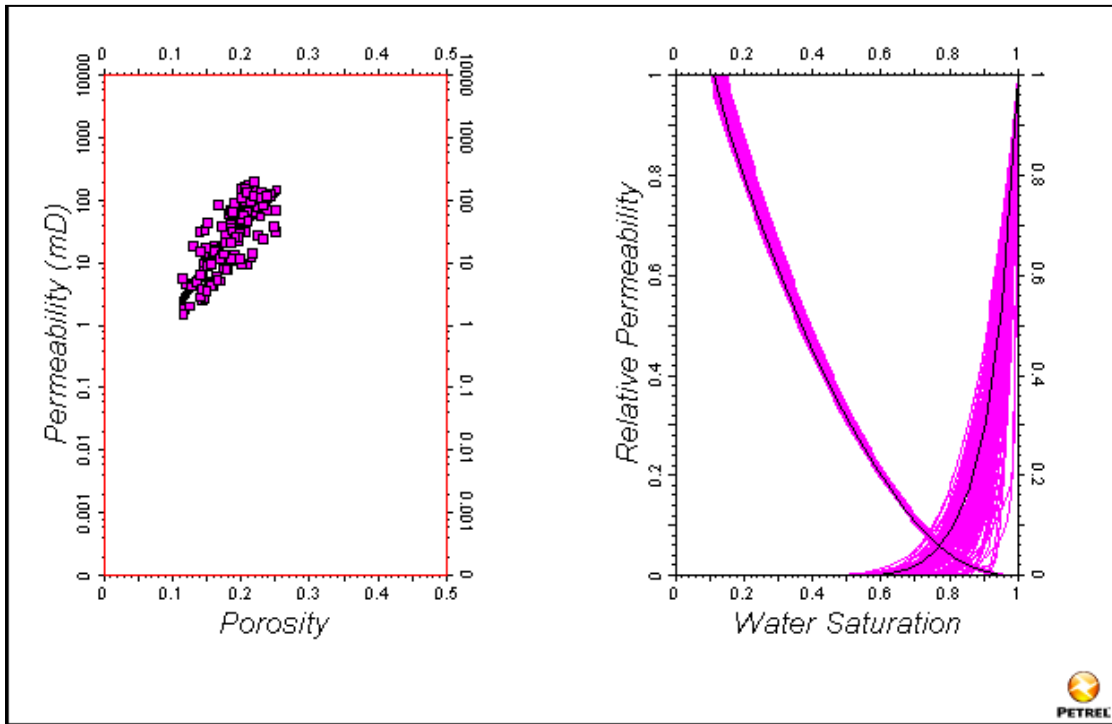
HFU#1



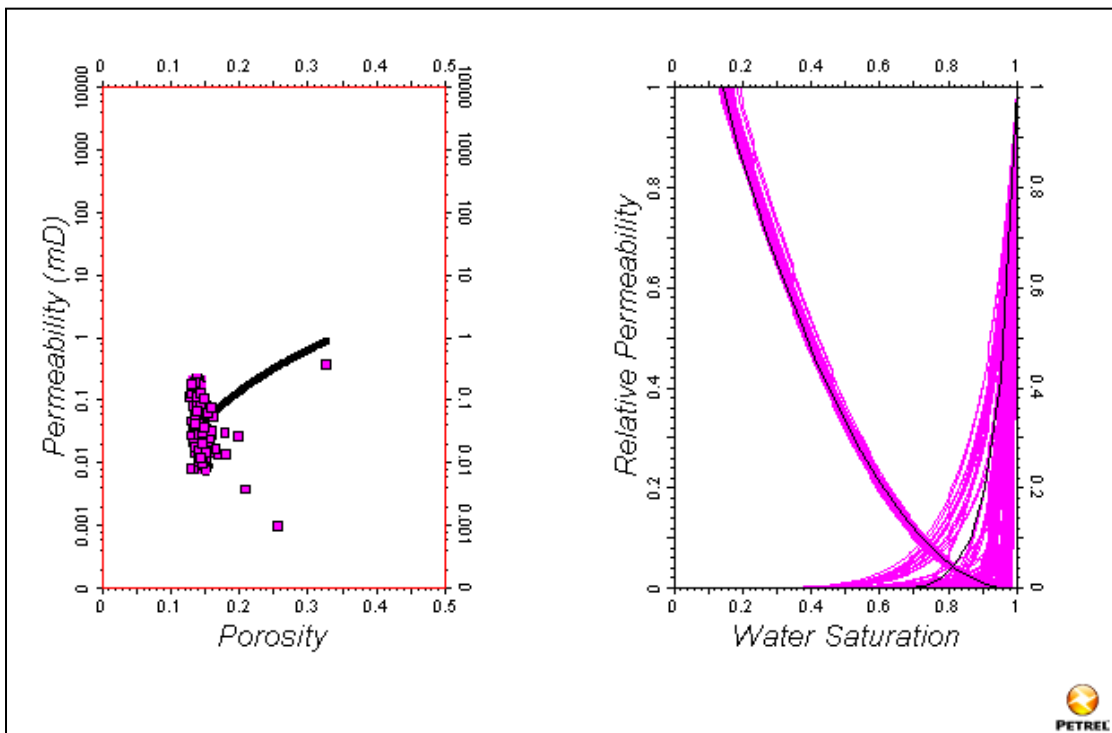
HFU#2



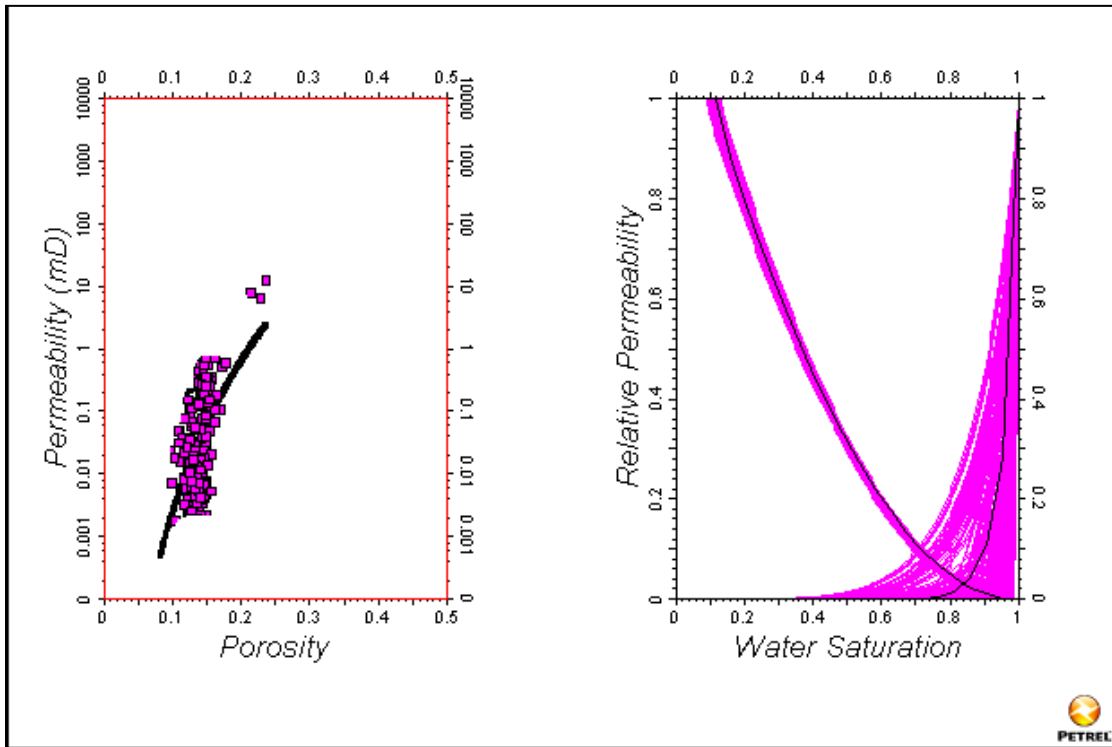
HFU#3



HFU#4

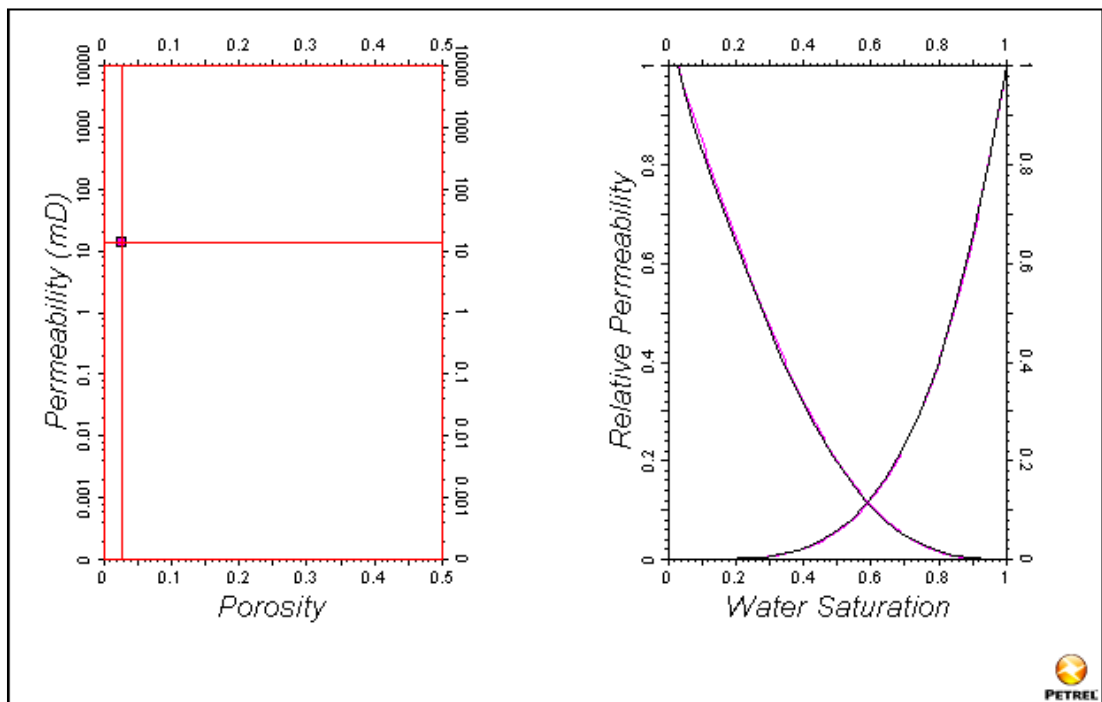


HFU#5

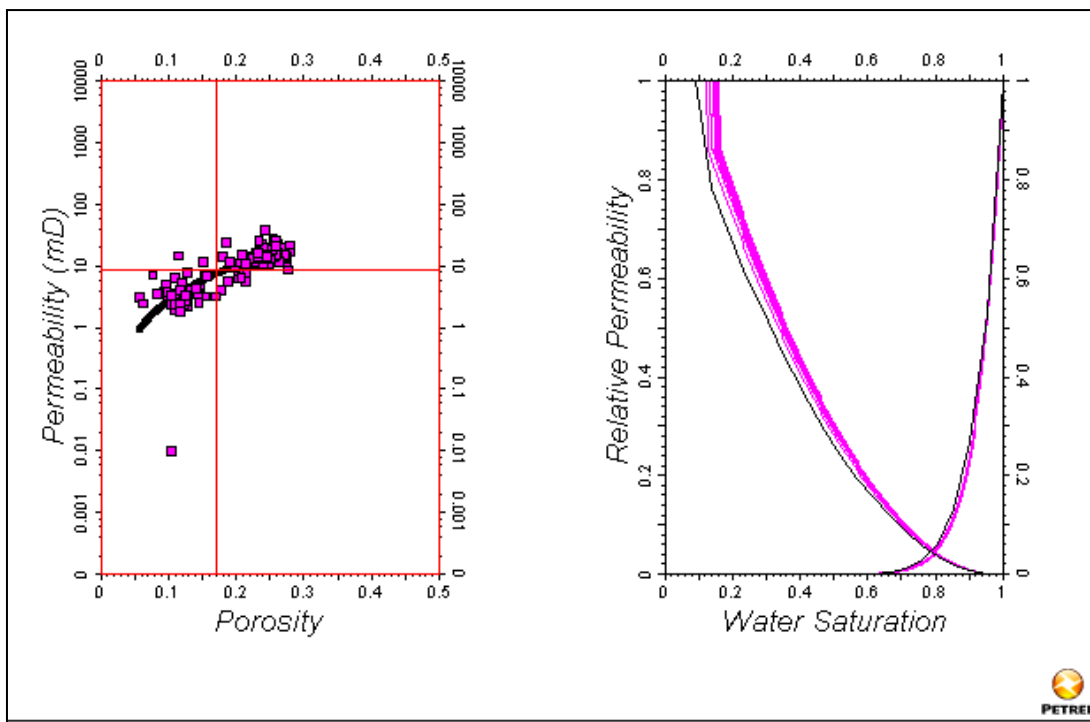


Hydraulics Flow Units (HFUs) of Single Well Model of Borehole Electrical Image Based Method

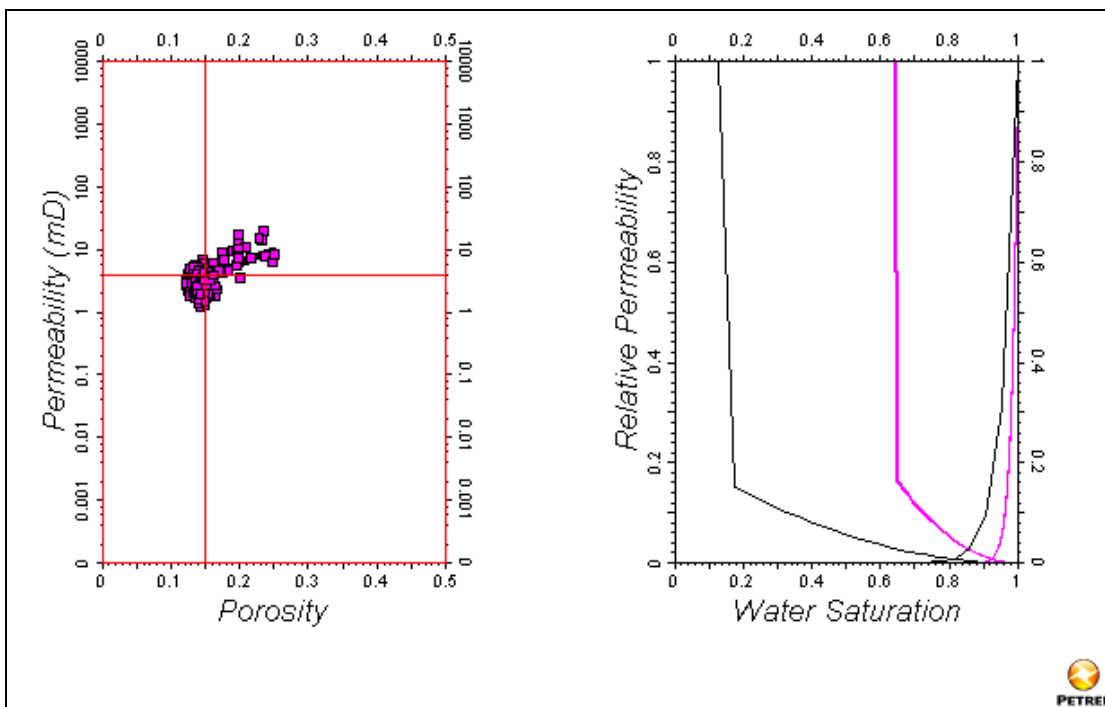
HFU#1



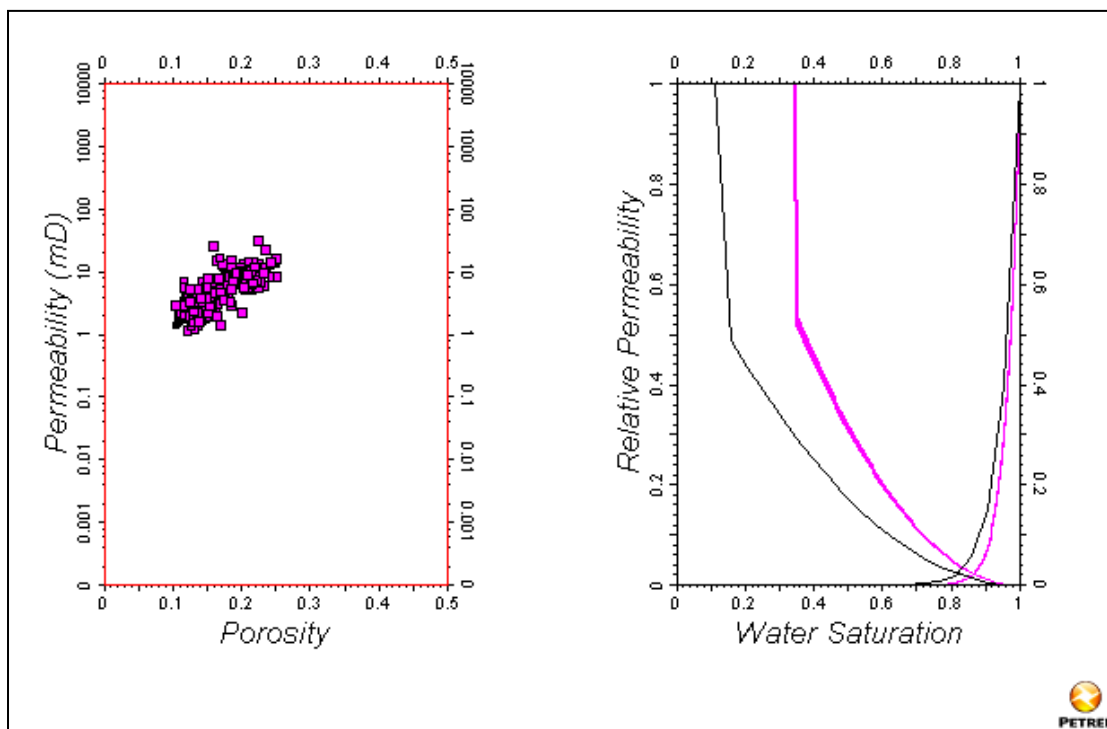
HFU#2



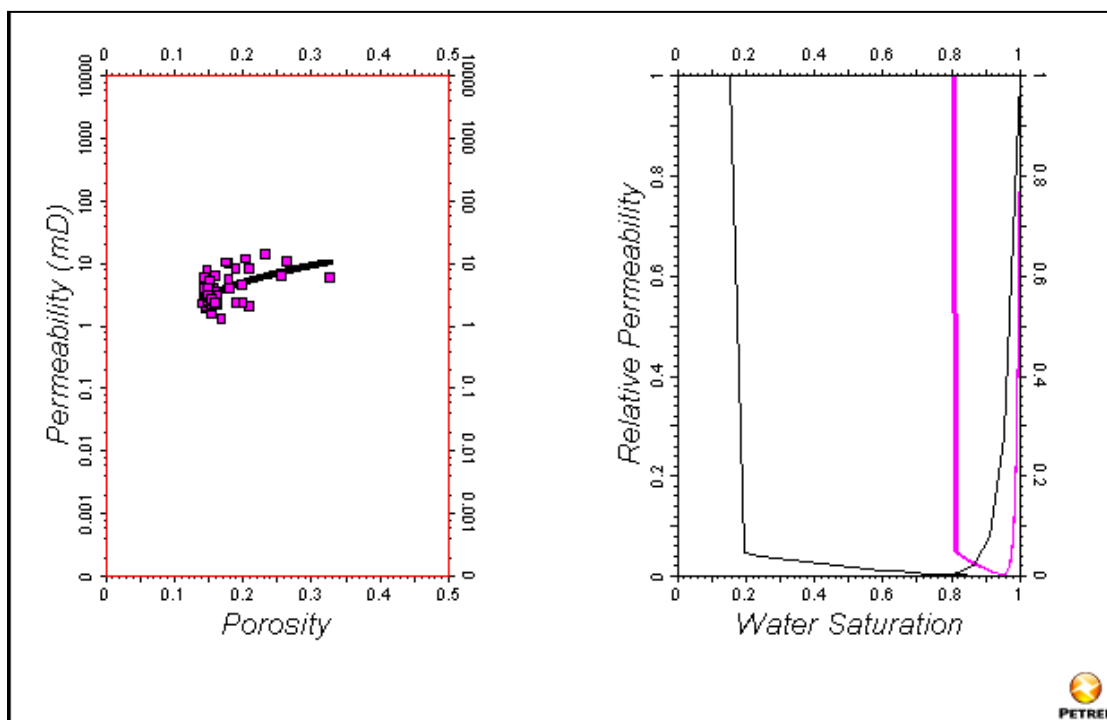
HFU#3



HFU#4



HFU#5



VITAE

Suchart Chokthanyawat was born on August 28, 1981 in Chaing Rai, Thailand. He received his B.Eng. in Computer Engineering from the Faculty of Engineering, King Mongkut's University of Technology Thonburi in 2004. After graduating, he had worked in Reuters Software (Thailand) for a year. He joined Schlumberger Overseas S.A. as IT Support Engineer, and Log Data Processor, accordingly. In 2009, he started to work as Reservoir Engineer and also studied in the Master of Petroleum Engineering program at the Department of Mining and Petroleum Engineering, Faculty of Engineering, Chulalongkorn University.